Efficient strengthening technique to increase the flexural resistance of existing RC slabs: NSM CFRP laminates and compressive thin bonded SFRC overlay

Everaldo Bonaldo,
Joaquim O. Barros, Paulo B. Lourenço

Report 09-DEC/E-06

The present research has been carried out under the financial support of FCT, under PhD grant number SFRH / BD / 11232 / 2002

Date: May 2006
No. of pages: 118

Keywords: flexural strengthening, reinforced concrete slabs, CFRP laminate, thin-bonded overlay, steel fibre reinforced concrete.

Escola de
Engenharia

Departamento de
Engenharia Civil

Universidade
do Minho

Azurém, 4800-085 Guimarães - Tel. +351 253 510 200 - Fax +351 253 510 217 - E-mail secG@civil.uminho.pt

Contents

Summary

The use of composites materials is a remarkable strengthening technique for increasing and upgrading the flexural load carrying capacity of reinforced concrete (RC) members. The Near Surface Mounted (NSM) strengthening technique consists of applying carbon fiber-reinforced polymer (CFRP) laminate strips into slits opened in the concrete cover of the elements to be strengthened. A normal cold cured epoxy based adhesive is used to bond the CFRP laminate strips to concrete.

Laboratory tests have shown that the NSM technique is an adequate strengthening strategy to increase the flexural resistance of RC slabs. However, in RC slabs of low or medium concrete strength, the increment of the flexural resistance that NSM can provide is limited by the maximum allowable compressive strain in the compressed part of the slab, in order to avoid concrete crushing or unadvisable damage. This restriction reduces the efficiency of the strengthening, being questionable the use of the NSM technique in these cases.

A new layer of concrete bonded, by an epoxy compound, to the existing concrete at the compressed region is suitable to overcome this limitation. Since a thin layer (three to five centimetres) is enough for the aforementioned purpose, the volumetric contraction due to shrinkage and thermal effects can induce uncontrolled cracking in the concrete of this layer. Adding steel fibres to concrete (steel fibre reinforced concrete - SFRC), the post cracking residual stress can be increased in order to prevent the formation of uncontrolled crack patterns.

In the present work, the combined strengthening strategy, a SFRC overlay and NSM CFRP laminate strips, was applied to increase, significantly, the flexural resistance of existing RC slabs. Experimental results of four-point bending tests, carried out in concrete slabs strips unstrengthened and strengthened, are presented and analysed.

1 Introduction

In the following a brief background of the hybrid strengthening system is presented, as well as the objectives and scope of the present work.

Brief Background

The Near-Surface Mounted (NSM) strengthening technique has been used in the recent years, with remarkable efficiency, to increase the flexural strength (ALKHRDAJI & NANNI, 1999, ALKHRDAJI et al, 1999, NANNI, 2000; FIB, 2001; CAROLIN, 2003; ROSENBOOM et al 2004; BARROS & FORTES, 2005; KOTYNIA, 2005a) and shear resistance (DE LORENZIS & NANNI, 2001a/2001b; BARROS & DIAS, 2003) of reinforced concrete elements. The NSM technique involves the embedment of CFRP bars - of circular, square or rectangular cross-section - into grooves opened on the concrete surface. The CFRP bars are bonded to concrete using an epoxy-based adhesive (see ***Figure 1.1***). A simple procedure is used to open the grooves for NSM strengthening: a concrete saw moves on supporting rails which are fastened to the bottom surface of the element (see ***Figure 1.2***). Entire cleanness of the sawing task is totally guaranteed attaching a receptacle for the dust powder to the concrete saw machine.

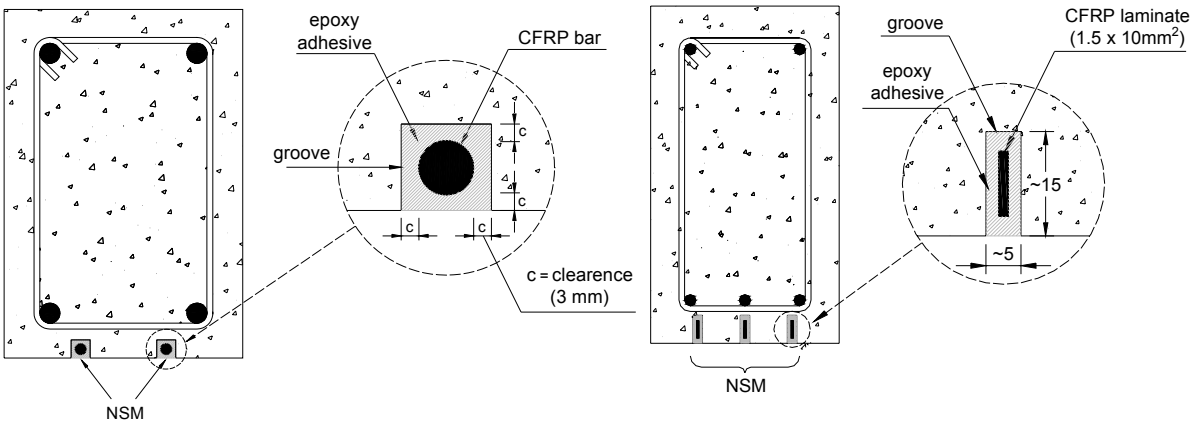

Figure 1.1 *- Details of the NSM technique for the flexural strengthening of RC beams: (a) CFRP bars of circular cross-section, and (b) CFRP bars of rectangular cross-section [(a) ALKHRDAJI & NANNI, 1999; CAROLIN, 2001 and 2003; ROSENBOOM et al 2004, (b) BARROS & FORTES, 2005; KOTYNIA, 2005a; ROSENBOOM et al 2004].*

When compared to the Externally Bonded Reinforcement (EBR) technique, the NSM technique assures a higher anchoring capacity to the FRP reinforcing material (see ***Figures 1.3*** - ***1.5***). As a consequence, a high tensile stress can be mobilized in the

CFRP, as long as the member load carrying capacity is not limited by a premature failure mode (BLASCHKO & ZILCH, 1999; FIB, 2001; CAROLIN, 2003).

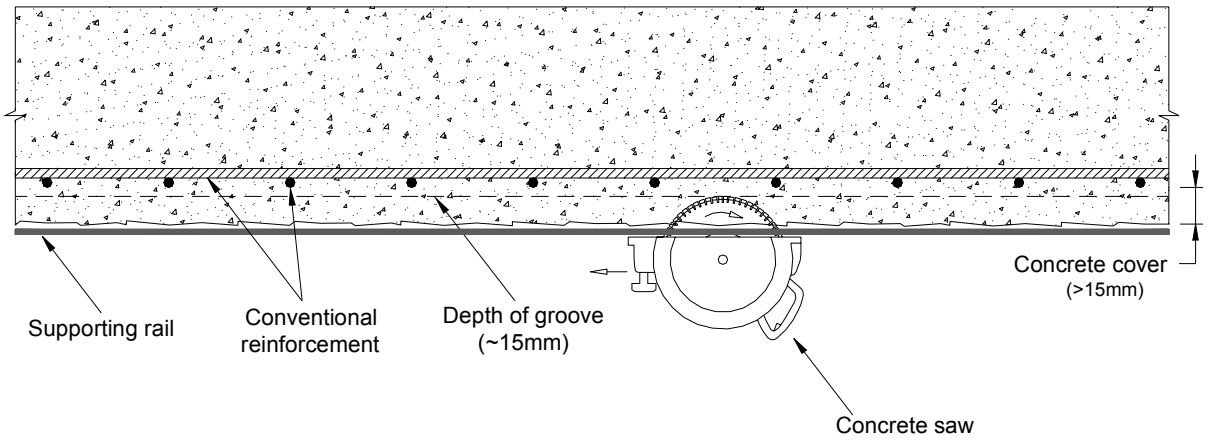

Figure 1.2 *- Making the grooves for NSM technique [adapted from TÅLJSTEN & CAROLIN, 2001; CAROLIN, 2001; CAROLIN, 2003].*

For RC slabs of low or medium concrete strength, the augment of the flexural resistance that NSM can provide might be limited by the maximum allowable compression strain in the extreme compressed concrete fibre. This drawback can be overcome by adding a concrete layer in the compression zone of the existent slab (BARROS & SENA-CRUZ, 2001).

To attain the desired structural performance (e.g. full composite action), the new concrete overlay and the existent concrete slab should behave monolithically. A sound bond between the new layer and the existing concrete slab can be guaranteed if a proper epoxy compound is used (BONALDO, BARROS & LOURENÇO, 2004).

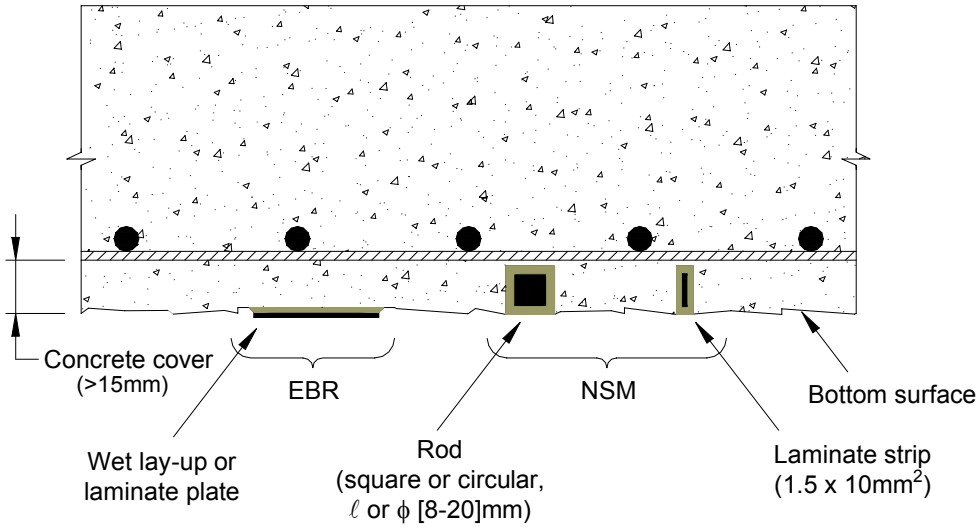

Figure 1.3 *- Strengthening techniques: externally bonded reinforcement, EBR, and near surface mounted, NSM [adapted from TÅLJSTEN & CAROLIN, 2001; CAROLIN, 2001; CAROLIN, 2003].*

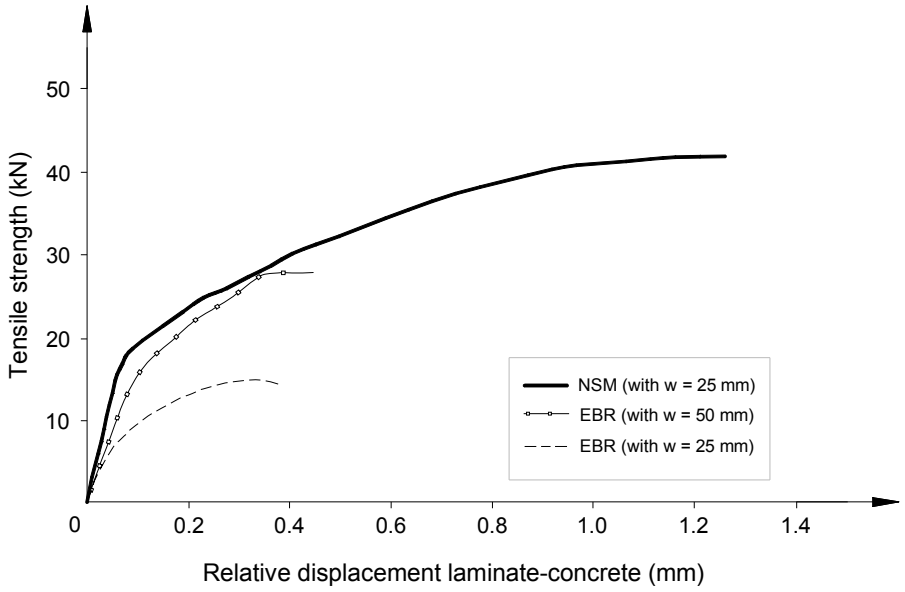

Figure 1.4 *- Strength-slip relationships for NSM e EBR (bond length 250 mm, refer to Figure 1.5). [BLASCHKO & ZILCH, 1999]*

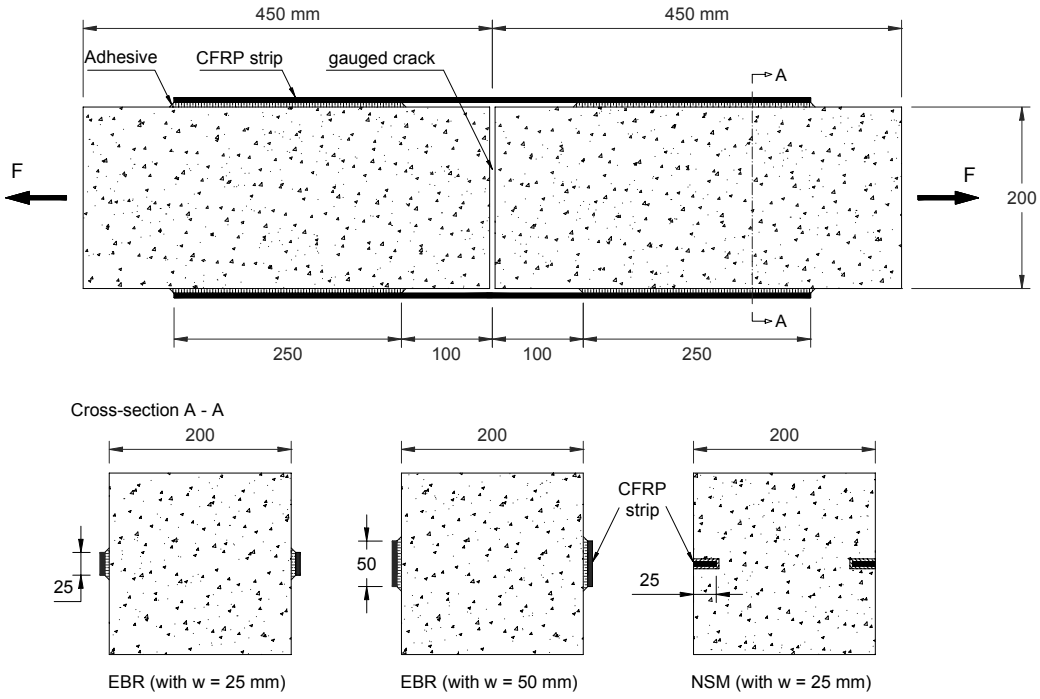

Figure 1.5 *- Geometry of the double-shear specimen for the bond tests carried out by BLASCHKO & ZILCH, 1999.*

Since a thin concrete layer is enough for the aforementioned purpose, the restrained shrinkage and the temperature variation can induce uncontrolled cracking in the

concrete of this layer. Adding discrete fibres to concrete, such as steel fibres, the crack widths resulting from drying restrained shrinkage can be substantially reduced (refer to ***Figure 1.6***). Even the addition of a small content of fibres (as small as 0.25 percent by volume) gives significant reductions of crack widths. Moreover, the post cracking residual tensile strength can be increased (BARROS et al, 2004), in order to prevent the formation of uncontrolled crack patterns. ***Figure 1.7*** shows the influence of the steel fibre addition on the concrete tensile stress-strain behaviour. While plain concrete has a very large stress-strain slope decay after cracking, which is typical of quasi-brittle materials, composite SFRC is able to withstand large strains, while restraining the cracks.

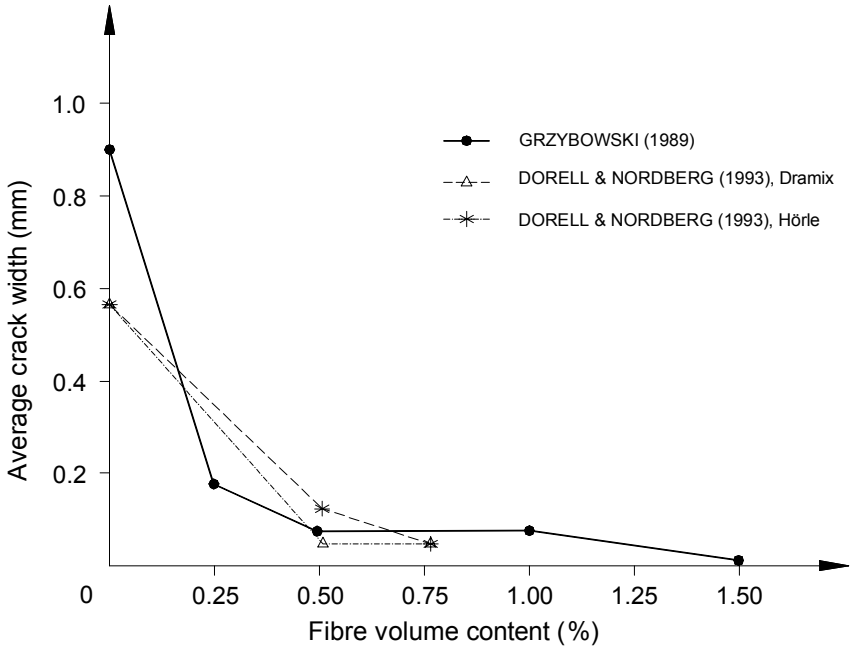

Figure 1.6 *- Beneficial effects of steel fibres on reducing average crack widths reported in literature. [GRZYBOWSKI, 1989; GRZYBOWSKI & SHAH, 1990 and DORELL & NORDBERG, 1993]*

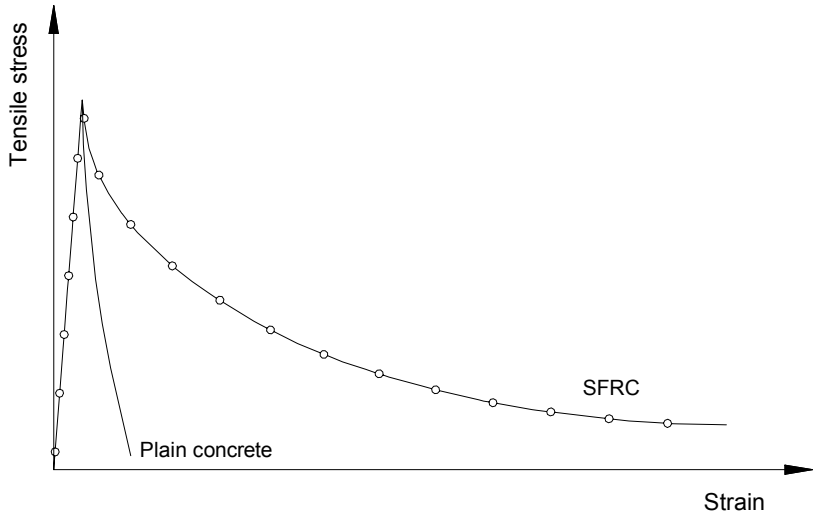

Figure 1.7 *- Sketch of steel fibre influence on the concrete tensile stress-strain behaviour. [FISCHER & LI, 2003]*

The influence of the fibre content on the concrete compressive stress-strain behaviour is presented in ***Figure 1.8***. In plain concrete, the post-peak strength decreases abruptly after peak load, while a significant residual strength is retained in the softening phase of the fibrous concrete. This residual strength increases with the fibre content, which means that increasing the fibre content results in a tougher and much more ductile material (SOROUSHIAN & LEE, 1989; BALAGURU, 1992; WAFA & ASHOUR, 1992; TAERWE, 1992). However, other than the volume fraction (V_f), the composite behaviour also depends on the aspect ratio of the fibres (ℓ_f/d_f where: ℓ_f = fibre length and d_f = fibre diameter), matrix mix proportion and maximum aggregate size. Moreover to avoid concrete crushing, these favourable effects of fibre composite materials can be used to enhancing the compressive behavior of the top concrete layer in the strengthening of RC slabs.

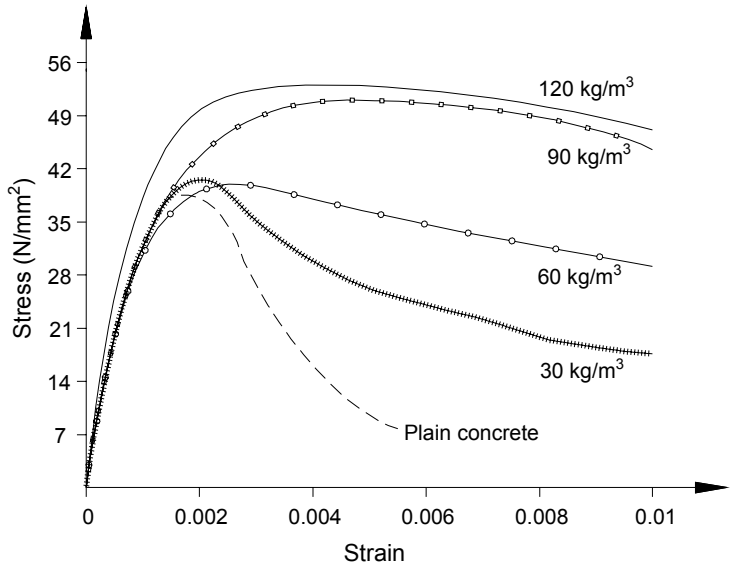

Figure 1.8 *- Steel fibre influence on the concrete compressive stress-strain behaviour, obtained in specimens reinforced with Dramix 50/50 [BALAGURU, 1992].*

BARROS & SENA-CRUZ (2001) proposed a strengthening strategy, combining SFRC and CFRP materials. To increase, for a certain level, the flexural resistance of a RC slab, these authors studied three strengthening alternatives. One solution comprises of CFRP laminates, but the tensile stress that can be installed in the CFRP laminates was limited by the concrete compressive strain. Adding a thin layer of SFRC to the slab compression zone, this restriction was overcome and the ultimate flexural capacity was increased around 45%. The moment-curvature relationship, obtained by the numerical analysis, is depicted in ***Figure 1.9*** for the three studied situations: slab strengthened with a thin layer of SFRC, slab strengthened with CFRP, and slab strengthened with CFRP and overlaid with a thin layer of SFRC. This figure also includes the moment-curvature of the unstrengthened slab.

In the present report, a strengthening strategy for increasing the load carrying capacity of RC slabs, firstly engineered by BARROS & SENA-CRUZ (2001), was experimentally investigated. This strategy consists of applying CFRP laminates in the

tensile bottom slab surface, according to the NSM technique, and bonding, with appropriate epoxy-based adhesive, a SFRC layer in the compression top slab surface (see ***Figure 1.10***). To assess the efficacy of the NSM strengthening technique for increasing the flexural resistance of slabs strips failing in bending, four-point bending tests with RC slab strips were carried out in displacement control.

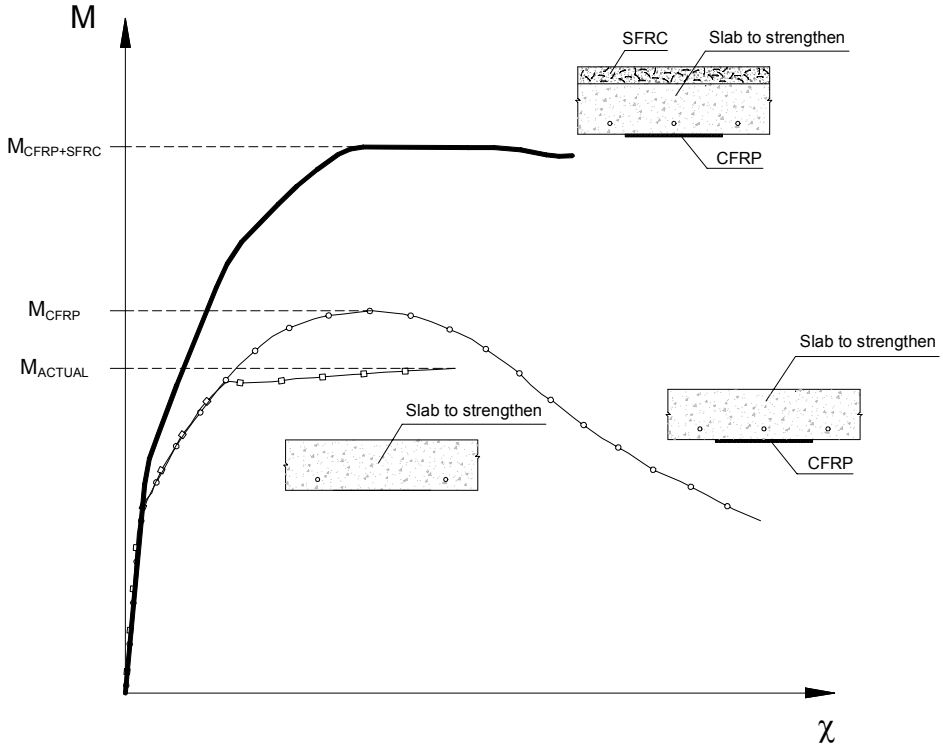

Figure 1.9 *- Moment-curvature relationships from the numerical analysis [adapted from BARROS & CRUZ, 2001].*

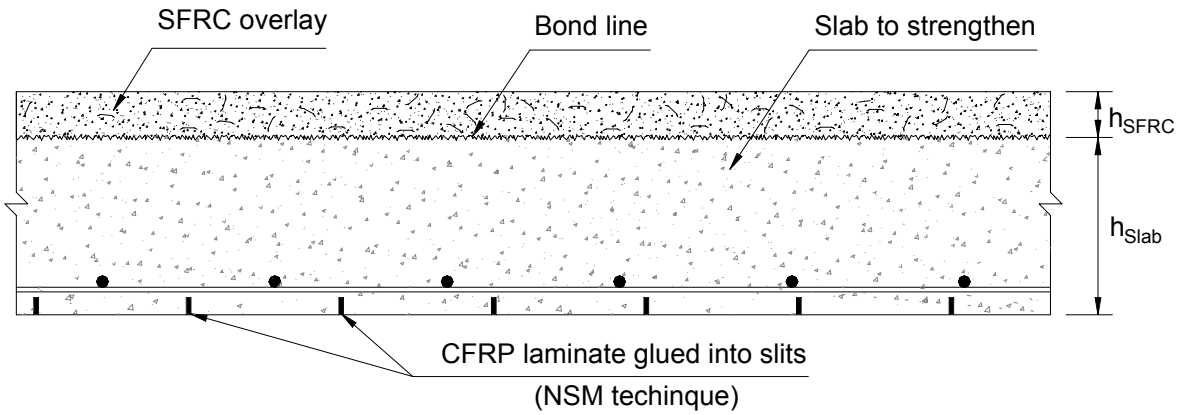

Figure 1.10 *- The hybrid strengthening technique for concrete slabs.*

Objectives and Scope

The present study has the following objectives:

- Evaluate the strengthening efficacy of the NSM technique for RC slabs;

- Evaluate the structural performance of the hybrid strengthening technique: CFRP laminates and SFRC overlay for RC slabs.

The experimental program is composed of eight slab strips: two control slabs, three NSM CFRP strengthened slabs, and three slabs strengthened with NSM CFRP and a SFRC overlay, simultaneously.

2 Experimental Program

The following sections detail the test specimens, test configuration, measuring devices, and test program.

Specimen and Test Configuration

To assess the efficacy of the hybrid strengthening technique for the increase of flexural load carrying capacity of RC slabs, the slab strip specimens represented in ***Figure 2.1*** were used. The test set up and the cross section dimensions of the tested slab strip specimens are also illustrated in ***Figure 2.1***.

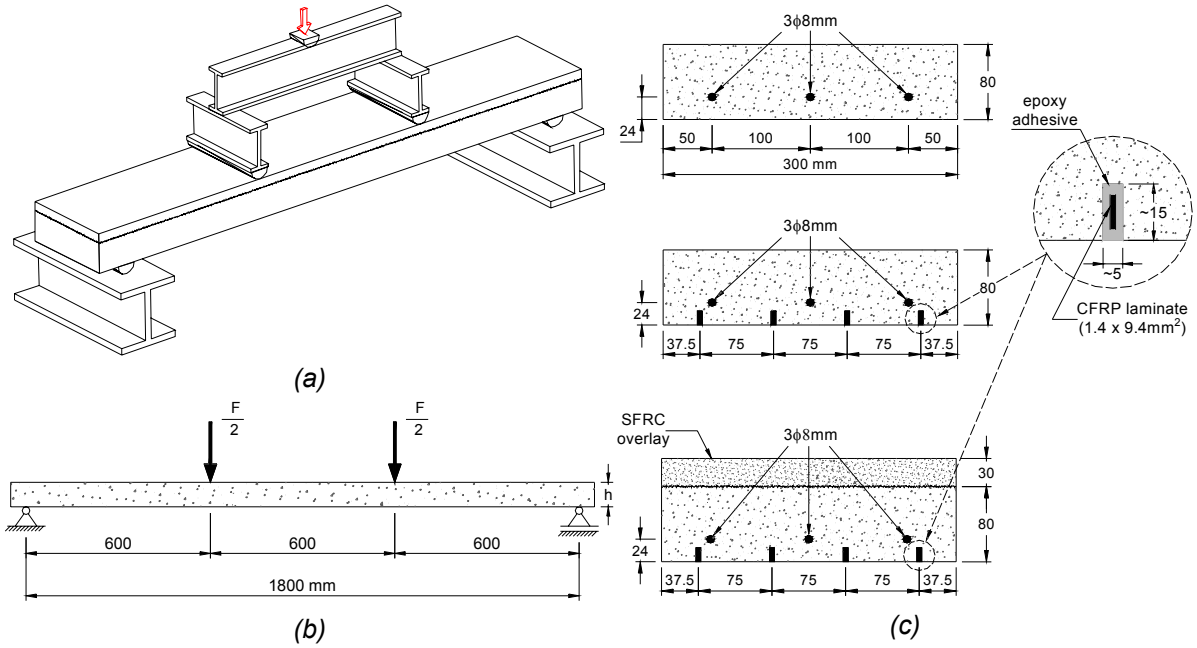

Figure 2.1 *- Test setup (a), test configuration (b), and specimens cross-section dimensions (c).*

The number of CFRP laminate strips applied in each RC slab was evaluated in order to increase 50% the service load (assumed equal to the load producing a mid-span displacement of ℓ/250 = 1800 mm/250 = 7.2 mm). The NSM strengthening is further detailed in ***Figure 2.1*** *(c)*.

The width of the slit where the CFRP is installed usually ranges from 4.0 to 5.0 mm for the NSM strengthening with CFRP strips. To assess the influence of cross section of the adhesive layers that bond the CFRP strip to concrete, and consequently the influence of the adhesive deformability on the performance of NSM strengthening, three different widths for the slits were considered. NSM slits having width of about

4.0 mm, 7.5 mm and 14.0 mm were selected for the hybrid slab specimens. For the slabs strengthened only with NSM, the width of the slits was about 4.0 mm.

Measuring Devices

To measure the deflection of the slab strip, five displacement transducers (LVDT 61472, LVDT 19906, LVDT 3558, LVDT 3468 and LVDT 63796) were applied (see ***Figure 2.2***). The LVDT 3558, positioned at the slab strip mid-span, was also used to control the test at 20 μm/s up to the deflection of 49 mm. After this deflection, the actuator internal LVDT was used to control the test at 25 μm/s displacement rate. The applied force (F) was measured using a load cell (±200 kN and accuracy of 0.5%) placed between the loading steel frame and the actuator of 600 kN load capacity.

Three electrical resistance strain gauges were installed on the internal steel reinforcement (SG1, SG2 and SG3), at the mid span position, to measure the strain in the steel reinforcements, see ***Figure 2.2***. Five strain gauges were installed at one CFRP laminate (SG4, SG5, SG6, SG7 and SG8) for evaluating the strain variation along the laminate. Two strain gages (SG9 and SG10) were also bonded on the top concrete surface to determine the maximum concrete compressive strain. In this experimental program FLA-3-11, BFLA-5-3 and PFL-30-11 strain gauges from TML (TML, 2004) were used, in steel bars, CFRP laminates and concrete, respectively.

The main technical characteristics of the used displacement transducers are included in ***Table 2.1***.

Table 2.1 *- Technical characteristics of the LVDTs, extracted from technical datasheet (RDP, 1995).*

LVDT	**Linear Range** (mm)	**Linearity** (%)
61472	±12.5	±0.04
19906	±25	±0.07
3558	±25	±0.08
3468	±25	±0.08
63796	±12.5	±0.04

Figure 2.3 shows the full arrangement of the bending test set up, while ***Figure 2.4*** includes a photo of a specimen being tested. A servo-controlled test machine was used in the experimental program.

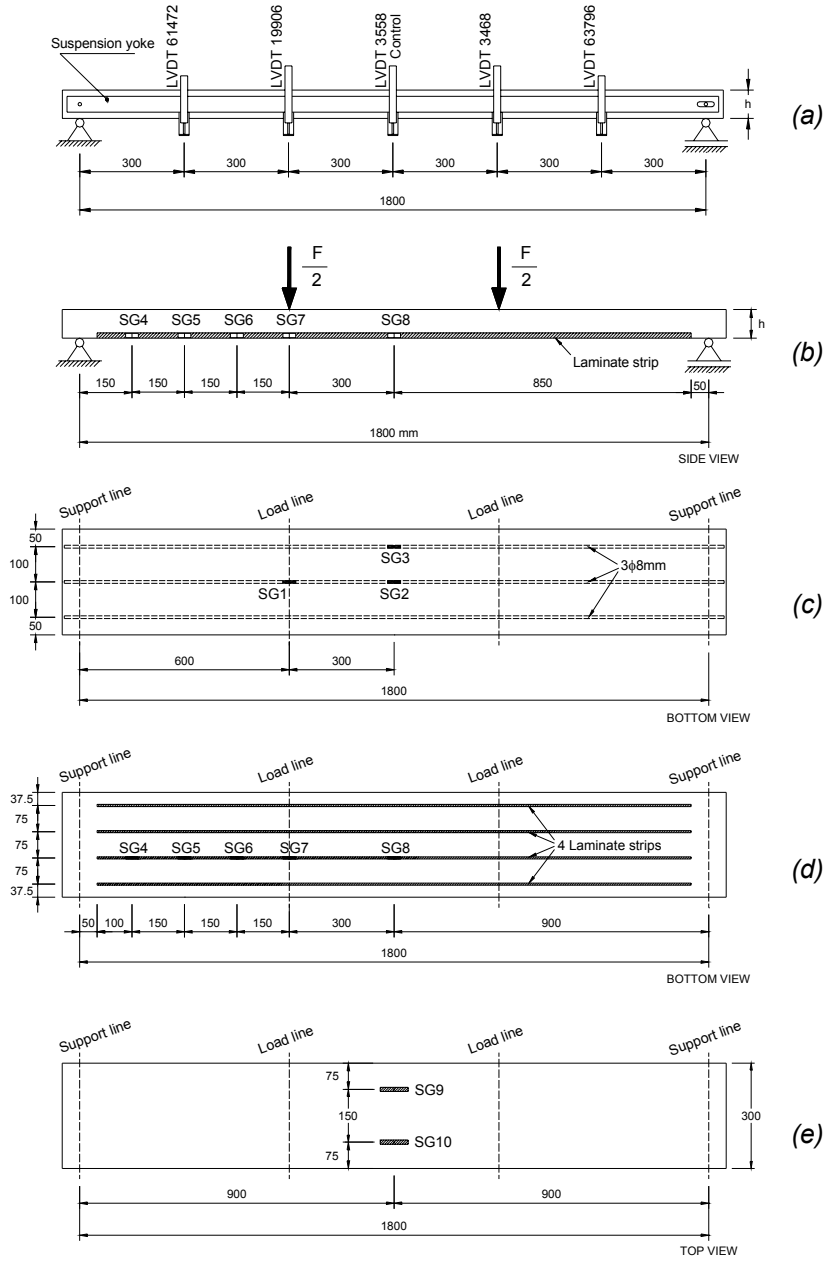

Figure 2.2 *- Arrangement of displacement transducers and strain gauges: displacement transducers (a), position of the strain gauges at the CFRP laminate - side view (b), lay-out of the strain gauges at the steel bars (c), lay-out of the strain gauges at the CFRP laminate - bottom view (d), and strain gauges at the concrete slab top surface - top view (e).*

Test Program

In the present experimental program the influence of the CFRP laminate strengthening and the SFRC overlay strengthening on the flexural behaviour of reinforced concrete slabs is analyzed. For this purpose, unstrengthened (control), strengthened with CFRP laminates, and simultaneously strengthened with CFRP laminates and SFRC overlay specimens (***Figure 2.1****(c)*) were tested under monotonic loading.

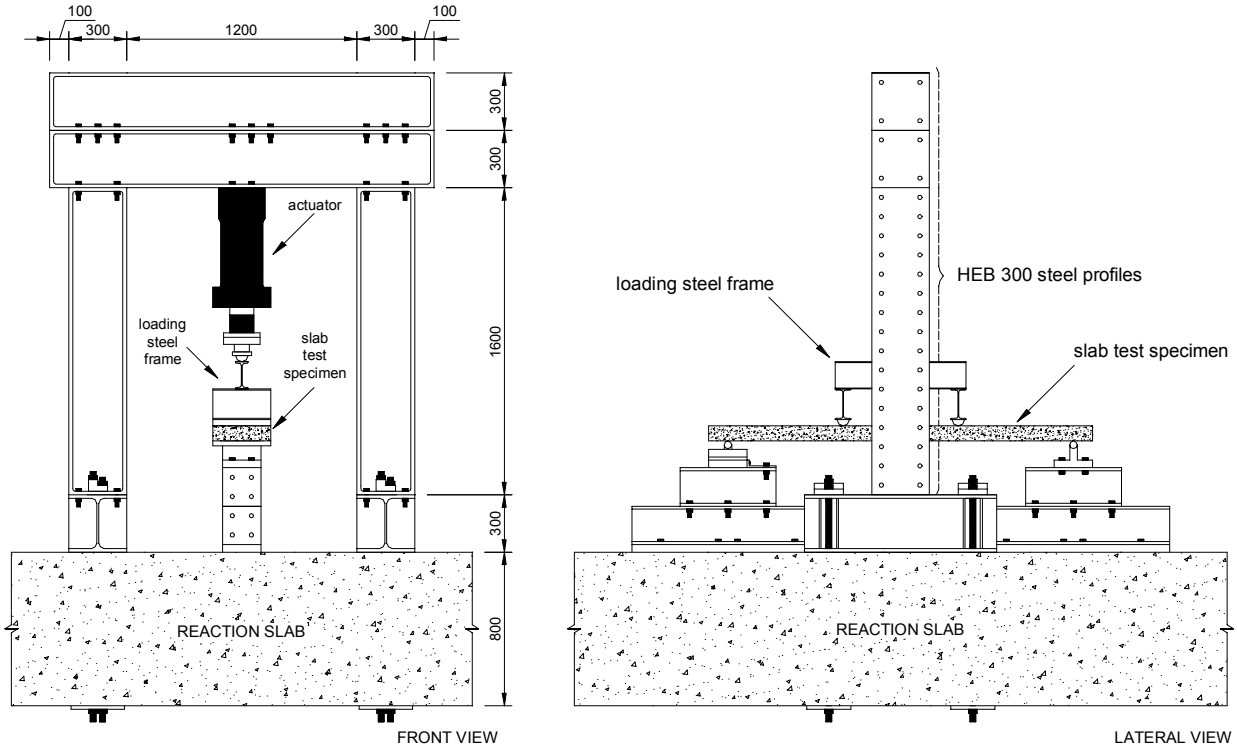

Figure 2.3 *- Layout of the four-point bending test (dimensions in millimetres).*

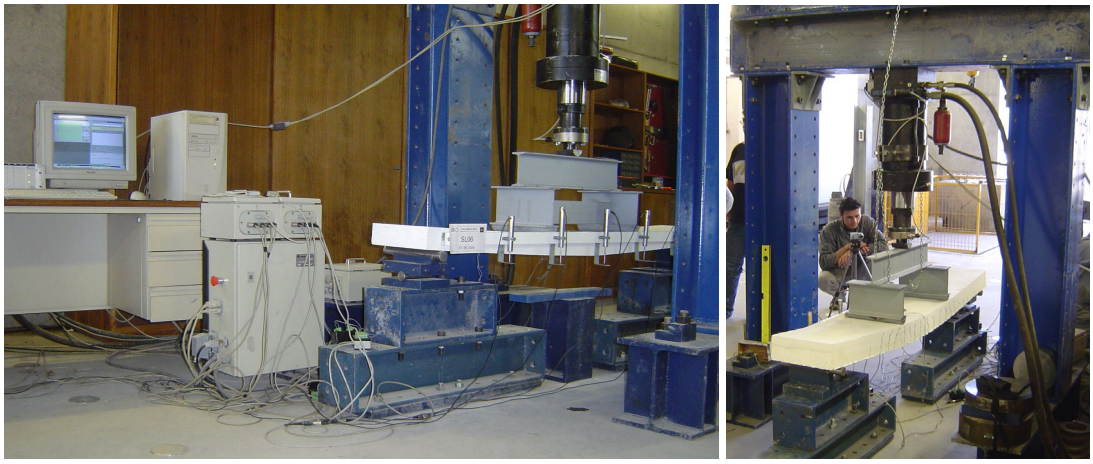

Figure 2.4 *- The SL2 specimen being tested.*

3 Materials Characterization

The following sections detail the various materials used in the present experimental program.

Concrete Slab and Concrete Overlay

A laboratory trial phase was developed at the Laboratory of the Structural Division of the University of Minho aiming to establish the following compressive strength grades (CEB-FIP Model Code, 1993): C20/25 for the concrete slab strips and C35/45 for the SFRC overlay.

For the purpose of defining the mix properties, a *Faury* mix design method was used, see e.g. COUTINHO (1988), using aggregates available in the Northern Region of Portugal (Minho). Details about the physical properties of the aggregates are given in **Annex A**. In **Annex B** the sieve analyses of the aggregates and the information about maximum aggregate size are included. Hooked ends DRAMIX® ZP305 steel fibres were used to reinforce the concrete overlay. This fibre has a length (ℓ_f) of 30 mm, a diameter (d_f) of 0.55 mm, an aspect-ratio (ℓ_f / d_f) of 55 and a yield strength of about 1100 N/mm^2 (DRAMIX, 1998). Previous work revealed that this fibre has high performance since significant increase in the ultimate load carrying capacity of the structural concrete elements was obtained (BARROS & FIGUEIRAS, 1998).

Fibres were added into the mix as the last concrete component. While concrete was being mixed, the steel fibre tablets were gradually and continuously charged into the mix at the same location, for all batches. This procedure was used as an attempt to ensure similar fibre dispersion conditions.

The concrete mix proportions and the main properties of the ordinary concrete (substrate) and SFRC overlay are shown in ***Table 3.1***. Here, W/B is the water-to-binder ratio (Portland cement for the plain concrete and Portland cement plus fly ash for the SFRC). The percentage of RHEOBUILD®1000 superplasticizer refers to the weight of cement plus fly ash. The cylinders compressive strength and static modulus of elasticity in compression were determined according to EN 12390-3 (2002) and RILEM TC14-CPC8 (RILEM, 1994), respectively. It can be noticed that the target concrete strength classes were satisfactorily achieved, and more details regarding the compressive strength of the manufactured concretes can be found in **Annex C**.

The flexural behaviour of the concretes was also characterized, carrying out three-point bending tests on notched beams, according to RILEM (1985) for ordinary concrete, and following the recommendations of to RILEM (2000, 2002) for SFRC. More details about the bending tests are described in **Annex D**.

Table 3.1 *- Mix proportions and main properties of the ordinary concrete (B1 and B2) and SFRC (O).*

Components	Mix designation		
	B1	B2	O
CEM I 42.5 R (kg/m^3)	260		330
Fly ash[a] (kg/m^3)	-		30
Fine river sand (kg/m^3)	394		228
Coarse river sand (kg/m^3)	510		620
Fine aggregate 4/11 (kg/m^3)	423		390
Coarse aggregate 11/16 (kg/m^3)	518		503
Superplasticizer (%)	2.5		2.5
Steel fibre (kg/m^3)	-		30
W/B ratio	0.67	0.71	0.38
Slump[b] (mm)	32.5	30	210[c] 210[d]
fc_{28d}[e] (MPa)	24.16	23.39	40.66
Ec_{28d}[e] (GPa)	26.61	27.69	30.08
fc[f] (MPa)	26.35	25.97	43.23

[a] Obtained from thermoelectric source
[b] Slump determined according to ASTM C143 (1998)
[c] Slump before adding the steel fibres
[d] Slump after adding the steel fibres
[e] Average value of at least three cylinder specimens (150 mm x 300 mm)
[f] Average value of at least three cylinder specimens (150 mm x 300 mm) at the daytime of the slab test

Table 3.2 includes the individual ($f_{ct,fl}$) and average ($f_{ctm,fl}$) values of flexural tensile strength, individual ($f_{ct,ax}$) and average ($f_{ctm,ax}$) values of axial tensile strength, and the individual (G_f) and average (G_{fm}) values of the fracture energy for the plain concrete mixes. ***Figure 3.1*** shows the load versus displacement curves for each plain concrete

mix obtained from flexural tests. Each curve is the average of the load-displacement relationship recorded in the three specimens of each mix.

Table 3.3 includes the values of the equivalent flexural tensile strength parameters (RILEM, 2000 and 2002) and the flexural modulus of elasticity for the SFRC mixes. ***Figure 3.2*** shows the average load versus displacement curve for each SFRC mix obtained from flexural tests. Each curve is the average of the load-displacement relationship recorded in, at least, three specimens of each mix.

Table 3.2 *- Flexural tensile strength, axial tensile strength and fracture energy of ordinary concrete.*

Plain concrete mix	Age at testing (days)	Beam	$f_{ct,fl}$ (N/mm^2)	$f_{ctm,fl}$ (N/mm^2)	$f_{ct,ax}$[a] (N/mm^2)	$f_{ctm,ax}$ (N/mm^2)	G_f (N/m)	G_{fm} (N/m)
B1	43	1	3.08	3.26 (*0.85*) [*26.19%*]	1.48	1.56 (*0.40*) [*25.75%*]	145	165 (*20.49*) [*12.43%*]
		2	4.19		1.99		163	
		3	2.51		1.20		186	
B2	36	1	3.03	2.91 (*0.61*) [*20.87%*]	1.45	1.39 (*0.29*) [*20.64%*]	156	135 (*26.93*) [*19.93%*]
		2	2.14		1.03		105	
		3	2.84		1.37		121	
		2	3.62		1.73		160	

[a] Computed using the CEB-FIP Model Code expression (confer equation D2 from Annex D)
(*value*) Standard deviation
[*value*] Coefficient of Variation (COV) = (Standard deviation/Average) x 100

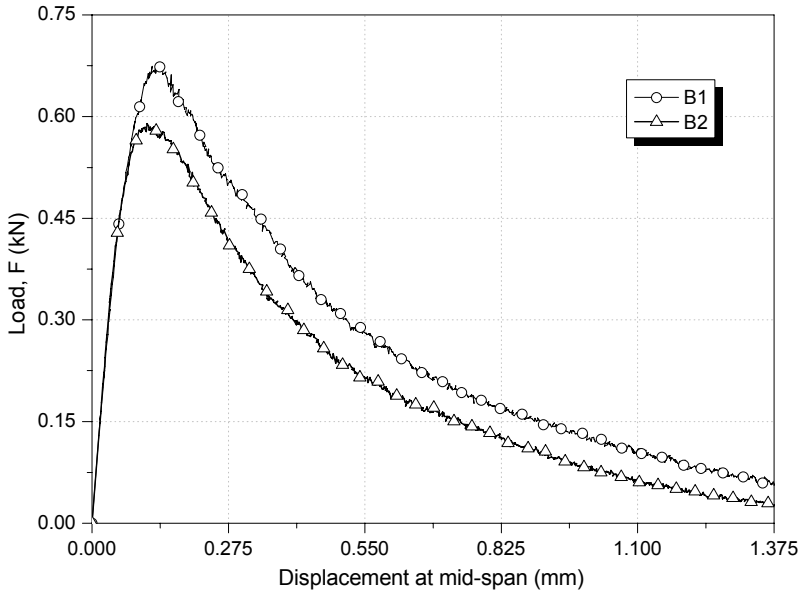

Figure 3.1 *- Load versus displacement curve for each plain concrete mix.*

Table 3.3 *- Equivalent flexural tensile strength parameters and flexural modulus of elasticity of SFRC.*

Beam[a]	$f_{eq,2}$ (N/mm^2)	$f_{eqm,2}$ (N/mm^2)	$f_{eq,3}$ (N/mm^2)	$f_{eqm,3}$ (N/mm^2)	E_{cf} (kN/mm^2)	E_{cfm} (kN/mm^2)
1	3.827		3.038		24.60	
2	3.484		2.892		29.03	
3	4.599		3.613		21.00	
4	5.072	4.313 (0.*526*)	4.106	3.469 (0.*407*)	21.97	24.87 (*2.94*
5	4.487		3.678		28.45	
6	4.786		3.707		24.63	
7	4.520		3.660		26.24	
8	3.732		2.980		26.40	
9	4.308		3.543		21.49	

[a] Testing at the age of 37 days
(*value*) Standard deviation

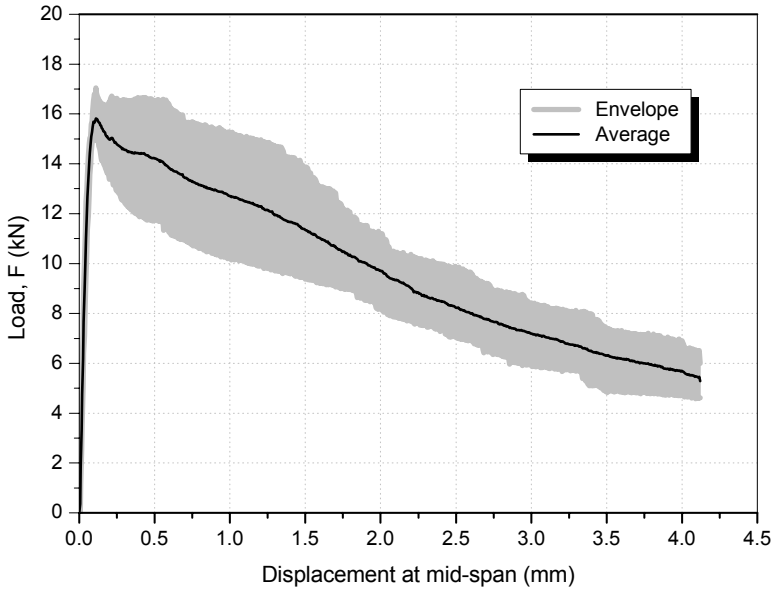

Figure 3.2 *- Load versus displacement curve for the SFRC mix.*

Overlay Bond Product

Epoxy resin is widely used as the bond product for most materials used in construction, such as concrete, masonry units, wood, glass, and metals. Since epoxy-based bond products used in the present experimental program are unaffected by moisture, they are appropriated to bond fresh to hardened concrete. Bonding fresh concrete overlay to an existing concrete slab is an example of such application (ACI 503R-93).

An epoxy resin-based bond agent with a Trademark of Sikadur®32N (see ***Figure 3.3***), supplied by Sika® Portugal, was selected to bond fresh SFRC overlay to hardened reinforced concrete slab. This resin was composed of two components (A and B), and was available in packages of 1.2 kg (0.8 kg component A and 0.4 kg component B). Information about the bond product is summarized in ***Table 3.4***.

Figure 3.3 *- Bond product packaging, 1.2 kg unit.*

In a previous study, the selected bond coat provided excellent performance in bonding fresh SFRC to hardened concrete substrate (BONALDO et al, 2004).

Table 3.4 *- Main properties of the product, extracted from commercial datasheet (SIKA, 2002).*

Properties				
Specific gravity	**Bond strength**	**Mechanical resistance**	***Pot life*[a] and open time[b] at 20 °C**	**Mixing ratio**
Approximately 1.4 kg/l	to concrete: 2.5 - 3.0 N/mm^2 (concrete failure) to steel: 18 - 20 N/mm^2	Compressive strength: ~60 - 70 N/mm^2 Tensile strength: ~18 - 20 N/mm^2 Flexural strength: ~30 - 35 N/mm^2	Approximately 20 min, and Approximately 3 h	Comp. A: 2 parts by weight Comp. B: 1 parts by weight

[a] The maximum time between final mixing and application during which a resin or adhesive remains usable (COMYN, 1997). Also known as *working life* or *usable life*.
[b] The open time starts when the adhesive has been applied to the parts to be joined, and it represents the time limit during which the joint has to be closed (MAYS & HUTCHINSON, 1992).

Mechanical properties of the overlay bond coating adhesive

To assess the tensile mechanical properties of the hardened epoxy resin, seven tensile tests in machined specimens (see ***Figure 3.4***) were carried out according to ISO 527-2 (1993). A testing machine Instron 4505 with 150 mm distance between grips (see ***Figure 3.5***) was used. A test speed of 1 mm/min, as is required for this type of material, was selected for all the tests. The tensile test results are displayed in ***Table 3.5****,* and the specimens before and after testing are shown in ***Figure 3.6***. The recorded stress-strain curves are depicted in ***Figure 3.7***. The strain was measured from the displacements recorded in the displacement transducer of the actuator.

The bond coating adhesive was applied onto dry and clean sandblasted concrete surface, i.e., free from surface contaminants such as dust, laitance, oil or grease, following the manufacturer specifications. A bond coating dosage of 0.90 kg/m^2 was adopted (BONALDO et al, 2004).

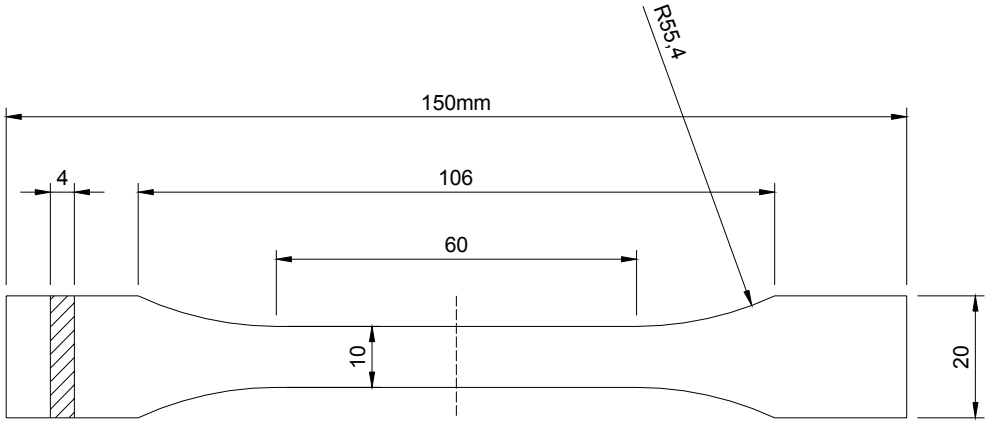

Figure 3.4 *- Shape and dimensions of the test specimens (type 1B - ISO 527-2, 1993).*

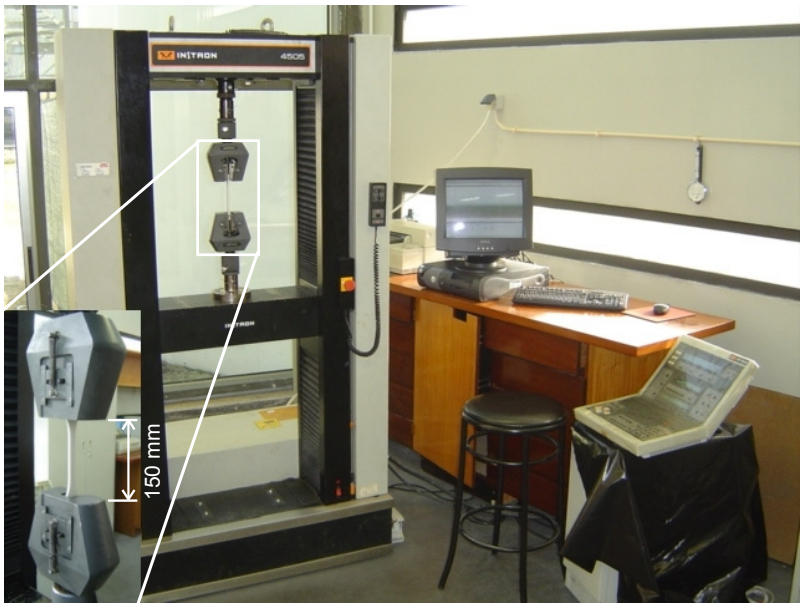

Figure 3.5 *- The testing machine Instron 4505.*

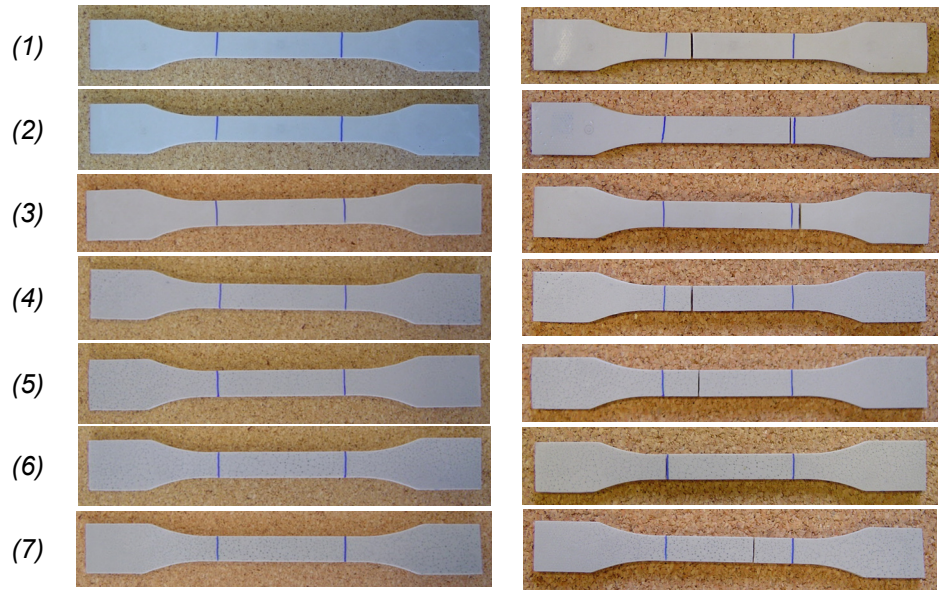

Figure 3.6 *- Test specimens before testing (a) and, after testing (b).*

Table 3.5 *- Results of the tensile tests on the overlay bond coating adhesive specimens.*

Specimen	Ultimate tensile stress (N/mm^2)	Ultimate tensile strain (‰)	Modulus of elasticity[a] (kN/mm^2)
1	28.79	11.63	3.67
2	26.39	9.82	3.76
3	24.04	9.51	3.51
4	27.92	10.87	3.75
5	25.93	10.76	3.56
6	25.96	10.81	3.54
7	26.86	11.80	3.59
Average	26.56	10.74	3.62
Std.Dev.	1.53 (*5.76%*)	0.85 (*7.89%*)	0.10 (*2.78%*)

[a] *Tensile Modulus of Elasticity* calculated from the stress-strain data using a linear regression procedure applied over the strain range 0-1.80 ‰
(*value*) Coefficient of Variation (COV) = (Standard deviation/Average) x 100

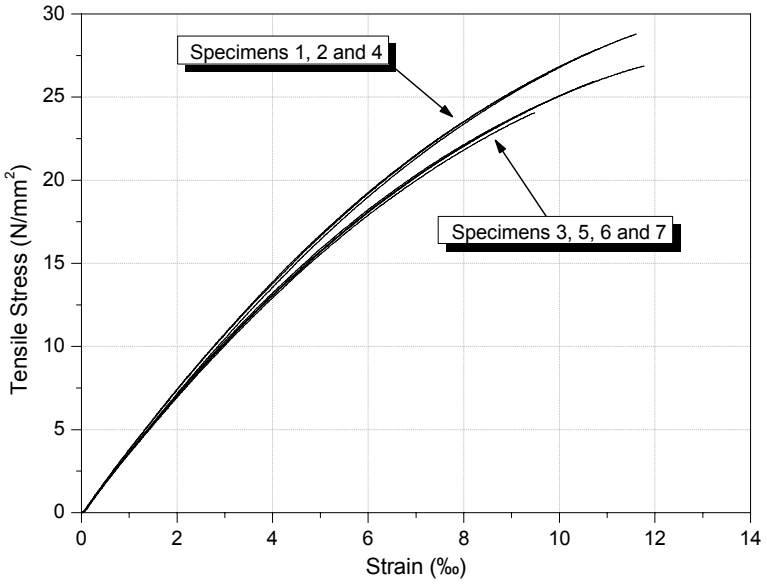

Figure 3.7 *- Tensile stress-strain curves for the Sikadur®32N epoxy resin.*

CFRP-Concrete Bond Product

A low viscosity epoxy based adhesive with a Trademark of MBrace®Resin 220, supplied by Bettor MBT® Portugal, was used to bond the prefabricated CFRP laminates to the concrete, into the grooves. The epoxy resin adhesive two component,

resin and activator, are provided in 5 kg unit packaging (see ***Figure 3.8***). According to the supplier, the epoxy adhesive has the properties indicated in ***Table 3.6***.

Table 3.6 *- Main properties of the MBrace®Resin 220, extracted from datasheet (BETTOR MBT, 2005).*

Properties			
Density (at 20 °C)	**Mechanical resistance**	***Pot life*, open time and hardening** (at 20 °C)	**Mixing ratio**
1.7 kg/l	Tensile strength: > 2.5 N/mm^2 (concrete failure) Shear strength: > 1.8 N/mm^2 (concrete failure)	Minimum 3 min, ≈ 60 min, ≈ 3 days	Comp. I: 3.805 parts by weight Comp. II: 1.195 parts by weight

Figure 3.8 *- CFRP bond product packaging, 5 kg unit.*

Mechanical properties of the CFRP-concrete bond product

Uniaxial tensile tests were performed on moulded specimens to determine the tensile behavior of the epoxy adhesive used for bonding the CFRP laminate to concrete. The tests followed the procedures outlined in ISO 527-2 (1993). The shape and dimensions of test specimens are shown in ***Figure 3.9***. Due to the low viscosity of the epoxy resin and to avoid the presence of voids, specimens of reduced dimensions have been adopted and moulded under pressure. The moulding steps of the test specimens are shown in ***Figure 3.10***.

A testing machine Instron 4505 (see ***Figure 3.5***) was used and a test speed of 1 mm/min was selected for all the tests, complying with the procedures outlined by ISO 527-2 (1993). The tensile test results are included in ***Table 3.7*** and represented in ***Figure 3.11***.

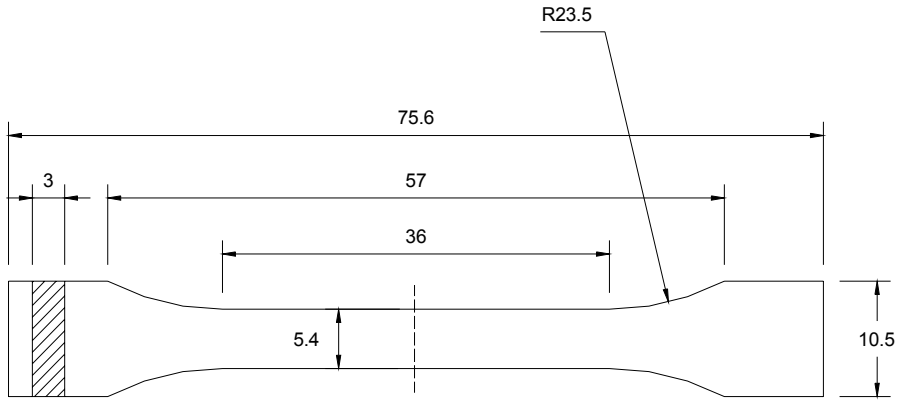

Figure 3.9 *- Shape and dimensions of the test specimen (dimensions in millimeters).*

(a) *(b)* *(c)*

Figure 3.10 *- Preparation of the test specimens: (a) test specimen mould, (b) resin casting, and (c) applying pressure.*

Table 3.7 *- Results of the MBrace®Resin 220 tensile tests.*

Specimen	Ultimate tensile stress (N/mm^2)	Ultimate tensile strain (‰)	Modulus of elasticity[a] (kN/mm^2)
1	32.75	4.62	7.530
2	38.38	5.72	7.341
3	33.49	4.62	7.646
4	27.91	3.93	7.448
5	30.66	4.45	7.496
6	35.40	4.60	8.230
7	34.60	5.71	7.025
8	32.39	5.29	7.188
9	31.64	4.58	7.352
Average	33.03	4.83	7.473
Std.Dev.	2.81 (*8.52%*)	0.57 (*11.80%*)	0.320 (*4.28%*)

[a] *Tensile Modulus of Elasticity*, calculated from the stress-strain data using a linear regression procedure over the strain range 0-2.20 ‰

(*value*) Coefficient of Variation (COV) = (Standard deviation/Average) x 100

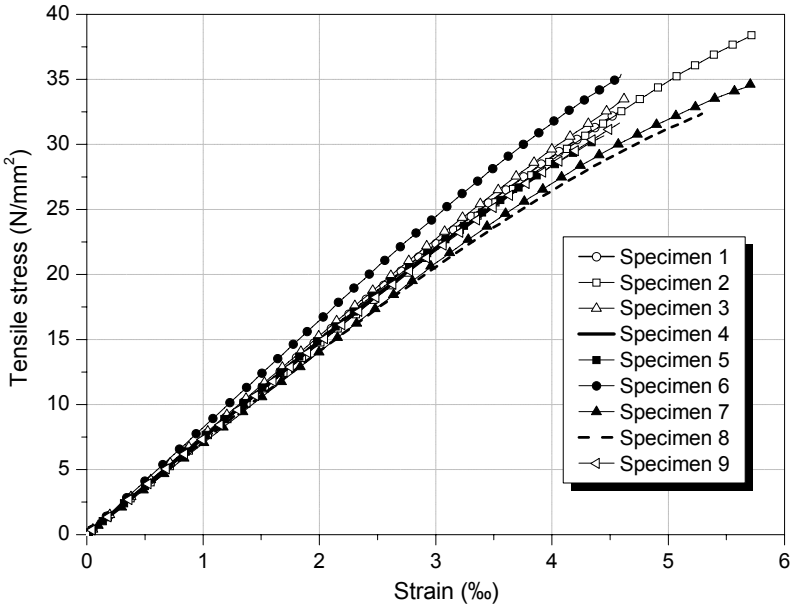

Figure 3.11 *- Tensile stress-strain curves for the MBrace®Resin 220 resin.*

CFRP Laminate

The CFRP laminate was provided in a roll and was produced by S&P® Clever Reinforcement Company (S&P, 2004) and distributed by Bettor MBT® Portugal (BETTOR MBT, 2004), see ***Figure 3.12***. The laminate had the trademark *MBrace Laminado LM* (BETTOR MBT, 2003), and was composed of unidirectional carbon fibres, agglutinated by an epoxy adhesive. According to the supplier, the *MBrace Laminado LM* has the main properties included in ***Table 3.8***.

Twenty measurements of the thickness and the width were carried out to determine the dimensions of the cross-section of the CFRP laminate strip. A thickness of 1.411±0.013 mm and a width of 9.372±0.038 mm were obtained.

To determine the tensile mechanical properties of the CFRP laminate, four tensile tests in coupon specimens (see ***Figure 3.13***) were carried out according to ISO 527-5 (1993) and ASTM 3039 (1993). A testing machine Instron 4208 with 150 mm distance between grips and gauge length of 50 mm (see ***Figure 3.14***) was used. A displacement rate of 2 mm/min was selected for all the tests. The failure tensile stress, failure tensile strain and modulus of elasticity are listed in ***Table 3.9***. The CFRP laminate tensile stress-strain curves are shown in ***Figure 3.15***.

Figure 3.12 *- CFRP laminate packaging, roll of 150 m length.*

Table 3.8 *- Main properties of the "MBrace Laminado LM" (BETTOR MBT, 2003).*

Property	Value
Width (mm)	10
Thickness (mm)	1.4
Tensile strength (N/mm^2)	> 2000
Elasticity modulus (kN/mm^2)	> 150
Ultimate strain (‰)	14

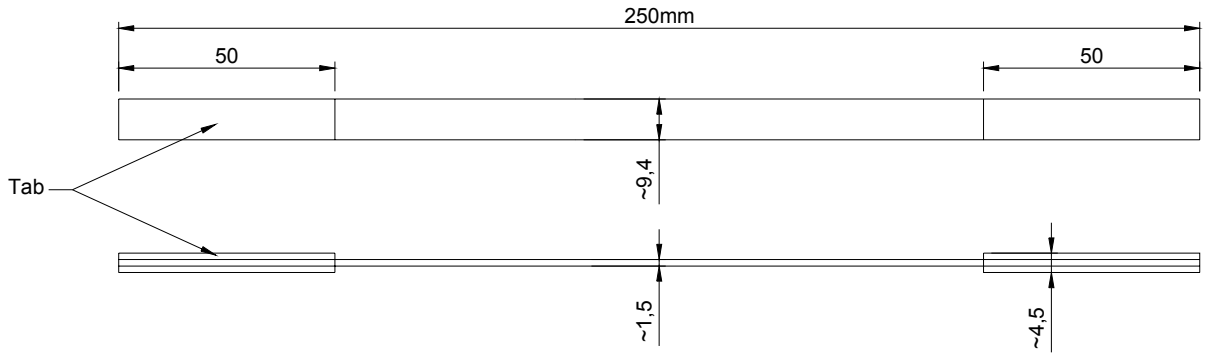

Figure 3.13 *- Test specimen shape and dimensions (type 1B - ISO 527-5, 1993).*

Figure 3.14 *- The Instron 4208 testing machine used in the CFRP tensile tests.*

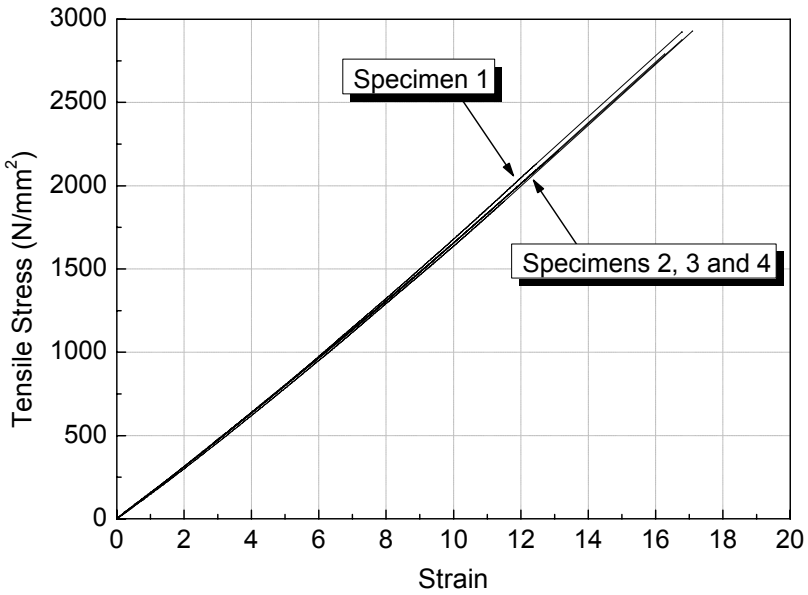

Figure 3.15 *- CFRP laminate tensile stress-strain curves.*

The ultimate tensile strain in ***Table 3.9*** was evaluated using the following equation:

$$\varepsilon_u = \frac{\sigma_u}{E} \tag{3.1}$$

where

ε_u is the ultimate tensile strain;
σ_u is the ultimate tensile stress; and
E is the tensile modulus of elasticity, in accordance with ISO 527-1/5 (1997).

Table 3.9 *- Results of the CFRP laminate tensile tests.*

Specimen	Ultimate tensile stress (N/mm^2)	Ultimate tensile strain (‰)	Modulus of elasticity[a] (kN/mm^2)	Modulus of elasticity[b] (kN/mm^2)
1	2922.10	18.84	155.080	167.740
2	2927.42	19.11	153.150	164.300
3	2876.15	18.12	158.690	165.230
4	2790.86	17.72	157.540	164.820
Average	2879.13	18.45	156.100	165.500
Std. Dev.	63.19 (*2.19%*)	0.64 (*3.49%*)	2.48 (*1.59%*)	1.53 (*0.92%*)

[a] According to ISO 527-1 and ISO 527-5 (1997)
[b] *Tensile Chord Modulus of Elasticity*, according to ACI (2002) and ASTM 3039 (1993)
(*value*) Coefficient of Variation (COV) = (Standard deviation/Average) x 100

Reinforcing Steel

Steel bars of grade 400 with nominal diameter, ϕ_s, of 8 mm, were used for the longitudinal reinforcement of the slabs (CEB-FIP Model Code, 1993). No shear reinforcement was used in the slabs.

Six tension coupons from the ϕ_s = 8 mm conventional reinforcing steel bars were tested to acquire their modulus of elasticity, yield stress and ultimate tensile strength. The coupons were tested in direct tension, using a DARTEC universal testing machine with a load cell of 600 kN capacity and an accuracy better than ± 2% (see ***Figure 3.16***) The samples were loaded at a constant stress rate of 18 N/mm^2 s^{-1}. The bar elongation was measured using a clip-gauge of 100 mm gage length. The tensile tests were conducted according to the standard procedures found in ASTM A 370 (2002) and EN 10 002-1 (1990).

Figure 3.16 *- The testing machine used in the steel bar tensile tests.*

The six obtained stress-strain curves are depicted in ***Figure 3.17***. The mechanical properties of the steel reinforcing bars, evaluated from the direct tensile tests, are reported in ***Table 3.10***. The results of the six tests were almost identical, and all tests exceeded the specified yield strength of 400 N/mm^2. All stress-strain curves showed a linear elastic behavior up to a yield stress of about 470 N/mm^2 and strain of 2.38 ‰. This tested yield strain was slightly higher than the expected yield strain of 2.35 - 2.24 ‰. This results in a tested elastic modulus of about 200 kN/mm^2, which is equals to the lower limit of the range that is typically used for steel reinforcement (200 - 210 kN/mm^2). Above the yield plateau, the steel experienced strain hardening up to the ultimate strength. The clip-gauge was removed at a strain of approximately 50 ‰ to protect it from damage.

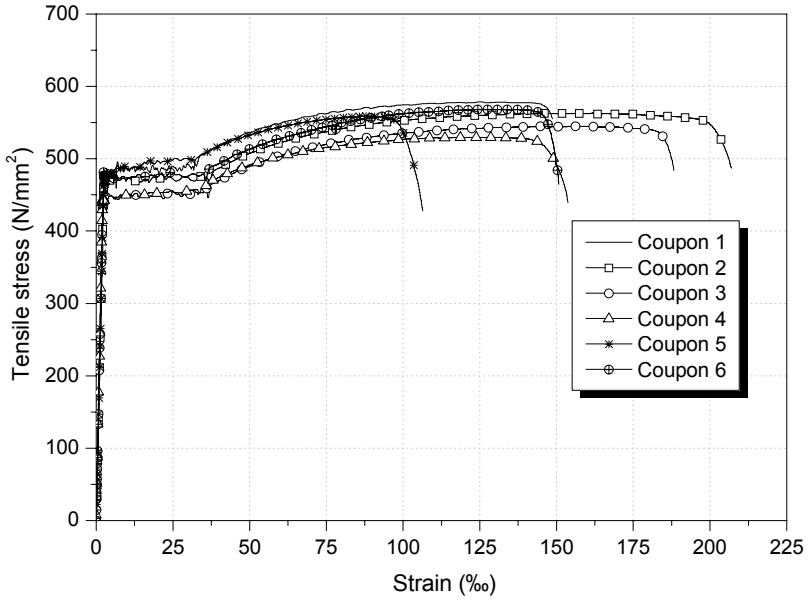

Figure 3.17 *- Stress-strain diagram of reinforcing steel.*

Table 3.10 *- Steel bars mechanical properties evaluated from the direct tensile tests.*

Sample	Modulus of elasticity (kN/mm^2)	Yield strength (0.2 %)[a] (N/mm^2)	Strain at yield stress[b]	Tensile strength (N/mm^2)
1	183.582	479.03	0.0028	578.75
2	191.344	470.38	0.0027	563.27
3	212.478	450.34	0.0024	544.60
4	216.988	442.60	0.0022	529.58
5	195.258	475.39	0.0026	558.72
6	202.256	476.75	0.0026	567.83
Average	200.318	465.75	0.0025	557.12
Std.Dev.	*12.77* (*6.38%*)	15.40 (*3.31%*)	0.0002 (*8.19%*)	17.54 (*3.15%*)

[a] Yield strength determinated by the "*Offset Method*", according to ASTM 370 (2002)
[b] Strain at yield point, for the 0.2 % offset stress
(*value*) Coefficient of Variation (COV) = (Standard deviation/Average) x 100

4 Preparation of the Slab Specimens

Eight reinforced concrete slabs strips of 300 mm x 1965 mm, with 80 mm thickness, were cast at distinct periods from different concrete mixes. For each concrete batch, four cylindrical concrete specimens, of 150 mm diameter and 300 mm depth, and three beams of 100 mm x 100 mm cross section and 850 mm length, were cast. The slabs, cylinders and beams moulds used are shown in ***Figure 4.1****(a)*. For each concrete batch, each slab, cylinder and beam specimen was cast in two layers, each one vibrated using an electrical concrete poker vibrator with a 25 mm tip and 50 Hz frequency, see ***Figure 4.1****(b)*.

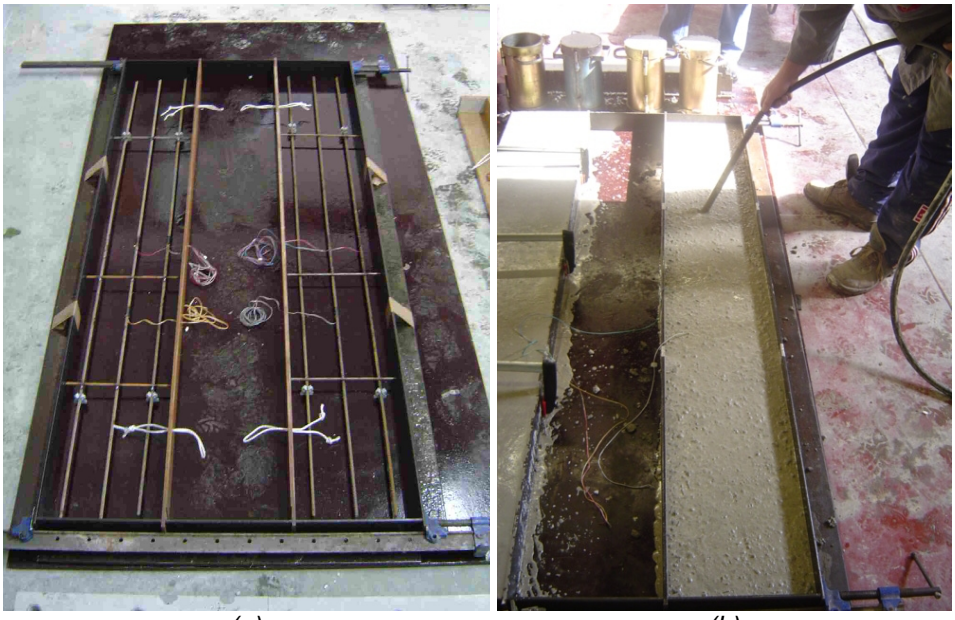

(a) *(b)*

Figure 4.1 *- Slab strips, cylinders and beam specimens: (a) formwork set up and moulds used, and (b) plain concrete consolidation.*

A detail of one strain gauge installed on a reinforcing bar, the bar plastic support used to set the bar correctly, and the constructive reinforcement ϕ3 mm is shown in ***Figure 4.2***.

After the slabs, the cylinder, and beam concrete specimens have been cast, their top surfaces were finished manually using a smooth plastic float and were covered with wet burlap sacks. The burlap sacks were monitored and kept wet for two days (see ***Figure 4.3***). After this curing period, the slabs, the cylinder and the beam specimens were removed from the moulds and maintained in natural laboratory environmental conditions up to 28 days.

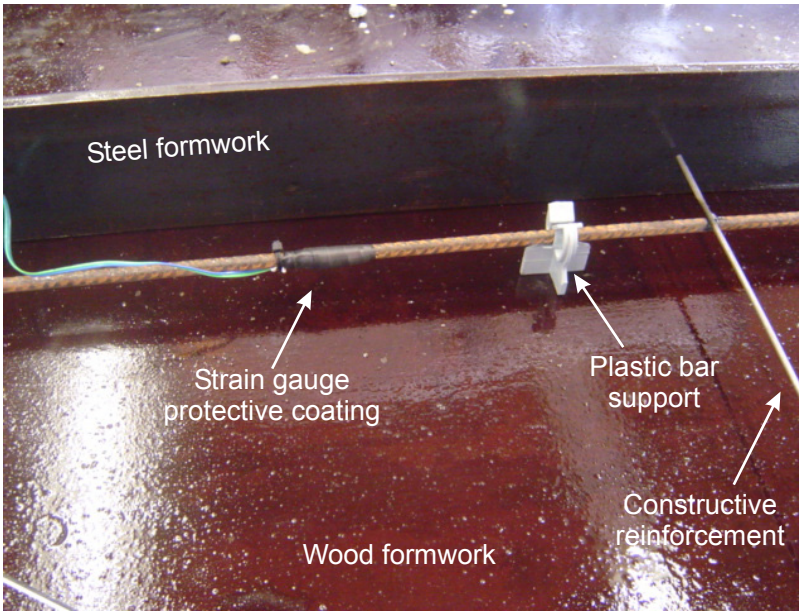

Figure 4.2 *- Detail of the strain gauge at the steel bar, bar plastic support and constructive reinforcement.*

(a) *(b)*

Figure 4.3 *- Curing with water-retaining covering (a), and final aspect of the specimens (b).*

5 Strengthening Steps

The procedures of the hybrid strengthening technique are described in this chapter.

NSM Strengthening Technique

When the concrete slabs attained approximately 28 days of age, the slab specimens to be strengthened were placed outside the laboratory and the grooves were made using a Hilti diamond saw cutter machine, model DC 230-S (HILTI, 2004), see ***Figure 5.1***. The slits had about 4.5 mm width and 15 mm depth on the concrete cover of the slab's surface that will be in tension.

(a) *(b)*

Figure 5.1 *- Making the slits (a), and diamond saw cutter machine detail (b).*

In order to eliminate the dust resultant from the sawing process, the slits were cleaned with compressed air before bonding the laminate strips to the concrete into to slits (***Figure 5.2***). The CFRP laminates were cleaned with acetone to remove any possible dirt.

Figure 5.3 shows an overview before installing the CFRP laminates into the slits. The laminate strips were fixed to the concrete slits using the aforementioned epoxy adhesive (Section "CFRP-Concrete Bond Product"). The slits were filled with the epoxy adhesive using a spatula, and the CFRP laminates were then introduced into the slits (***Figure 5.4***).

Figure 5.2 *- Cleaning the slits using compressed air.*

Figure 5.3 *- A specimen before being strengthened; the adhesive compound recipients; the acetone bottle; the CFRP laminate strips; and the tools used to mix and to apply the epoxy adhesive into the slits.*

SFRC Overlay Strengthening

The slab specimens to be overlaid were placed outside of the laboratory and the top surface was sandblasted, see ***Figure 5.5***. To ensure good adhesion between new concrete overlay and the old concrete, a fast layer should be removed up to get aggregates uncovered. Therefore, the surface preparation technique of sandblasting the old concrete was employed.

(a) *(b)* *(c)* *(d)*

Figure 5.4 *- NSM application procedure: Mixing the thixotropic epoxy adhesive (a), detail of the strain gauges at the CFRP laminate (b), filling the slit with epoxy (c), and placing the CFRP laminate (d).*

To eliminate the dust resultant from the sandblasting process, before applying the bond product, the top surface of the specimen was cleaned with compressed air (***Figure 5.6***).

Figure 5.5 *- Sandblasting the top surface specimen.*

Figure 5.6 *- Cleaning the sandblasted surface with compressed air jet.*

The SFRC overlay was bonded to the concrete slab sandblasted surface using the epoxy adhesive indicated in Section “Overlay Bond Product”. The main bond steps are shown in ***Figure 5.7***. An overview before applying the bond product and the freshly SFRC is shown in ***Figure 5.7****(a)*. The bond product was spread over the substrate top surface with a spatula ***Figure 5.7****(b,c)*. The fresh concrete overlay was cast as is illustrated in ***Figure 5.7****(d)*. A mini slipform showed in ***Figure 5.8****(a,b)* was used to consolidate the thin SFRC overlay and beam SFRC specimens. The mini slipform intends to simulate the real conditions of compaction of a thin SFRC overlay. The SFRC beam specimens were cast in three layers (about 50 mm thickness) and each one was consolidated using the mini slipform. The SFRC cylinder specimens were cast in two layers, each one consolidated using a vibratory compaction table during about 5 seconds.

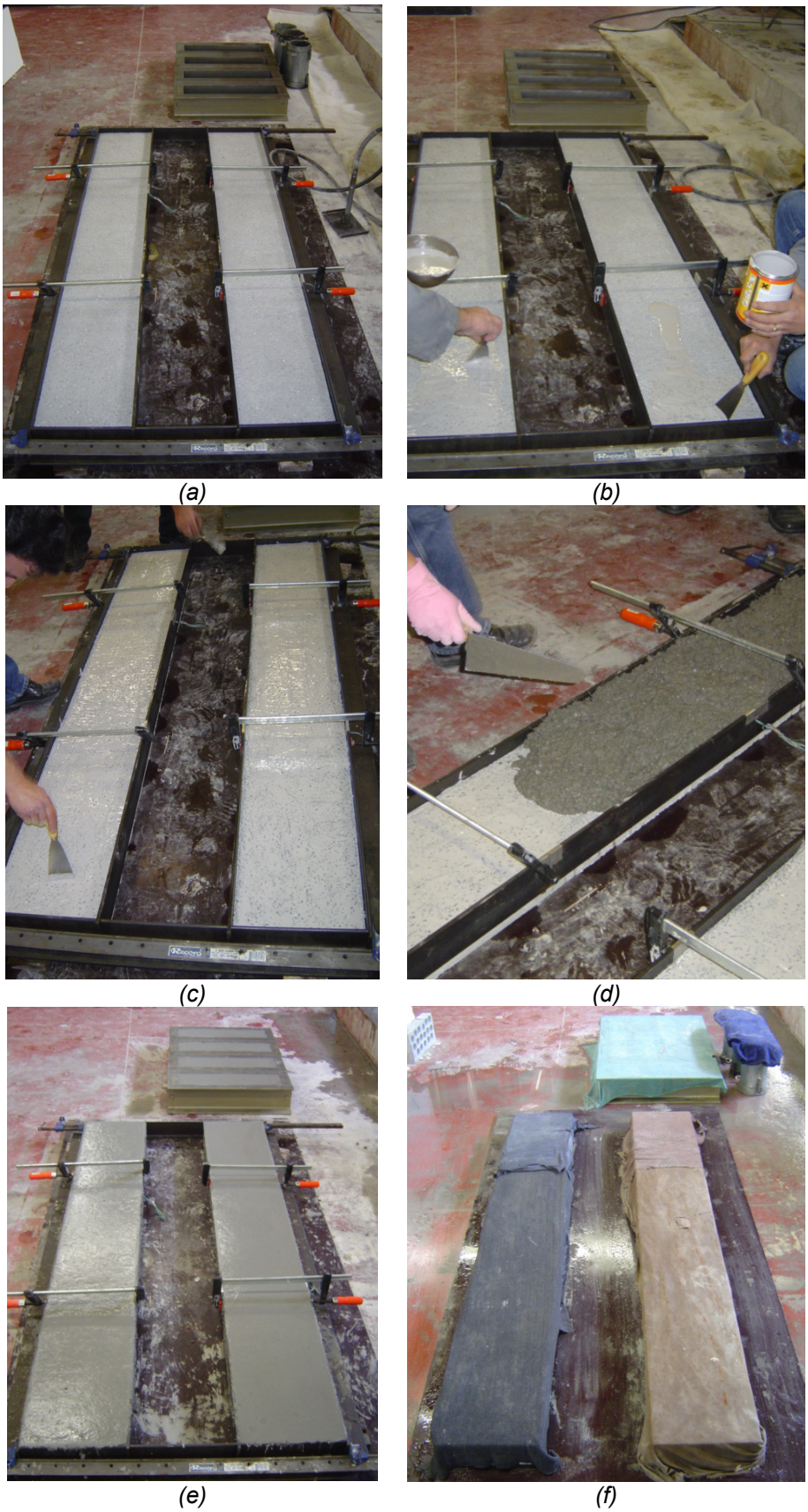

Figure 5.7 *- Overview of the specimens and the moulds before applying the SFRC overlay: (a) formwork set up and moulds used, (b, c) applying overlay bond product, (d) placing fresh SFRC overlay, (e) final aspect of the finished surface (f) curing with wet burlap.*

The work of bonding the fresh SFRC overlay to the hardened concrete followed the manufactures specifications (SIKA, 2002) and the ACI guidelines (ACI 503.2-92, ACI 503.5R-92 and ACI 503.6R-97). In the present experimental program, an overlay thickness of approximately 30 mm of SFRC layer was adopted.

For each SFRC batch, three cylinder concrete specimens (150mm x 300mm) and four beams (150 mm x 150 mm, with 600 mm length) were cast and tested at the testing age of the slab. The curing process adopted for the plain concrete was also used for the thin bonded SFRC overlay, cylinder and beam SFRC specimens (see ***Figure 5.7****(f)*).

(a) *(b)*

Figure 5.8 *- SFRC consolidation with a mini slipform: (a) SFRC overlay, and (b) beam specimens.*

6 Results

The notation adopted to identify each slab specimen is: **SLxSO**, where:

SL = slab strip base;
x = slab specimen number (1 to 8);
S = strengthened with CRFP laminates (if this is the case); and
O = slab overlaid with SFRC layer (if this is the case).

Therefore, the slab with signature SL7SO refers to the slab specimen number 7, strengthened with CFRP laminates in the tensile zone and overlaid with 30 mm thickness SFRC in the compressive zone.

Reference Slabs

- The SL1 unstrengthened slab strip is shown in ***Figures 6.1***, before and after having been tested. The mid-span deflection, steel reinforcement strain and concrete strain are shown in ***Figures 6.2***, ***6.3*** and ***6.4***, respectively.

(a) (b)

Figure 6.1 *- Specimen SL1 before (a), and after having been tested (b).*

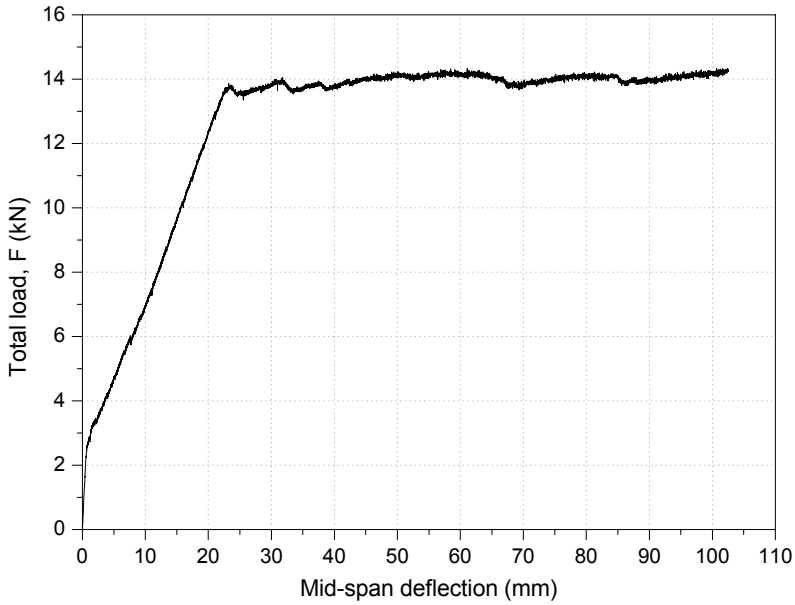

Figure 6.2 *- Relationship between applied load and deflection at mid-span of the slab SL1.*

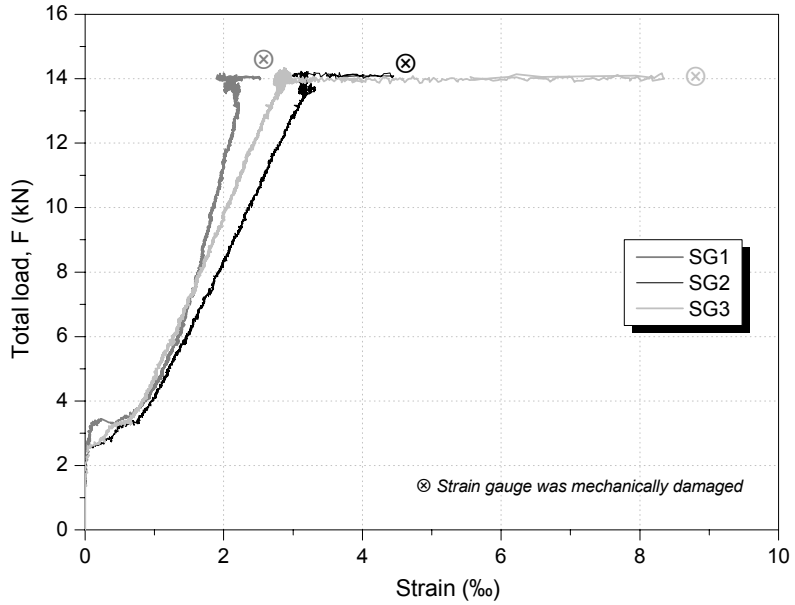

Figure 6.3 *- Relationship between applied load and tensile strain of the steel reinforcement for the slab SL1 (refer to* ***Figure 2.2****(c)).*

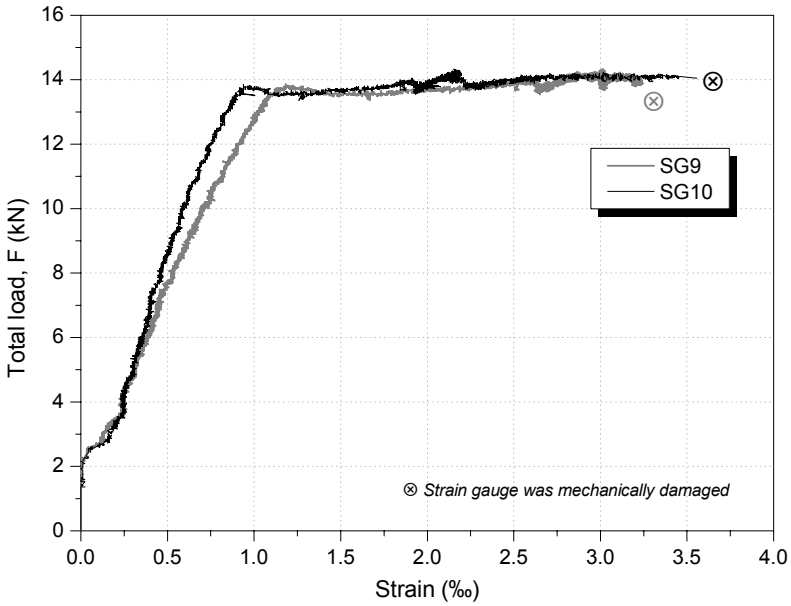

Figure 6.4 *- Relationship between applied load and compressive strain of the concrete at top surface for the slab SL1 (refer to* ***Figure 2.2****(d)).*

- The SL2 unstrengthened slab strip is shown in ***Figures 6.5***, before and after having been tested. The mid-span deflection, steel reinforcement strain and concrete strain are shown in ***Figures 6.6***, ***6.7*** and ***6.8***, respectively.

(a) *(b)*

Figure 6.5 *- Specimen SL2 before (a), and after having been tested (b).*

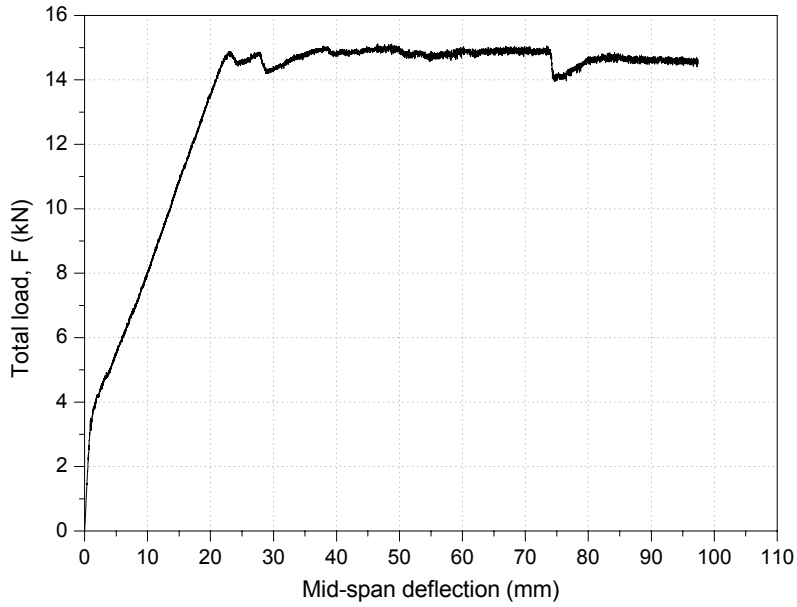

Figure 6.6 *- Relationship between applied load and deflection at mid-span of the slab SL2.*

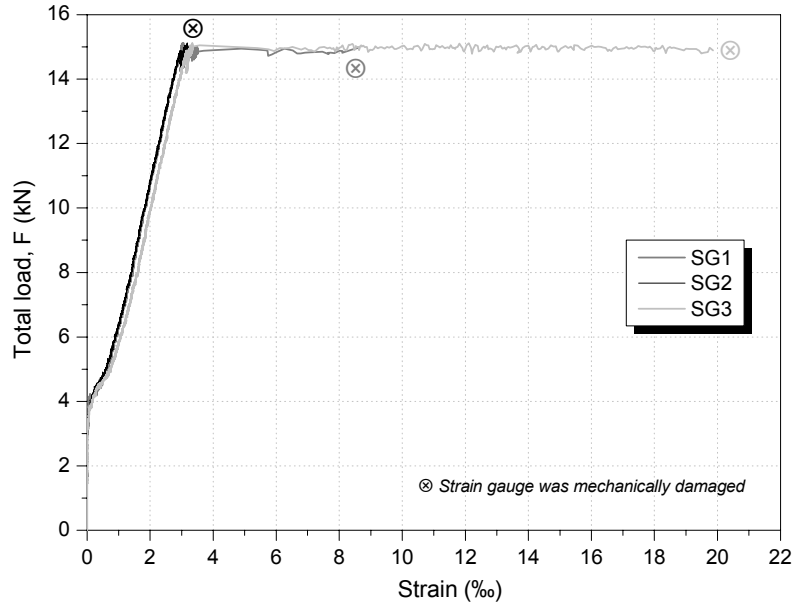

Figure 6.7 *- Relationship between applied load and tensile strain of the steel reinforcement for the slab SL2 (refer to* ***Figure 2.2****(c)).*

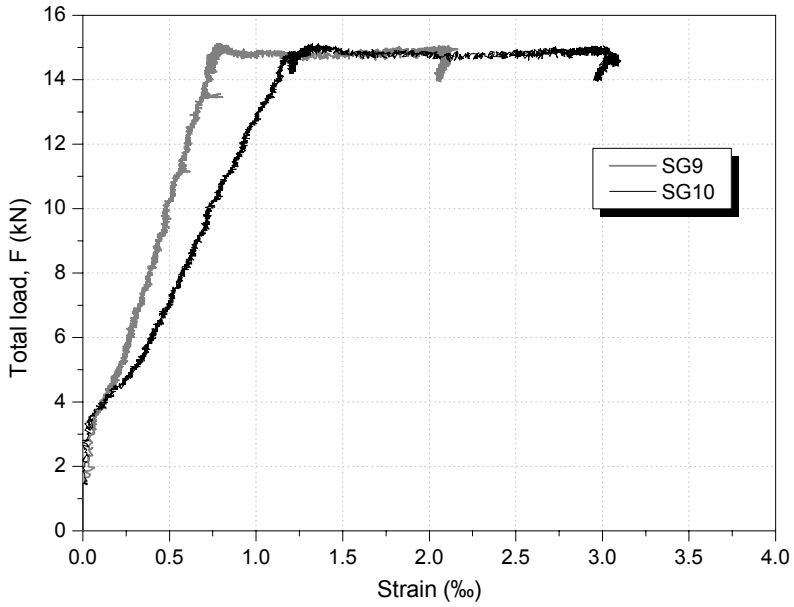

Figure 6.8 *- Relationship between applied load and compressive strain of the concrete at top surface for the slab SL2 (refer to* ***Figure 2.2****(d)).*

The bottom appearance of the unstrengthened slabs after having been tested is shown in ***Figure 6.9***.

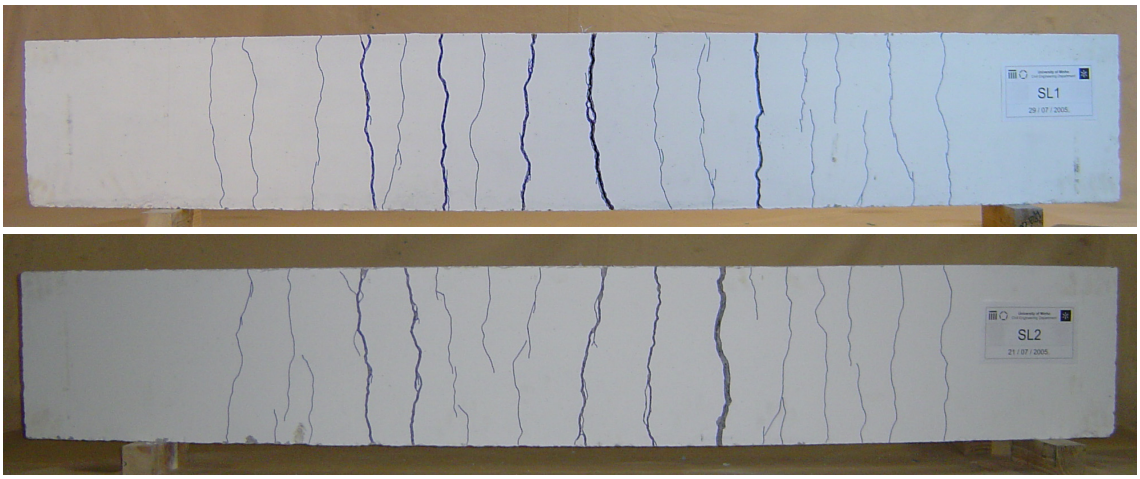

(a)

(b)

Figure 6.9 *- Crack pattern in reference slabs: (a) SL1, and (b) SL2.*

Slabs Strengthened with CFRP Laminate

- ***Figure 6.10*** shows the NSM CFRP strengthened SL3S slab strip before and after having been tested. The mid-span deflection, concrete strain and CFRP laminate strain are shown in ***Figures 6.11***, ***6.12*** and ***6.13***[§], respectively.

[§] **It was not possible to record data of the steel reinforcement strain gauge instrumentation for the slab strip SL3S**

(a) (b)

Figure 6.10 *- Specimen SL3S before (a), and after having been tested (b).*

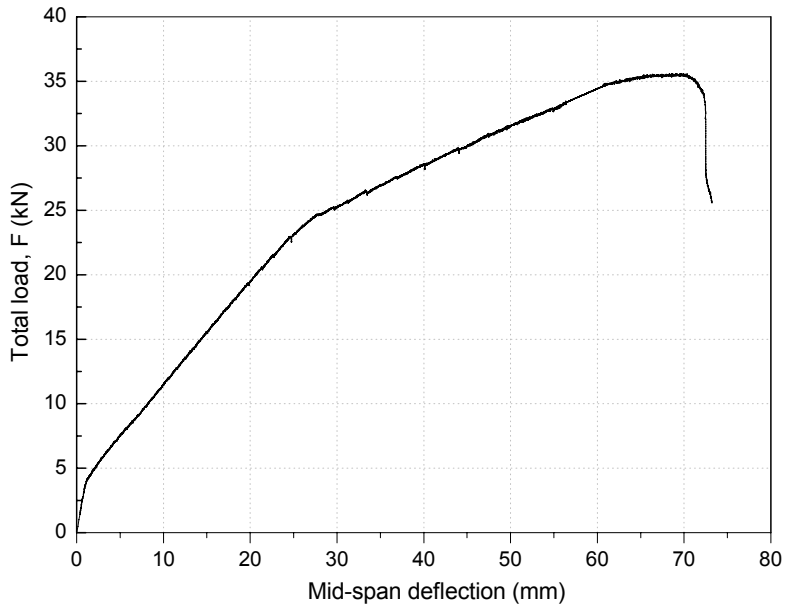

Figure 6.11 *- Relationship between applied load and deflection at mid-span of the slab SL3S.*

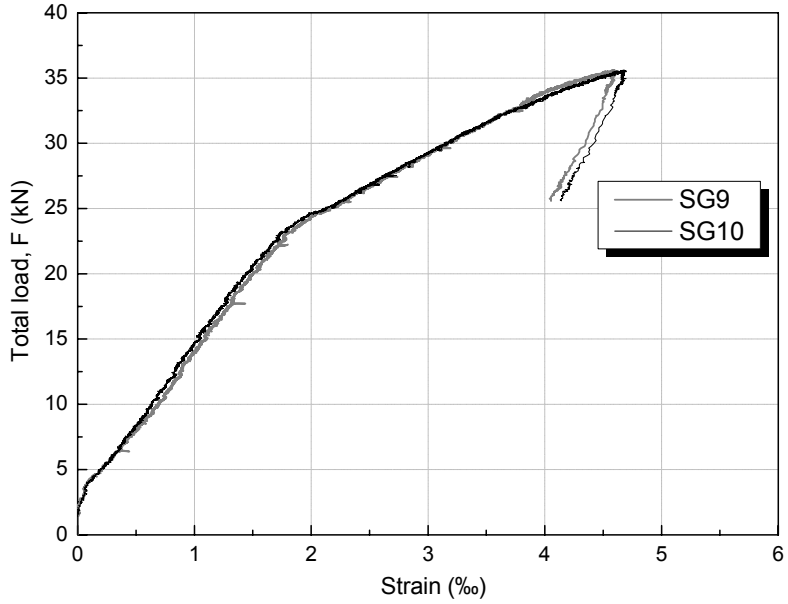

Figure 6.12 *- Relationship between applied load and compressive strain of the concrete at top surface for the slab SL3S (refer to* ***Figure 2.2****(d)).*

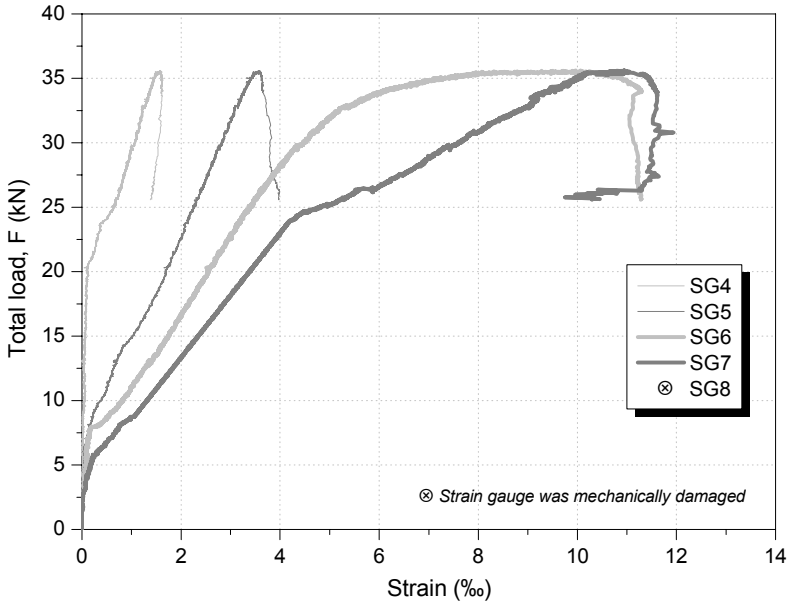

Figure 6.13 *- Relationship between applied load and tensile strain of the CFRP laminate for the slab SL3S[§] (refer to* ***Figure 2.2****(b,c)).*

[§] It was not possible to record the data of the SG8

- ***Figure 6.14*** shows the NSM CFRP strengthened SL4S slab strip before and after having been tested. The mid-span deflection is shown in ***Figures 6.15***.

(a) *(b)*

Figure 6.14 *- Specimen SL4S before (a), and after having been tested (b).*

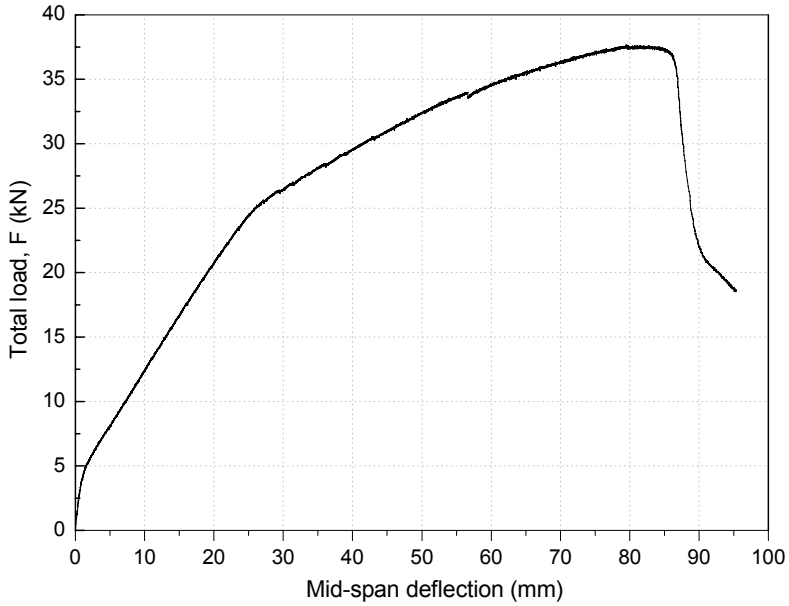

Figure 6.15 *- Relationship between applied load and deflection at mid-span of the slab SL4S.*

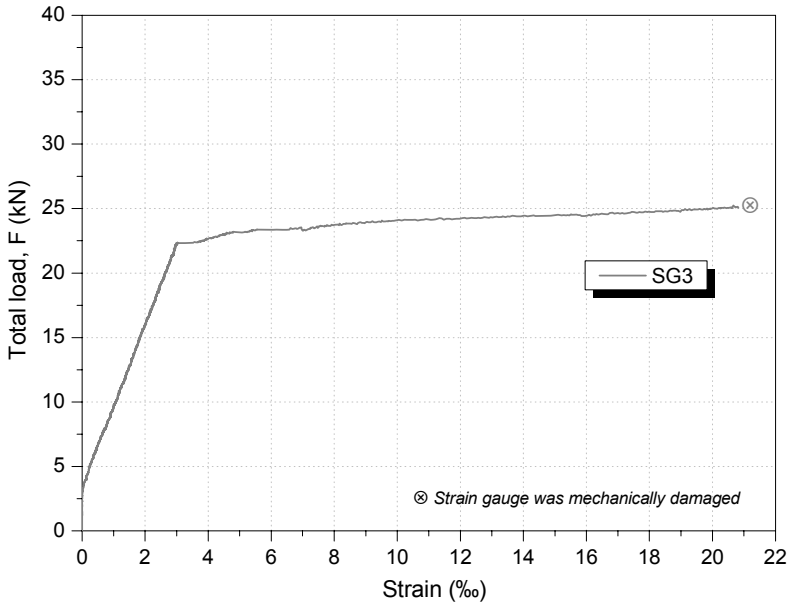

Figure 6.16 *- Relationship between applied load and tensile strain of the steel reinforcement for the slab SL4S[§] (refer to* ***Figure 2.2****(c)).*

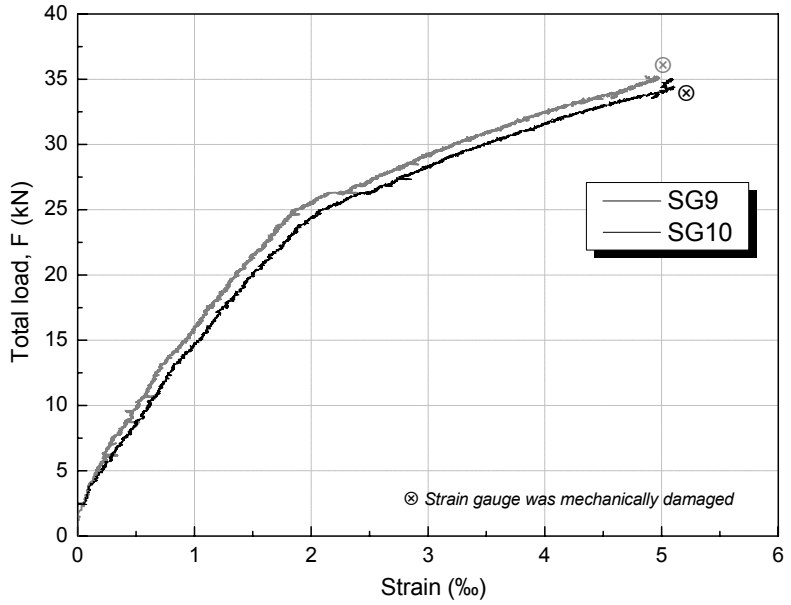

Figure 6.17 *- Relationship between applied load and compressive strain of the concrete at top surface for the slab SL4S (refer to* ***Figure 2.2****(d)).*

[§] It was not possible to record the data of the SG1 and SG2

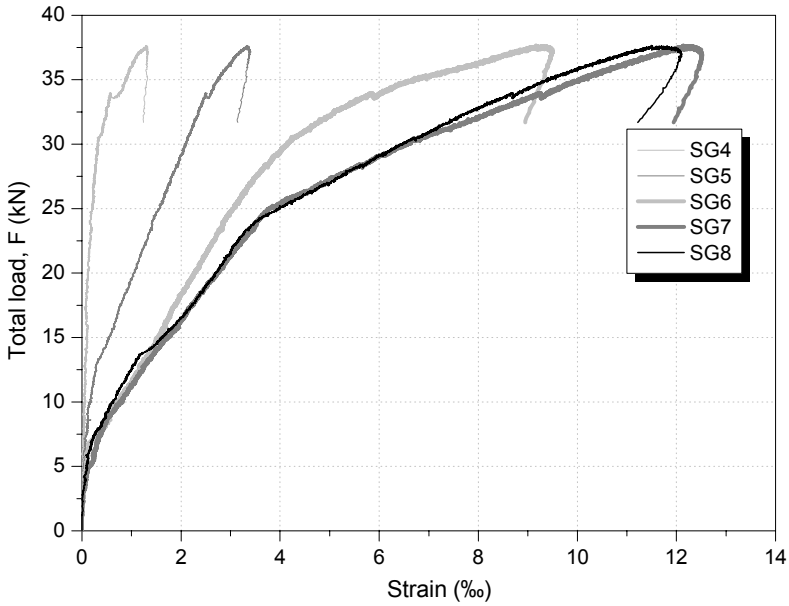

Figure 6.18 *- Relationship between applied load and tensile strain of the CFRP laminate for the slab SL4S (refer to* ***Figure 2.2****(b,c)).*

The bottom appearance of the slabs strengthened with CFRP laminates after having been tested is shown in ***Figure 6.19***.

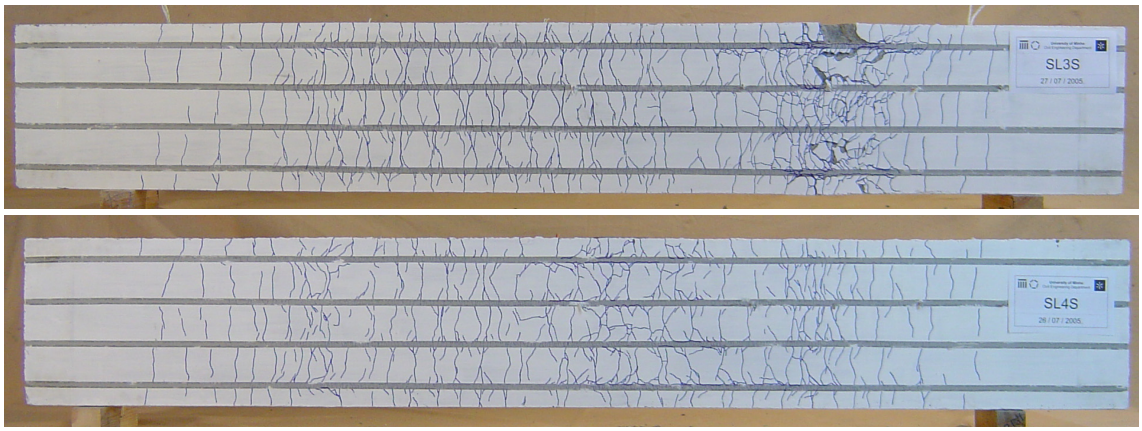

(a)

(b)

Figure 6.19 *- Crack pattern in CFRP strengthened slabs: (a) SL3S and (b) SL4S.*

Slabs Strengthened with CFRP Laminate and SFRC Overlay

- SL5SO is a slab strip strengthened by combining CFRP laminates, applied according to the NSM technique, and a SFRC compression overlay. ***Figures 6.20*** shows the SL5SO slab strip before and after having been tested The mid-span deflection, steel reinforcement strain, concrete strain and CFRP laminate strain are shown in ***Figures 6.21***, ***6.22***, ***6.23*** and ***6.24***, respectively.

(a) (b)

Figure 6.20 *- Specimen SL5SO before (a), and after having been tested (b).*

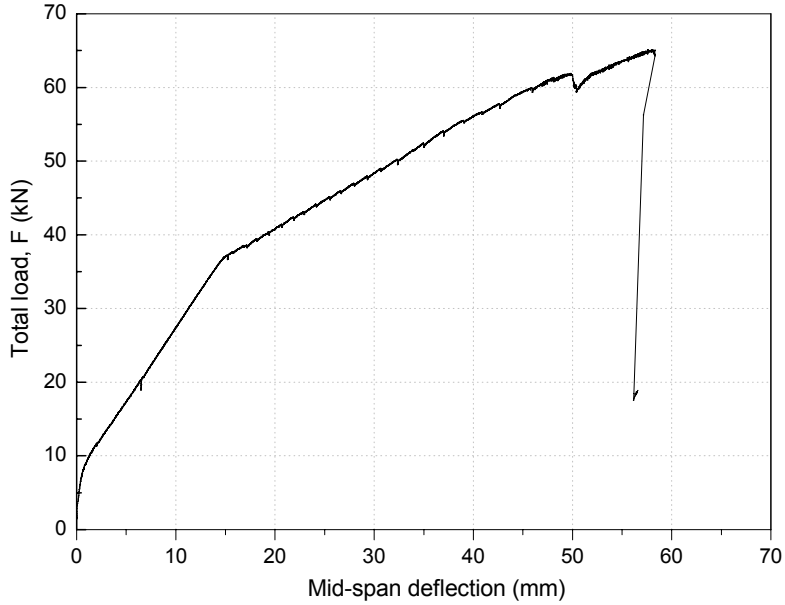

Figure 6.21 *- Relationship between applied load and deflection at mid-span of the slab SL5SO.*

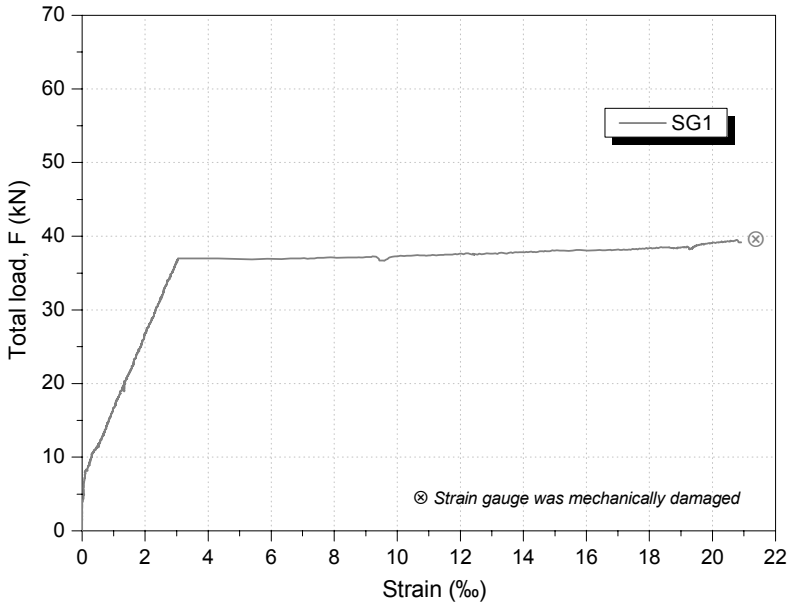

Figure 6.22 *- Relationship between applied load and tensile strain of the steel reinforcement for the slab SL5SO[§] (refer to* ***Figure 2.2****(c)).*

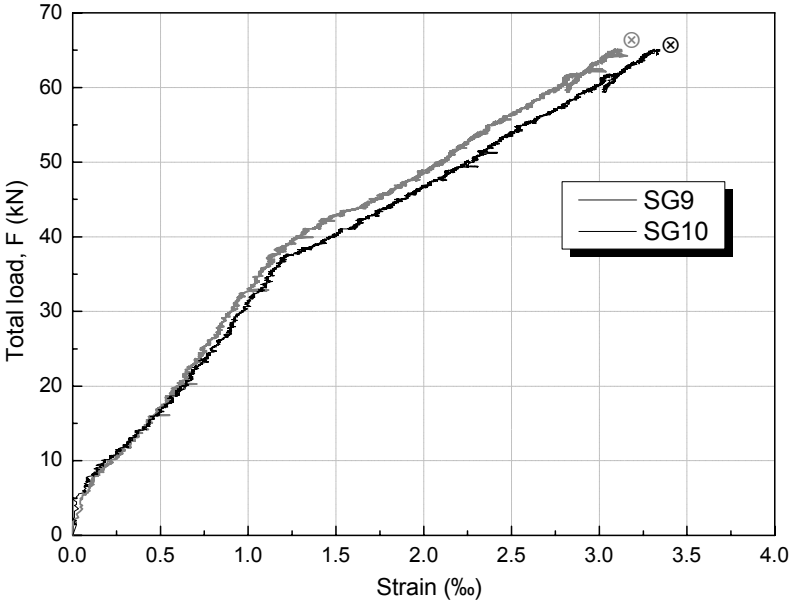

Figure 6.23 *- Relationship between applied load and compressive strain of the concrete at top surface for the slab SL5SO (refer to* ***Figure 2.2****(d)).*

[§] It was not possible to record the data of the SG2 and SG3

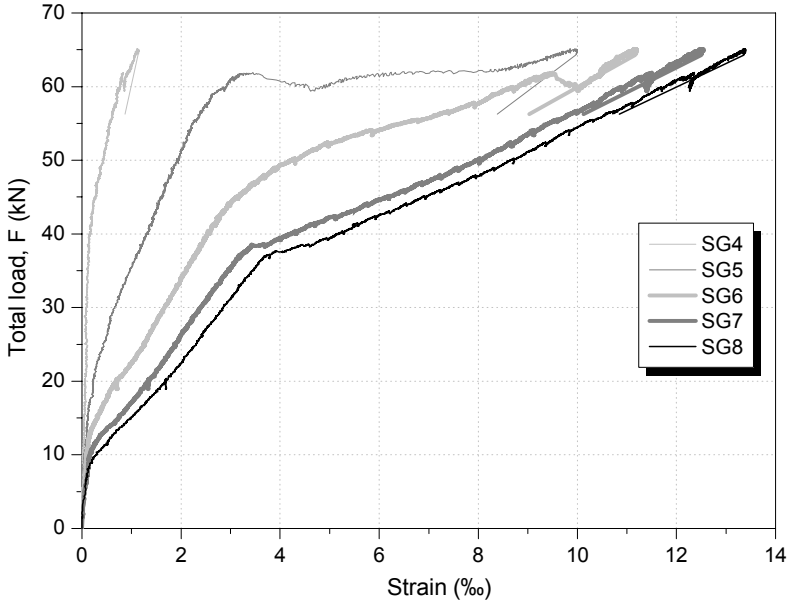

Figure 6.24 *- Relationship between applied load and tensile strain of the CFRP laminate for the slab SL5SO (refer to* ***Figure 2.2****(b,c)).*

- SL6SO is a slab strip strengthened by combining CFRP laminates, applied according to the NSM technique, and a SFRC compression overlay. ***Figures 6.25*** shows the SL6SO slab strip before and after having been tested The mid-span deflection, steel reinforcement strain, concrete strain and CFRP laminate strain are shown in ***Figures 6.26***, ***6.27***, ***6.28*** and ***6.29***, respectively.

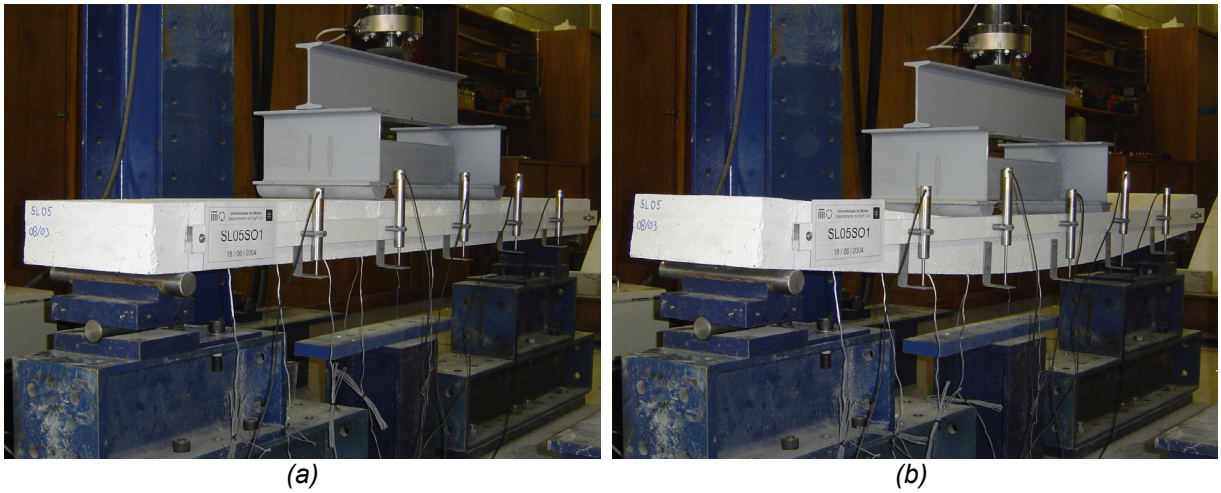

(a) *(b)*

Figure 6.25 *- Specimen SL6SO before (a), and after having been tested (b).*

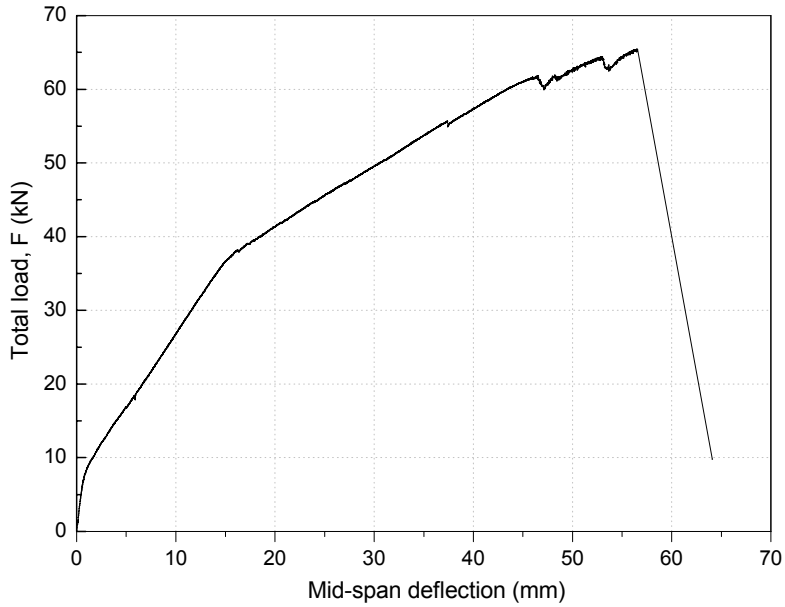

Figure 6.26 *- Relationship between applied load and deflection at mid-span of the slab SL6SO.*

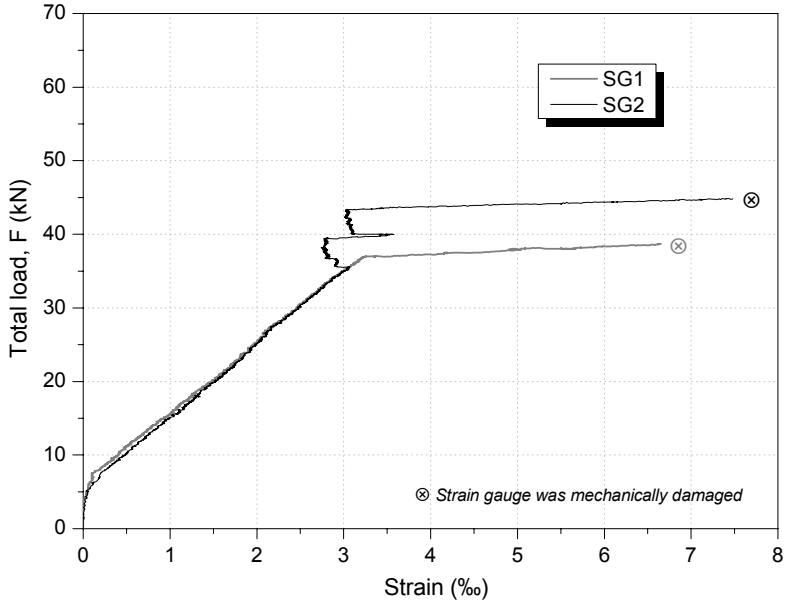

Figure 6.27 *- Relationship between applied load and tensile strain of the steel reinforcement for the slab SL6SO[§] (refer to* ***Figure 2.2****(c)).*

[§] It was not possible to record the data of the SG3

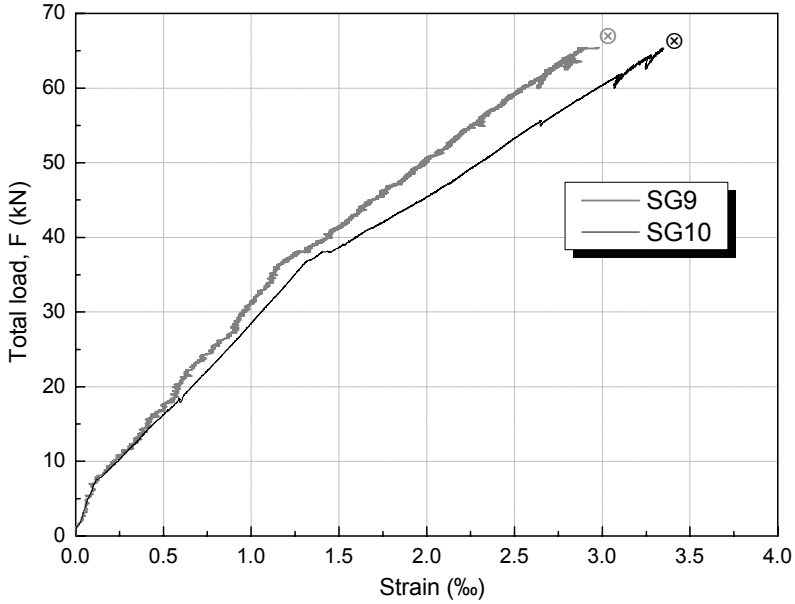

Figure 6.28 *- Relationship between applied load and compressive strain of the concrete at top surface for the slab SL6SO (refer to* ***Figure 2.2****(d)).*

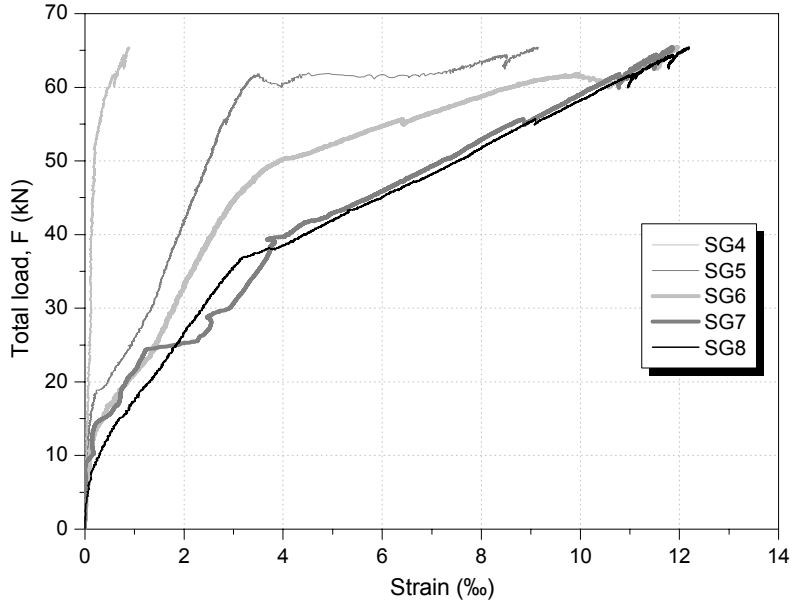

Figure 6.29 *- Relationship between applied load and tensile strain of the CFRP laminate for the slab SL6SO (refer to* ***Figure 2.2****(b,c)).*

- SL7SO is a slab strip strengthened by combining CFRP laminates, applied according to the NSM technique, and a SFRC compression overlay. ***Figures 6.30*** shows the SL7SO slab strip before and after having been tested The mid-span deflection, steel reinforcement strain, concrete strain and CFRP laminate strain are shown in ***Figures 6.31***, ***6.32***, ***6.33*** and ***6.34***, respectively.

(a) *(b)*

Figure 6.30 *- Specimen SL7SO before (a), and after having been tested (b).*

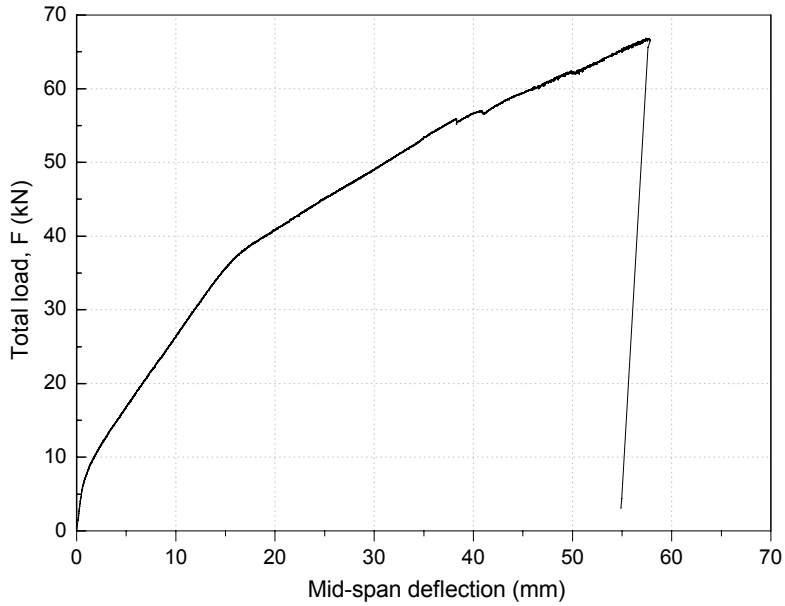

Figure 6.31 *- Relationship between applied load and deflection at mid-span of the slab SL7SO.*

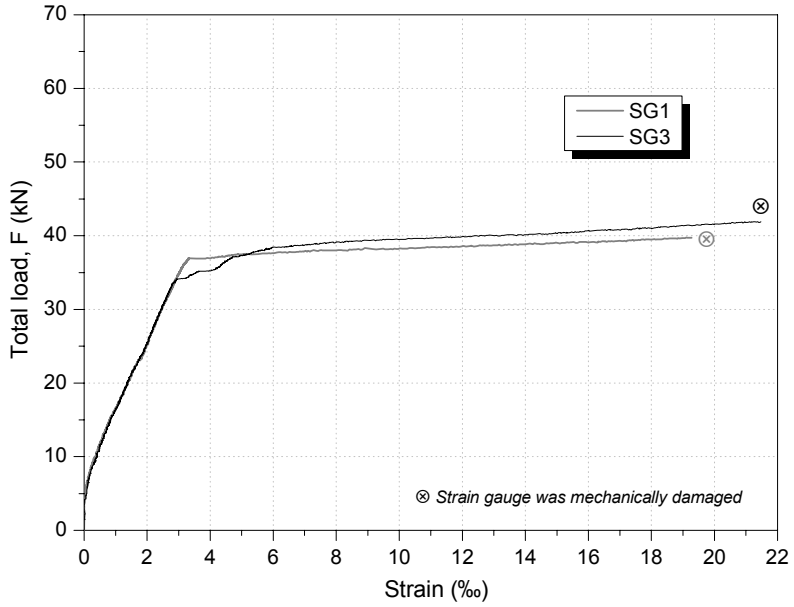

Figure 6.32 *- Relationship between applied load and tensile strain behaviour of the steel reinforcement for the slab SL7SO[§] (refer to* ***Figure 2.2****(c)).*

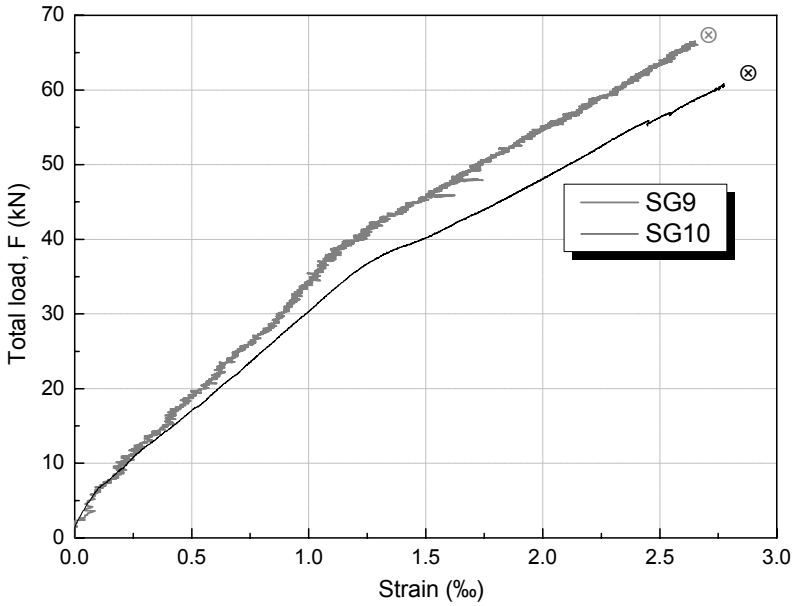

Figure 6.33 *- Relationship between applied load and compressive strain of the concrete at top surface for the slab SL7SO (refer to* ***Figure 2.2****(d)).*

[§] It was not possible to record the data of the SG2

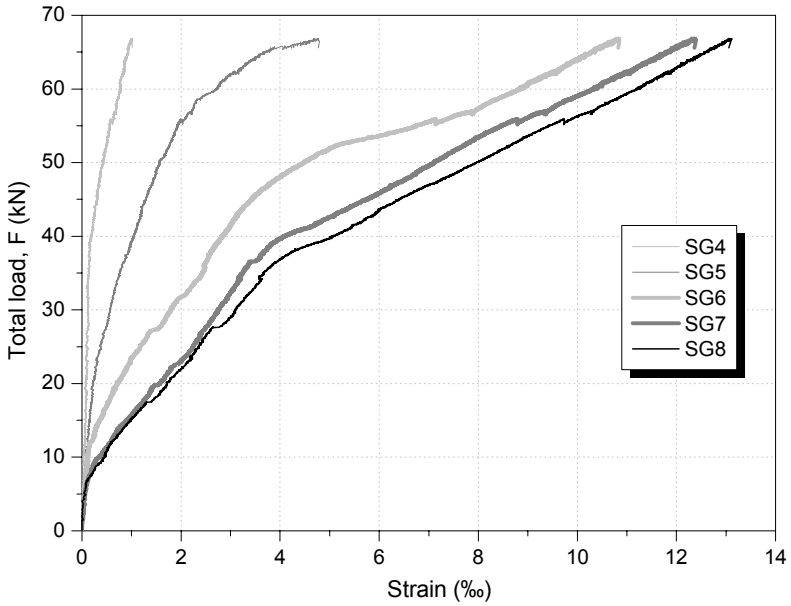

Figure 6.34 *- Relationship between applied load and tensile strain of the CFRP laminate for the slab SL7SO (refer to* ***Figure 2.2****(b,c))..*

- ***Figure 6.35*** shows the NSM CFRP strengthened SL8SO slab strip before and after having been tested. The mid-span deflection, steel reinforcement strain, concrete strain and CFRP laminate strain are shown in ***Figures 6.36***, ***6.37***, ***6.38*** and ***6.39***, respectively.

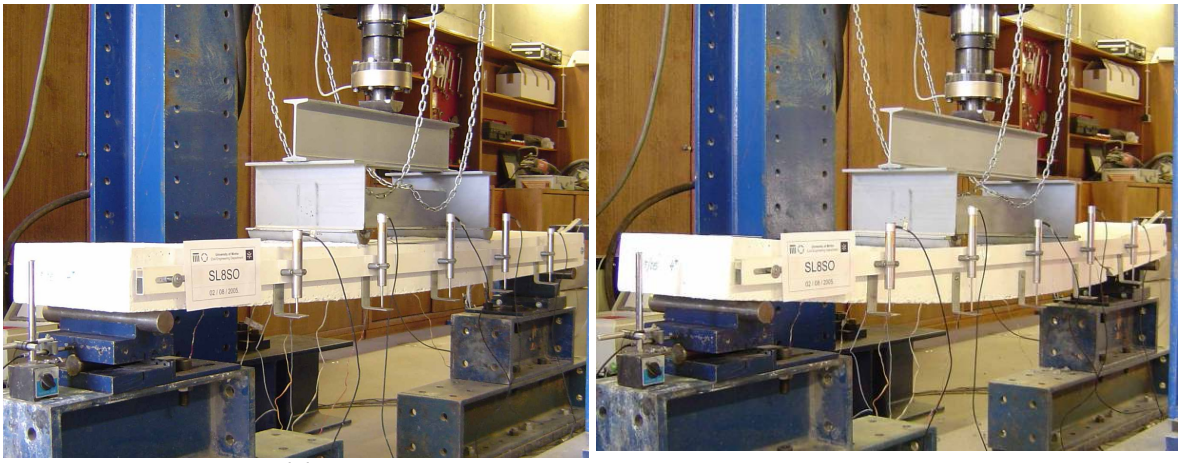

(a) *(b)*

Figure 6.35 *- Specimen SL8SO before (a), and after having been tested (b).*

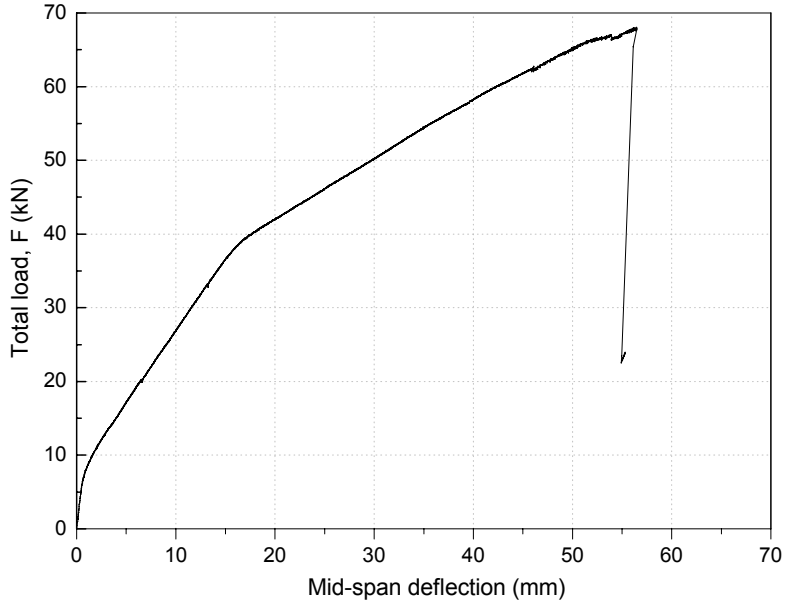

Figure 6.36 *- Relationship between applied load and deflection at mid-span of the slab SL8SO.*

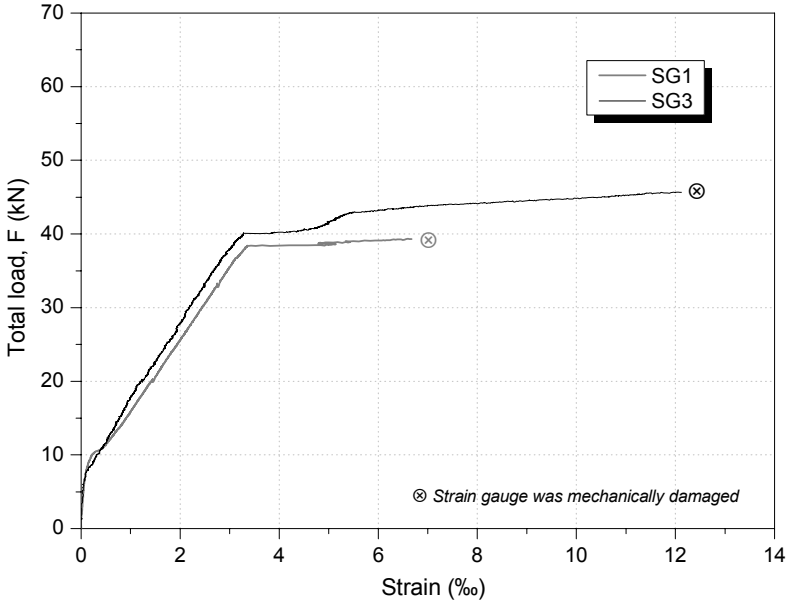

Figure 6.37 *- Relationship between applied load and tensile strain of the steel reinforcement for the slab SL8SO[§] (refer to* ***Figure 2.2****(c)).*

[§] It was not possible to record the data of the SG2

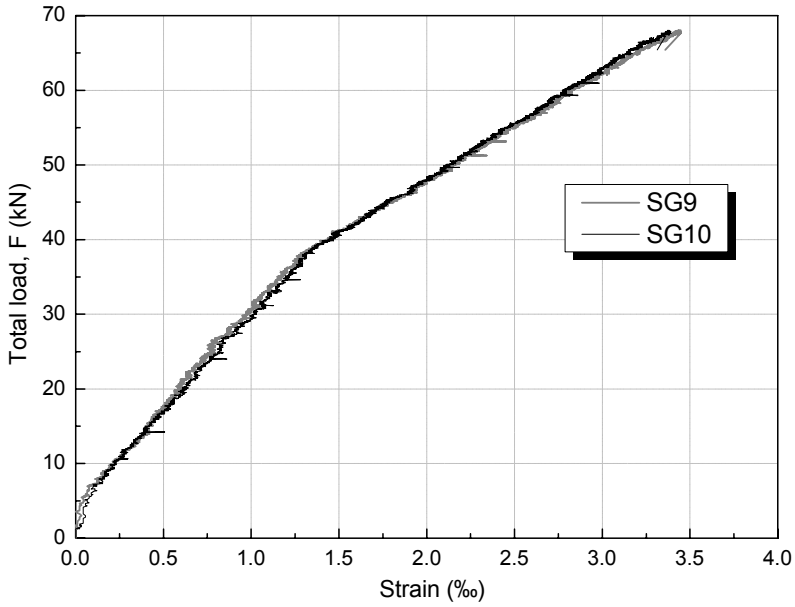

Figure 6.38 *- Relationship between applied load and compressive strain of the concrete at top surface for the slab SL8SO (refer to* ***Figure 2.2****(d)).*

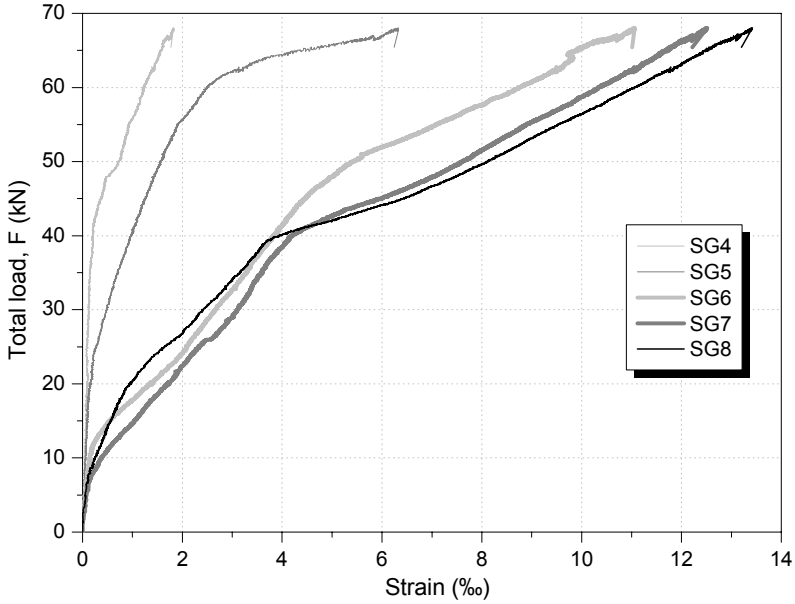

Figure 6.39 *- Relationship between applied load and tensile strain of the CFRP laminate for the slab SL8SO (refer to* ***Figure 2.2****(b,c)).*

The bottom appearance of the slabs strengthened with CFRP laminate and SFRC overlay after having been tested is shown in ***Figure 6.40***.

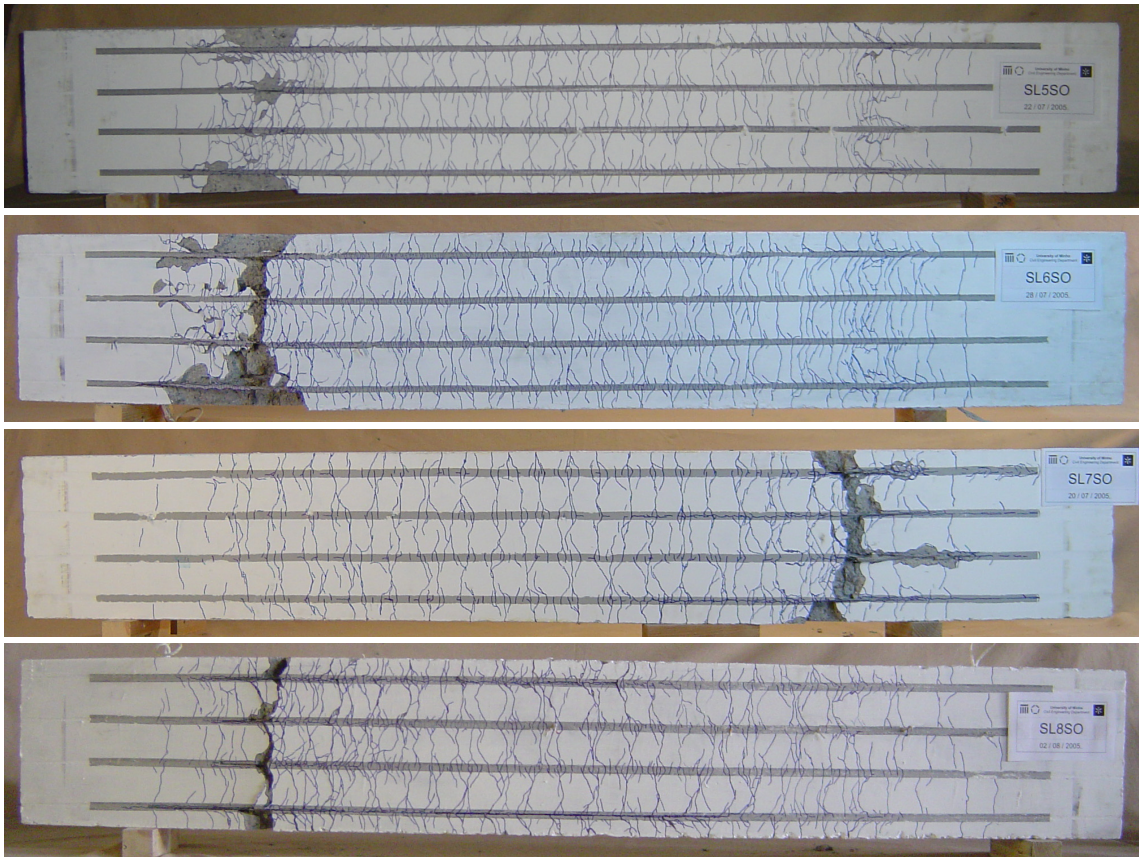

Figure 6.40 *- Crack pattern in CFRP strengthened and SFRC overlaid slabs: (a) SL5SO, (b) SL6SO, (c) SL7SO and (d) SL8SO.*

7 Analyses of Results

The analysis of the results of the eight tested slabs is presented in this chapter. Their behavior regarding load-displacement response, ultimate strength and mode of failure, bond stress along the laminate strips, crack spacing and ductility of the slab specimens tested, is described.

Load-displacement Response

The load-mid span deflection curves of the tested slabs are presented in ***Figure 7.1***. The relationship between the displacements recorded in the other LVDTs and load are included in **Annex F**. It can clearly be noticed in ***Figure 7.1*** that the experimental load-displacement curves of the unstrengthened and strengthened slabs have a typical trilinear diagram, which correspond to the following behavioural phases: the uncracked elastic; crack propagation with steel bars in elastic stage; steel reinforcement post-yielding stage. The unstrengthened control slabs behaved in a perfectly plastic manner in the post-yielding phase.

The cracking, yielding and maximum loads, and the strength increasing ratio are given in ***Table 7.1***. The strength increasing ratio, in ***Table 7.1***, was calculated using the following expressions:

- *CFRP strengthened slabs:* $\frac{F_{UL}^{CFRP} - F_{UL}^{U}}{F_{UL}^{U}}$, (7.1)

and

- *CFRP & SFRC strengthened slabs:* $\frac{F_{UL}^{CFRP\&SFRC} - F_{UL}^{U}}{F_{UL}^{U}}$ and $\frac{F_{UL}^{CFRP\&SFRC} - F_{UL}^{CFRP}}{F_{UL}^{CFRP}}$ (7.2) and (7.3)

where

F_{UL}^{CFRP} - is the average maximum load of CFRP strengthened slabs;

F_{UL}^{U} - is the average maximum load of unstrengthened slabs, and

$F_{UL}^{CFRP\&SFRC}$ - is the average maximum load of CFRP and SFRC overlay strengthened slabs.

The monitored strains at the mid-span, in the concrete top surface, steel bar and CFRP laminates are listed in ***Table 7.2***.

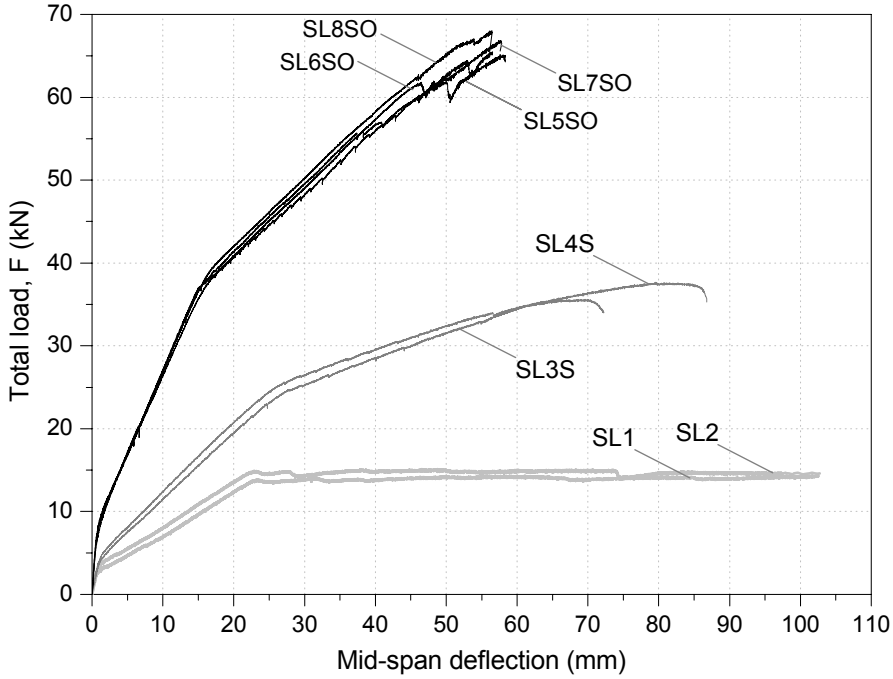

Figure 7.1 *- Load-deflection behaviour at mid-span of all slabs.*

The width of the slits where the CFRP laminate was installed, in the slabs SL3S, SL4S, SL5SO and SL6SO, was of about 4.0 mm. In the slabs SL7SO and SL8SO the width of the NSM slits was about 14.0 mm and 7.4 mm (c.f. **Annex I**). By examining the load-deflection curves in ***Figure 7.1***, it can be noticed that the width of the NSM slits had no influence on the overall behaviour of the slabs.

Table 7.1 *- Summary of the results in terms of loads.*

Strengthening	**Slab designation**	**Cracking load**[a] (kN)	**Yielding load**[b] (kN)	**Maximum load** (kN)	**Average ultimate load** (kN)	**Strength increasing ratio** (%)
Reference	SL1	2.57	10.56	14.34	14.73 (*3.74%*)	NA
	SL2	3.50	12.10	15.12		
CFRP laminate strengthening	SL3S	3.78	17.93	35.60	36.64 (4.00%)	148.71
	SL4S	3.77	19.15	37.67		
CFRP + SFRC overlay strengthening	SL5SO	7.61	31.55	65.13	66.37 (2.02%)	350.58[c] 81.17[d]
	SL6SO	6.98	30.08	65.46		
	SL7SO	6.79	30.57	66.85		
	SL8SO	6.96	30.64	68.04		

(*value*) Coefficient of Variation (COV) = (Standard deviation/Average) x 100

[a] In an experimental test, the cracking load is normally reported at a load step when cracking is detected for the first time. However, the cracking load is considered here as the load at which a significant change in the slope of the total load-deflection relationship is observed

[b] The yield load is defined herein as the load which leads to an elongation on steel reinforcement corresponding to the yield point from tension test in coupons. A significant change in the slop of the total load-deflection curve is also observed in the vicinity of yield load

[c] With respect to the reference

[d] With respect to the CFRP laminate strengthening

NA: not applicable

From the analysis of the strain values of ***Table 7.2***, it can be concluded that, at the onset of the slabs' failure, the maximum strain in the CFRP ranged from 11‰ to 13.4‰, which is 60% to 73% of the CFRP laminate ultimate strain (see ***Table 3.9***).

As expected, the concrete maximum compressive strain of the slabs only strengthened by CFRP laminates has exceeded 3.5‰, while in the hybrid strengthened slabs the concrete maximum compressive strain was below this value.

Table 7.2 *- Summary of the monitored strains.*

Strengthening	Slab	Concrete compression strain[a] (‰)	Steel strain[b] (‰)	CFRP laminate strain[c] (‰)
Reference	SL1	3.56[*14.05*][d]	8.35[*14.00*]	NA
	SL2	3.10[*14.56*]	19.86[*14.89*]	NA
CFRP laminate strengthening	SL3S	4.70[*35.49*]	NE	11.06[*35.58*]
	SL4S	5.12[*34.39*]	20.82[*25.07*]	12.52[*36.91*]
CFRP + SFRC overlay strengthening	SL5SO	3.35[*65.13*]	20.91[*39.20*]	13.41[*65.13*]
	SL6SO	3.35[*65.24*]	7.48[*44.84*]	12.20[*65.46*]
	SL7SO	2.78[*60.61*]	21.48[*41.87*]	13.12[*66.85*]
	SL8SO	3.45[*67.62*]	12.12[*45.64*]	13.42[*68.04*]

[*value*] Corresponding load in brackets
[a] Maximum value of SG9 and SG10
[b] Maximum value of SG1, SG2 and SG3
[c] Maximum value recorded in SG7 and SG8
[d] The load in bracket is the maximum load
NA: not applicable; NE: not evaluated

Strength and Failure Mode

Figure 7.2 illustrates the internal strain and stress distribution for the CFRP strengthened sections under flexure at the ultimate limit state. If the type of failure that can occur is assumed to be failure in the composite material with steel yielding, the nominal bending capacity can then be evaluated from:

$$M = A_s \cdot f_s \cdot \left(d_s - \frac{\beta_1}{2} \cdot c \right) + A_f \cdot \varepsilon_f \cdot E_f \cdot \left(h - h_f - \frac{\beta_1}{2} \cdot c \right) \tag{7.3}$$

The horizontal equilibrium equation for the section in ***Figure 7.2****(d)* gives:

$$\beta_1 \cdot \alpha \cdot f_c \cdot b \cdot c = A_s \cdot f_s + A_f \cdot \varepsilon_f \cdot E_f \tag{7.4}$$

That can be solved in terms of c (the neutral axis depth):

$$c = \frac{A_s \cdot f_s + A_f \cdot \varepsilon_f \cdot E_f}{\beta_1 \cdot \alpha \cdot f_c \cdot b} \tag{7.5}$$

The aforesaid assumptions can be also used to determine the nominal flexural strength of the hybrid strengthened section, CFRP and SFRC overlay strengthening, since the depth of the equivalent rectangular stress block does not extend beyond the bond line. ***Table 7.3*** includes the theoretical calculations of the load capacity, the experimental loads at failure, the ultimate deflections and the modes of failure of the slabs tested herein. The failure types of each slab specimens tested is further detailed separately hereafter. In the calculations of the load capacity the following values were taken:

- for the rectangular stress block factors:
  - α = is the ratio of the average concrete stress to the concrete strength (is taken equal to 0.85, according to ACI 318-02), and
  - β_1 = is the ratio of the depth of the equivalent rectangular stress block to the depth of the neutral axis (According to ACI 318-02, factor β_1 is 0.85 for concrete strength, f_c, up to and including 27.6 N/mm^2. For strengths above 27.6 N/mm^2, β_1 is reduced continuously at a rate of 0.05 for each 6.9 N/mm^2 of strength in excess of 27.6 N/mm^2, but β_1 shall not be taken less than 0.65. Therefore herein β_1 is taken equal to 0.72).

- for the material properties:
  - f_c = value corresponding to each slab (refer to ***Table 3.1***);
  - f_s = 550 N/mm^2 (refer to ***Table 3.10***);
  - ε_f = 18.45‰ (refer to ***Table 3.9***), and
  - E_f = 156.10 kN/mm^2 (refer to ***Table 3.9***).

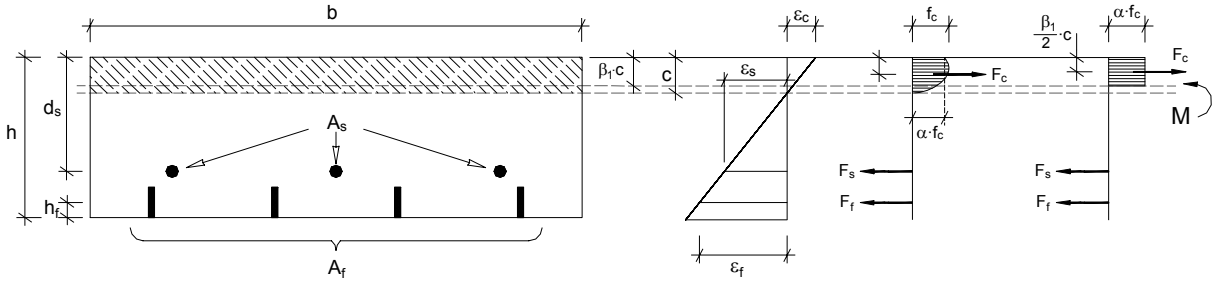

Figure 7.2 *- Internal strain and stress distribution for the strengthened section under flexure at ultimate stage.*

The failure mechanism of the reference slabs (SL1 and SL2) was governed by flexure failure mode, i.e. by yielding of internal reinforcement, with extensive cracking in the tension flange, followed by concrete crushing in compression. The failure mode of the reference slabs is illustrated in ***Figure 7.3***.

For the slab strips strengthened only with NSM technique (SL3S and SL4S) the failure mechanism was also governed by flexural failure: yielding of the internal steel reinforcement followed by the concrete compression failure at the top. However, the

slab specimen SL3S, after significant deflection failed in shear by intermediate shear crack mechanism (refer to ***Figure 7.4***). The failure modes of the slabs SL3S and SL4S are shown in ***Figure 7.5***.

Table 7.3 *- Theoretical calculations compared with loads at failure, ultimate deflection and mode of failure.*

Strengthening	Slab	Calculated load (kN)	Maximum load (kN)	Maximum/ calculated ratio	Ultimate deflection[a] (mm)	Type of failure
Reference	SL1	13.84	14.34	1.04	102.52	Flexure
	SL2	14.01	15.12	1.08	102.74	Flexure
CFRP laminate strengthening	SL3S	37.58	35.60	0.95	73.20	Flexure[b]
	SL4S	37.58	37.67	1.00	95.32	Flexure
CFRP + SFRC overlay strengthening	SL5SO	66.90	65.13	0.97	56.54	Flexo-shear[c]
	SL6SO	66.54	65.46	0.98	64.11	Flexo-shear
	SL7SO	66.36	66.85	1.01	57.84	Flexo-shear
	SL8SO	68.26	68.04	1.00	56.47	Flexo-shear

[a] Deflection registered at ultimate load in strengthened slabs
[b] Slab specimen with severe crushing of concrete followed by diagonal shear crack formation
[c] Flexo-shear failure mode is considered here as steel yielding and shear failure was observed after significant deflections

In the combined strengthening case, NSM and SFRC overlay, all slab strips (SL5SO, SL6SO, SL7SO and SL8SO) failed in shear, by intermediate shear crack mechanism with extensive cracking in the tension flange (refer to ***Figure 7.4***). The failure modes of the slabs strengthened with NSM and SFRC overlay are illustrated in ***Figure 7.6*** and ***7.7***.

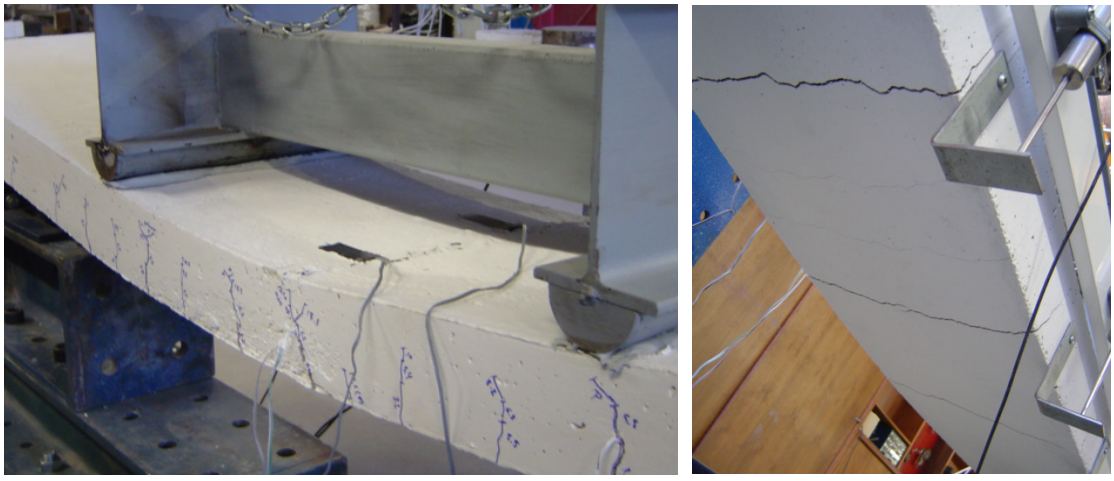

(a) *(b)*

Figure 7.3 *- Failure mode of the unstrengthened slabs: (a) lateral view of cracking pattern and concrete crushing at the top of slab, and (b) bottom view of cracking pattern of slab SL1.*

In all the tested slabs strengthened by NSM technique, on the contrary to what has been commonly verified experimentally for the extensively studied EBR strengthening technique (HOLLAWAY & LEEMING, 1999; AL-CHAAR & LAMB, 2002; BUYUKOZTURK et al, 2002; CHRISTOPHER & YANG, 2002; TENG et al, 2003;

MOSALLAM & MOSALLAM, 2003; SAYED et al, 2005; WO & HEMDAN, 2005; TANN, 2005; KOTYNIA, 2005b; ZHANG et al, 2006), no premature brittle failure occurred, i.e. loss of FRP effectiveness due to sudden CFRP debonding phenomena.

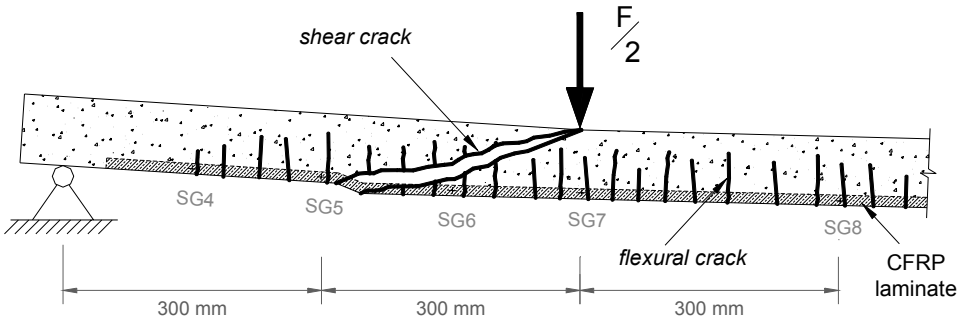

Figure 7.4 *- Intermediate shear crack away from the CFRP strip ends.*

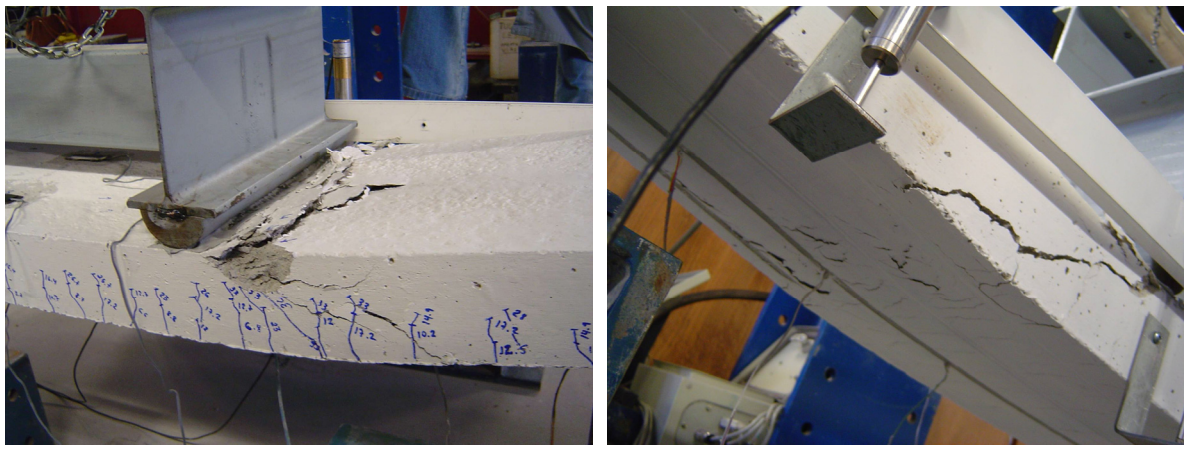

Figure 7.5 *- Failure mode of the slab strengthened with NSM: (a) lateral view of cracking pattern and concrete crushing at the top and (b) lateral and bottom view of shear crack in slab SL3S; (c) and (d) lateral views of concrete crushing in compression of slab SL4S.*

Early concrete cover delamination and plate-end failure, due to direct transverse tensile stress at the concrete cover-internal reinforcement interface and adhesive-concrete interface, respectively, are another common failure modes considered in RC

member strengthened with externally bonded FRP reinforcement (AHMED et al, 2001; AL-CHAAR & LAMB, 2002). Although this type of collapse has also been reported as a failure mechanism for the NSM strengthening technique (FORTES & BARROS, 2001; KOTYNIA, 2005a, 2005c), such occurrence was not observed in the present tests, even in the slab specimens having a concrete of low strength class (C20/25), a relative small distance between the NSM slits (about 70 mm) and a high CFRP strengthening ratio (A_s/A_{CFRP} = 35.05%, $^{1}\rho_{\ell,ef}$ = 1.08% and $\rho_{\ell,ef}$ = 0.71%, for slabs strengthened with NSM and slabs strengthened with NSM and SFRC overlay, respectively). However, surely it would be necessary to carry out a comprehensive experimental research about this subject taking into account variables such as, among others, the distance between the NSM slits, the concrete strength, the percentage and arrangement of internal steel reinforcement, the effective reinforcement ratio and/or ratio of CFRP strengthening to the internal steel reinforcement (A_{CFRP}/A_s).

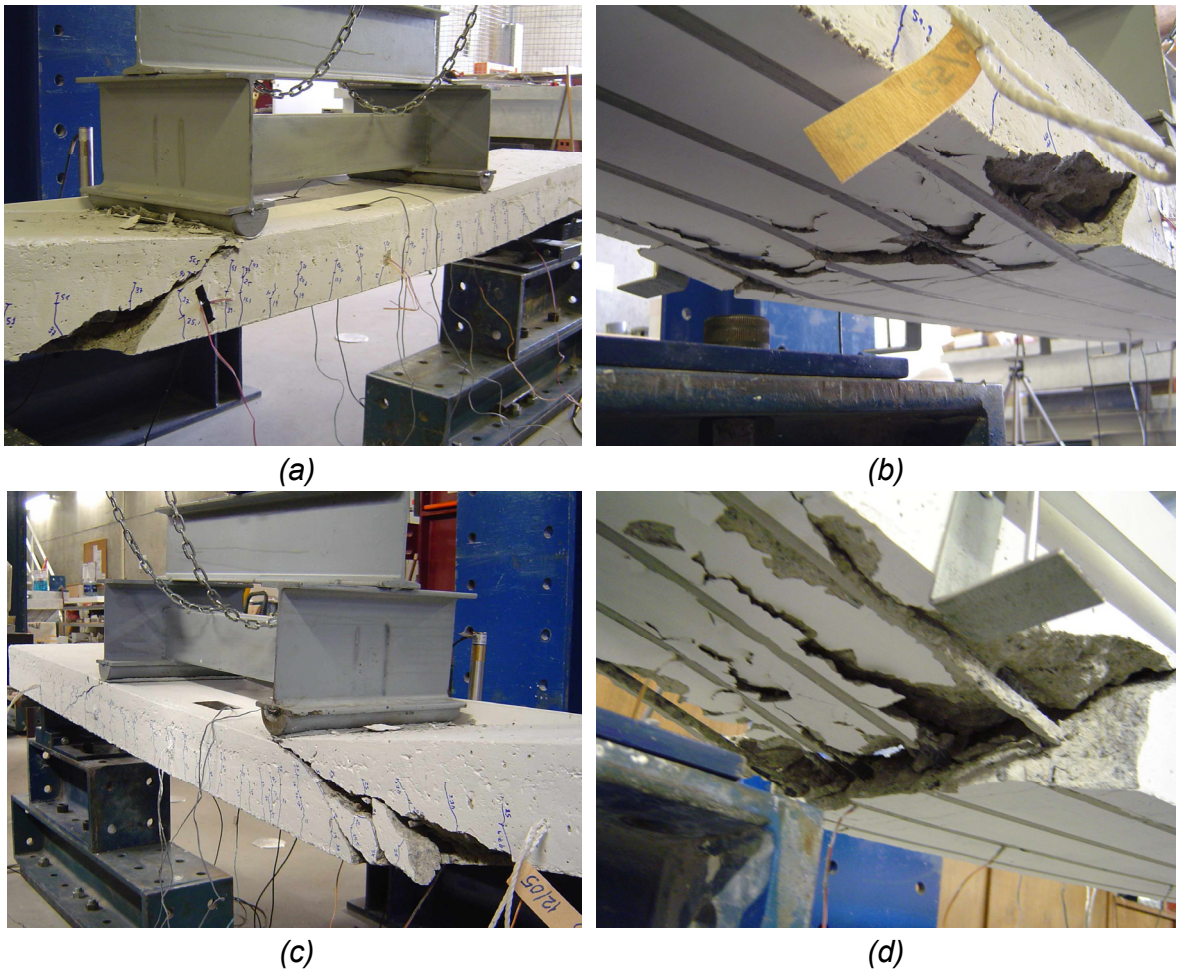

(a) *(b)*

(c) *(d)*

***Figure 7.6** - Failure mode of slab strengthened with NSM and SFRC overlay: (a) lateral view of the cracking pattern and diagonal tension crack of slab SL5SO, and (b) bottom view of the shear crack of slab SL5SO; (c) lateral view of the cracking pattern and shear crack of slab SL6SO, and (d) bottom view of the shear crack of slab SL6SO.*

$$^{1}\rho_{\ell,ef} = \frac{A_s}{b \cdot d_s} + n \cdot \frac{A_{CFRP}}{b \cdot d_{CFRP}} \; ; \; n = \frac{E_{CFRP}}{E_s}$$

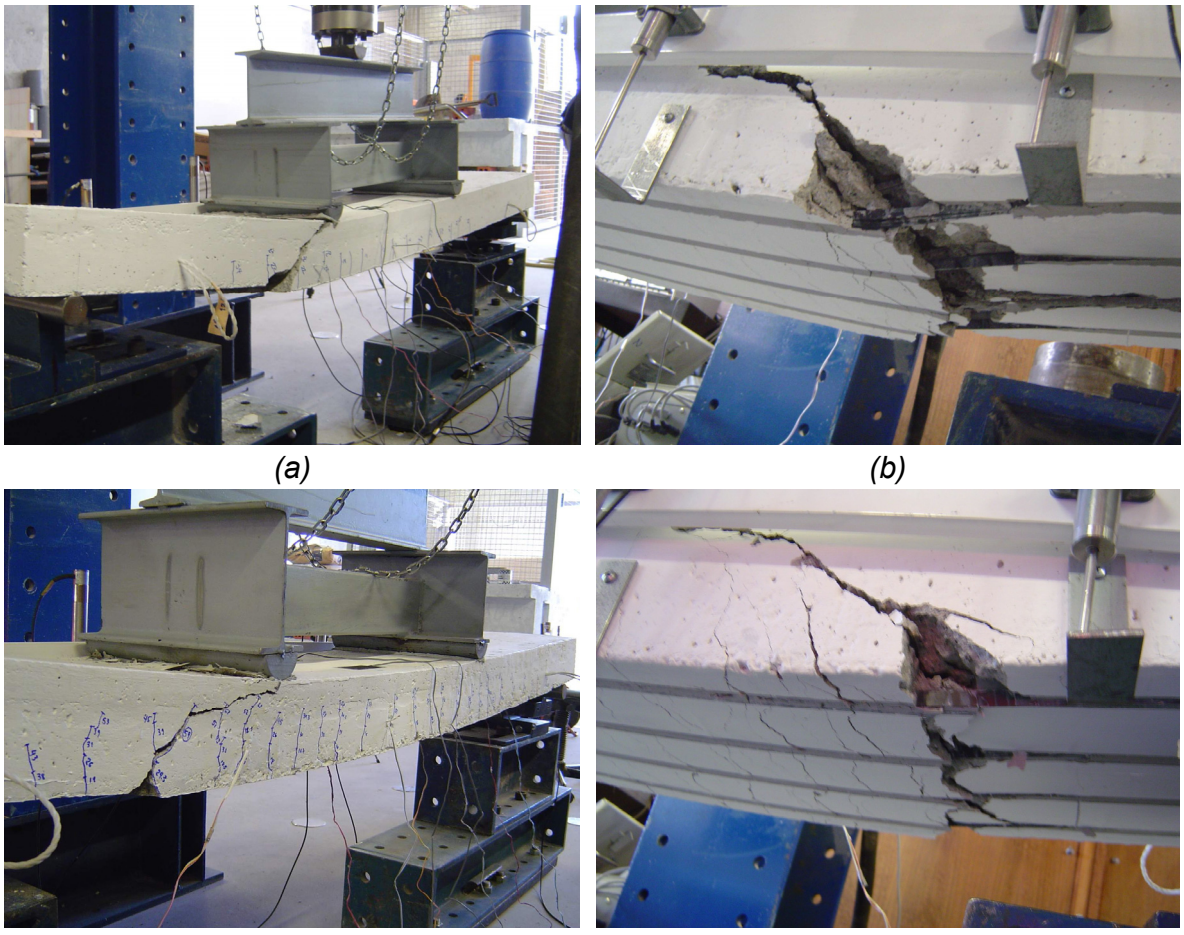

(a) *(b)*

(c) *(d)*

***Figure 7.7** - Failure mode of slab strengthened with NSM and SFRC overlay: (a) lateral view of the cracking pattern and shear crack* of slab SL7SO*, and (b) bottom close up view of the shear crack of slab SL7SO; (c) lateral view of the cracking pattern and shear crack* of slab SL8SO*, and (d) bottom close up view of the shear crack of slab SL8SO.*

The values of shear resistance of the slabs, obtained experimentally, and predicted from several codes are compared in ***Table 7.4***. From the analysis of the values in ***Table 7.4*** it can be concluded that the values predicted by the considered codes and those recorded experimentally are quite similar.

***Table 7.4** - Ratio between experimental shear crack loads and theoretical predictions.*

Strengthening	ACI 318 (2004)	REBAP (1983)	CEB (1993)	OKAMURA & HIGAI (1980)	NIWA et al (1987)	CSA (1984)	JSCE (1996)
CFRP laminate strengthening	0.95	1.05	1.01	0.87	0.87	0.89	1.04
CFRP + SFRC strengthening	0.98	1.03	1.26	0.96	0.98	0.89	1.15

Note: the values were obtained by dividing the experimental load when the diagonal shear crack was first observed by the theoretical predictions. Detailed formulas are included in **Annex G**.

Bond Stress Between CFRP Laminate Strips and Concrete

Using the strains recorded in the strain gauges installed to the laminate strips, the average CFRP-concrete bond stresses developed along the CFRP laminate strips can be evaluated. Therefore, the average bond stress (τ_{bm}^{RL}) in the CFRP laminate strips, in-between the strain gauges position, SG^L (left) and SG^R (right), was determined according to the following equations (refer to ***Figure 7.8***):

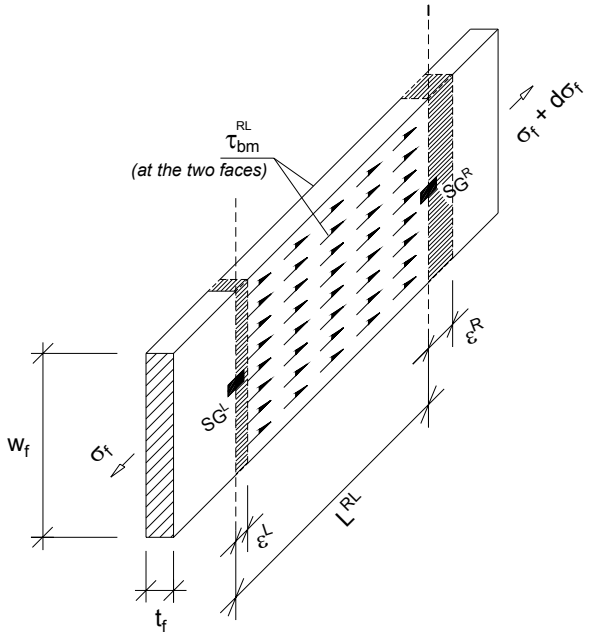

Figure 7.8 *- Average bond stress (τ_{bm}^{RL}) in-between two consecutive strain gauges installed to the CFRP laminate.*

$$\tau_{bm}^{RL} = \frac{\Delta F^{RL}}{A_b^{RL}} \tag{7.6}$$

where

ΔF^{RL} is the difference in axial force in the laminate, between the two strain gauges ($= E_{CFRP} \cdot \Delta\varepsilon^{RL} \cdot A_{CFRP}$)

A_b^{RL} is the area of the lateral CFRP faces in contact to the adhesive, in-between strain gauges position ($= p \cdot L^{RL}$)

E_{CFRP} is the Young's modulus

$\Delta\varepsilon^{RL}$ is the difference in axial strain between the strain gauges positioned at right and left sections ($= \left|\varepsilon_{SG}^R - \varepsilon_{SG}^L\right|$)

A_{CFRP} is the laminate cross sectional area

p is the perimeter of the contact surface between CFRP laminate and epoxy adhesive (considered here equals to $2 \cdot W_f$)

L^{RL} is the distance between two consecutive strain gauges

ε_{SG}^R is the axial strain registered experimentally in the *right* strain gauge

ε_{SG}^{L} is the axial strain registered experimentally in the *left* strain gauge

hence (7.6) takes the form:

$$\tau_{bm}^{RL} = \frac{E_{CFRP} \cdot A_{CFRP} \cdot \Delta\varepsilon^{RL}}{2 \cdot W_f \cdot L^{RL}} \ (N/mm^2) \tag{7.7}$$

In this approach, constant bond stress in-between the strain gauges SG^L and SG^R is assumed. This situation is illustrated in ***Figure 7.8***. The variation of the τ_{bm}^{RL} during the applied load is shown in ***Figures 7.9***, ***7.10*** and ***7.11***, for the slab specimens strengthened with NSM technique.

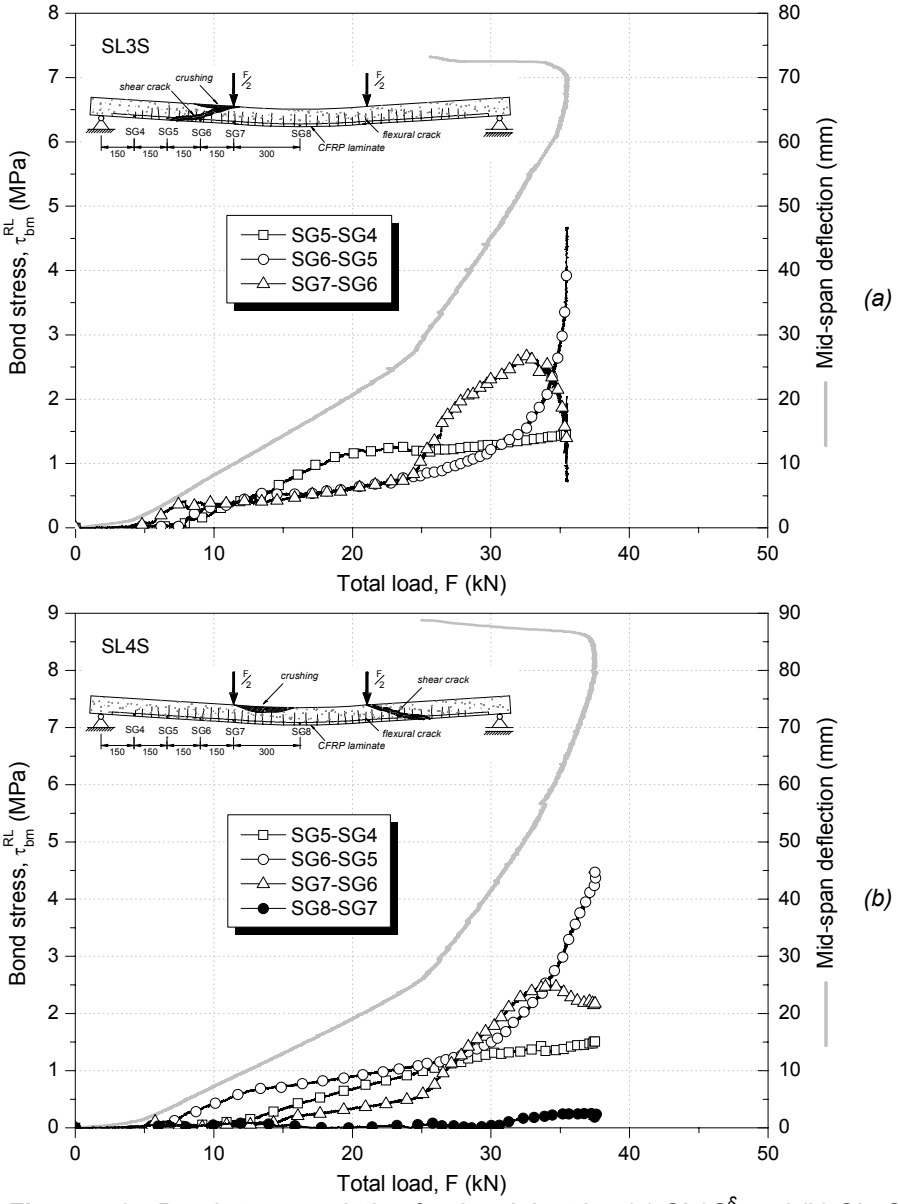

Figure 7.9 *- Bond stress variation for the slab strips (a) SL3S[§] and (b) SL4S.*

[§] **It was not possible to record the data of the SG8 for the slab strip SL3S**

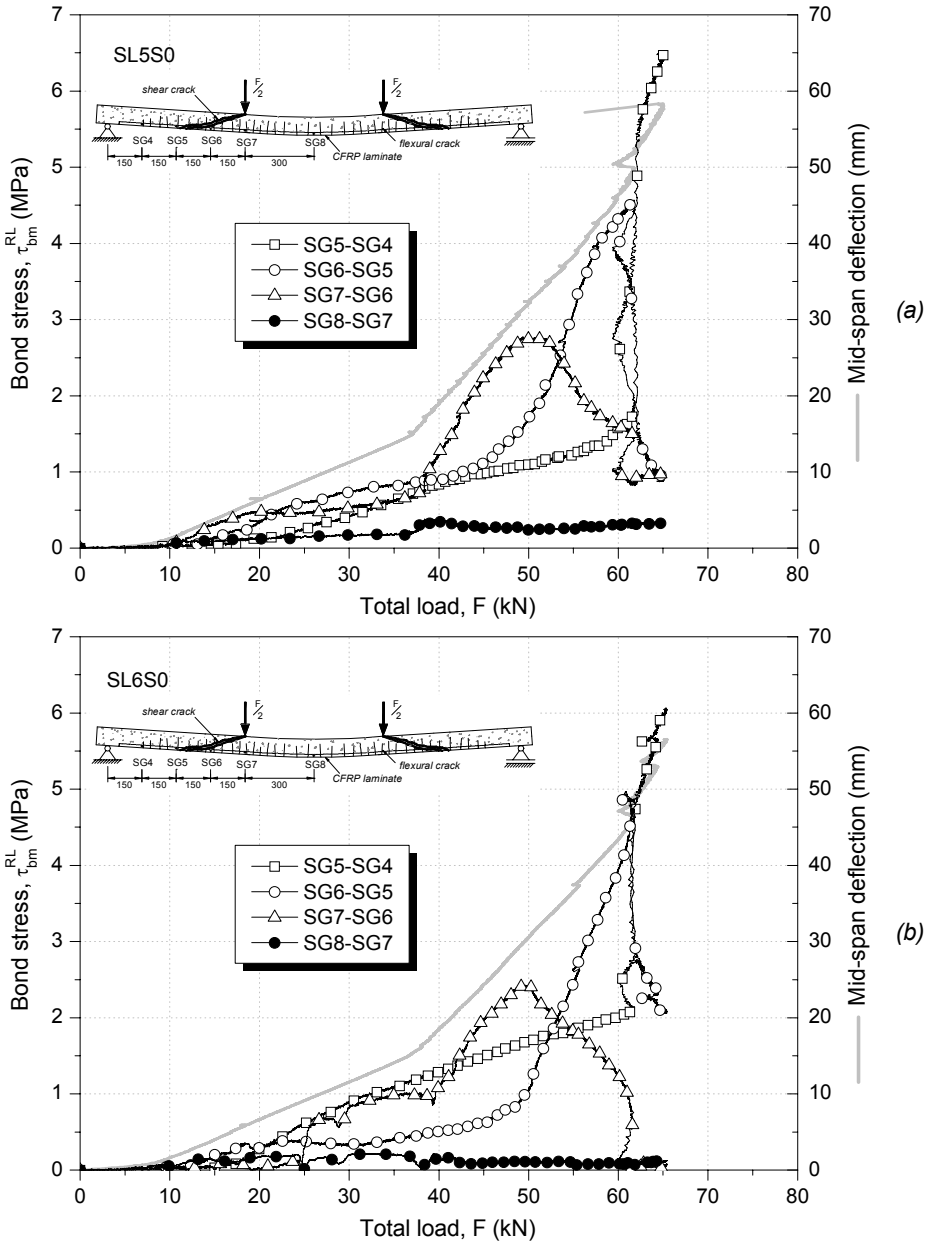

Figure 7.10 *- Bond stress variation for the slab strips (a) SL5SO and (b) SL6SO.*

Figures 7.9, ***7.10*** and ***7.11*** show that up to concrete cracking the strain in the CFRP laminates are marginal since the observed bond stresses are very low. In general, a very low bond stress profile is developed at the interfaces CFRP laminate-epoxy adhesive-concrete at the serviceability limit deflection, since the average bond stress computed at the service deflection, corresponding to a deflection of 7.2 mm at mid-span, was below 1.0 MPa.

Furthermore, it can be noticed that the average bond stress variation was below 6.5 MPa at the ultimate load.

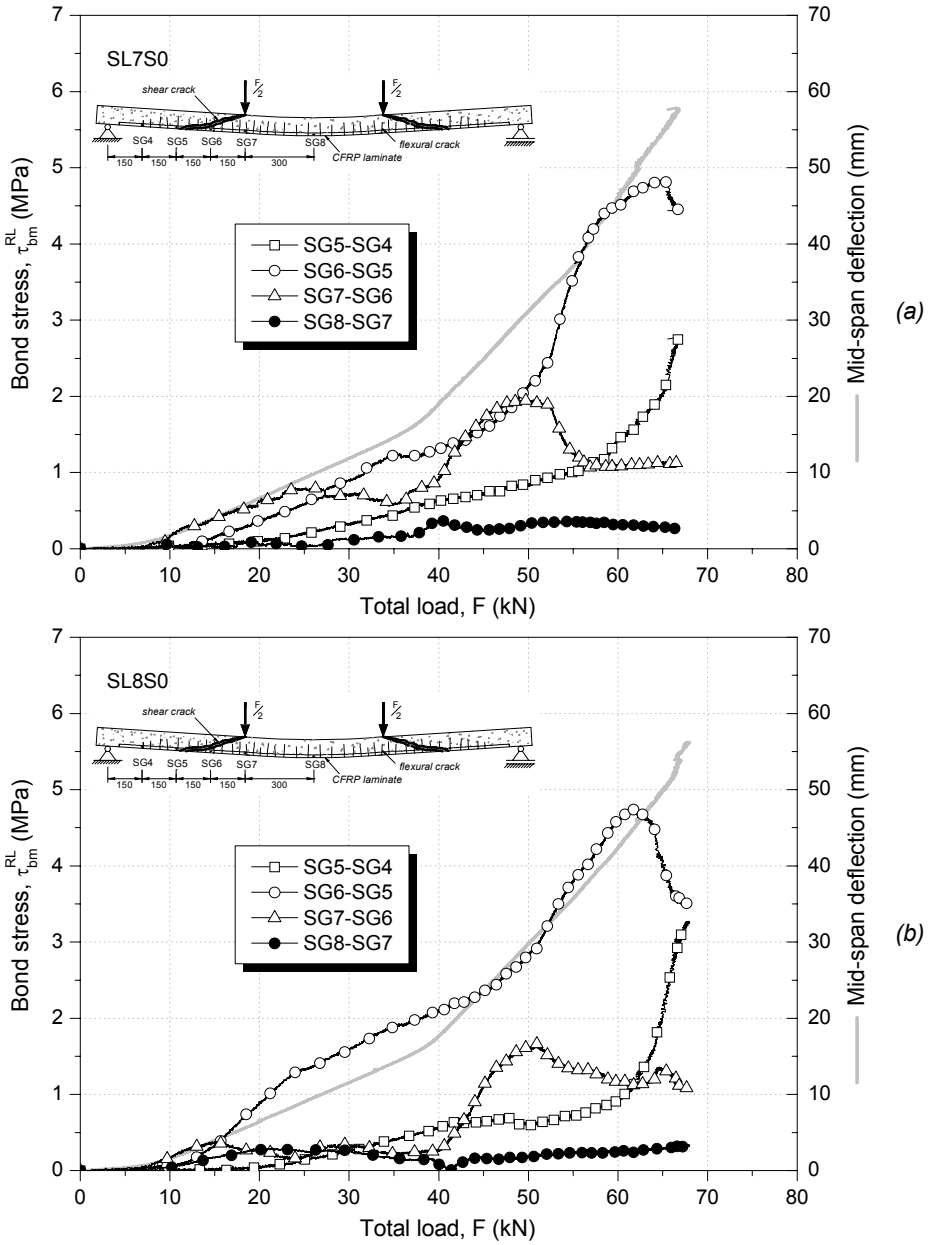

Figure 7.11 *- Bond stress variation for the slab strips (a) SL7SO and (b) SL8SO.*

An extensive experimental program was conducted to investigate the bond for the near-surface mounted CFRP laminate strips (SENA-CRUZ & BARROS, 2004a and 2004b). From the pullout-bending tests a bond stress $\tau_{bm} \geq 12$ MPa was registered. The maximum average bond stress (less than 6.5 MPa) observed in the slabs herein tested is, therefore, rather lower than the bond strength (12 MPa). A more extensive experimental and numerical description of bond between NSM CFRP laminate strips and concrete is given by SENA-CRUZ (2004).

In general the average bond stress was higher between SG5 and SG6. For the slabs failing in flexo-shear mode, the average bond stress between SG4-SG5 and SG5-SG6 showed a tendency to increase with load increasing, and a tendency to decrease between SG6-SG7 after about 33 kN for the slab SL3S and SL4S; and after about 50 kN for the slabs SL5SO, SL6SO, SL7SO and SL8SO. Such tendencies may be

explained among others by: (1) the anchorage of the CFRP laminate strips is located in the region between SG5 and the end of the laminate; and (2) the widening of the cracks in the region between the SG5-SG6 relieves the bond stress in the SG6-SG7 region.

Crack Spacing Analysis

The distinct crack feature of reference and strengthened slabs shown in ***Figures 6.9***, ***6.22*** and ***6.37*** clearly indicates the significant improvement in the crack behavior provided by the used strengthening strategies.

The expressions from the Portuguese design code of reinforced and pre-stressing concrete structures, CEB Model Code, EUROCODE 2, FIB and CERONI & PECCE (2005) were considered herein to calculate the theoretical mean spacing between cracks for the tested slab strips. The average crack spacing, experimentally measured after the slabs having been tested, was determined as schematically described in ***Figure 7.12*** (the **Annex H** provides further details of the crack patterns at the side view of the tested slabs).

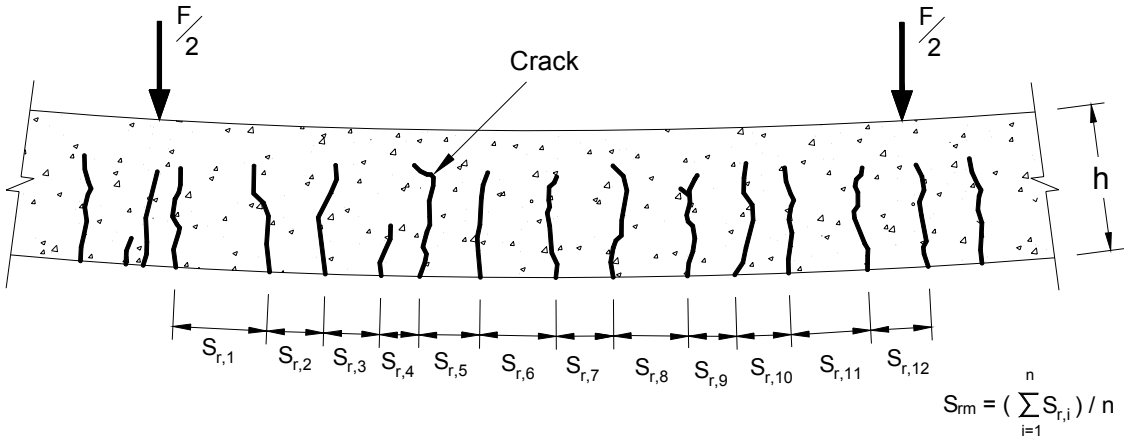

Figure 7.12 *- Determination of the average crack spacing (S_{rm}) in the tested slab strips.*

In the following, the analytical procedures are described, and in ***Table 7.5*** the obtained results are compared to the crack spacing measured experimentally.

Portuguese Design Code for Reinforced and Prestressing Concrete Structures (REBAP, 1983)

According to the Portuguese design code of reinforced and pre-stressing concrete structures, the following formula can be used to estimate the average crack spacing of the stabilized crack propagation phase, for RC members,

$$s_{rm} = 2 \cdot \left(c + \frac{s}{10} \right) + \eta_1 \cdot \eta_2 \cdot \frac{\phi}{\rho_r} \tag{7.8}$$

where

c is the concrete cover of the longitudinal reinforcement

s is the rebar spacing, and $s \leq 15 \cdot \phi$

η_1 is the steel reinforcement bond condition parameter, given by $\eta_1 = \begin{cases} 0.4 & \text{high bond rebars} \\ 0.8 & \text{normal bond rebars} \end{cases}$

η_2 is the coefficient that depends on the cross section strain distribution $\left(= 0.25 \cdot \frac{\varepsilon_1 + \varepsilon_2}{2 \cdot \varepsilon_1} \right)$

ε_1 and ε_2 are the strain in the bottom and top level of the concrete surrounding the tension reinforcement, respectively (see ***Figure 7.13***).

ϕ is the steel bar diameter

ρ_r is the effective reinforcement ratio $\left(= A_s / A_{c,r} \right)$

$A_{c,r}$ is the effective area of concrete in tension, the area of concrete surrounding the tension reinforcement (see ***Figure 7.13***)

In order to consider the contribution of the CFRP laminates each CFRP laminate is transformed in an equivalent steel bar of cross-section A_s^{eq} and diameter ϕ_s^{eq}, by applying the following expressions:

$$A_s^{eq} = \frac{E_{CFRP}}{E_s} \cdot A_{CFRP} \tag{7.9}$$

$$\phi_s^{eq} = 2 \cdot \sqrt{\frac{A_s^{eq}}{\pi}} \tag{7.10}$$

where

A_{CFRP} is the cross-sectional area of the CFRP laminate

E_{CFRP} is the modulus of elasticity of the CFRP laminate, and

E_S is the modulus of elasticity of the steel reinforcement

For the slabs including CFRP laminates, Eq. (7.8) is transformed into the following expression:

$$s_{rm} = 2 \cdot \left(c_m + \frac{s_m}{10} \right) + \eta_1 \cdot \eta_2 \cdot \frac{\phi_m}{\rho_r} \tag{7.11}$$

where

c_m is the mean concrete cover (average of steel and steel equivalent bars, $= \frac{c_s + c_s^{eq}}{2}$)

s_m is the mean rebar spacing ($= \frac{s_s + s_s^{eq}}{2}$ and $s_s \le 15 \cdot \phi_s$, $s_s^{eq} \le 15 \cdot \phi_s^{eq}$)

ϕ_m is the mean bar diameter (average of steel and equivalent steel bars, $= \frac{\phi_s \cdot A_s + \phi_s^{eq} \cdot A_s^{eq}}{A_s + A_s^{eq}}$)

η_1 is the bond condition parameter, considered equal to 0.8

η_2 is the coefficient that depends on the cross section strain distribution ($= 0.25 \cdot \frac{\varepsilon_1 + \varepsilon_2}{2 \cdot \varepsilon_1}$)

ρ_r is the effective reinforcement ratio ($= \frac{A_s + A_s^{eq}}{A_{c,r}}$)

$A_{c,r}$ is the area of concrete surrounding the tension reinforcement, steel and equivalent steel bars (see ***Figure 7.13***)

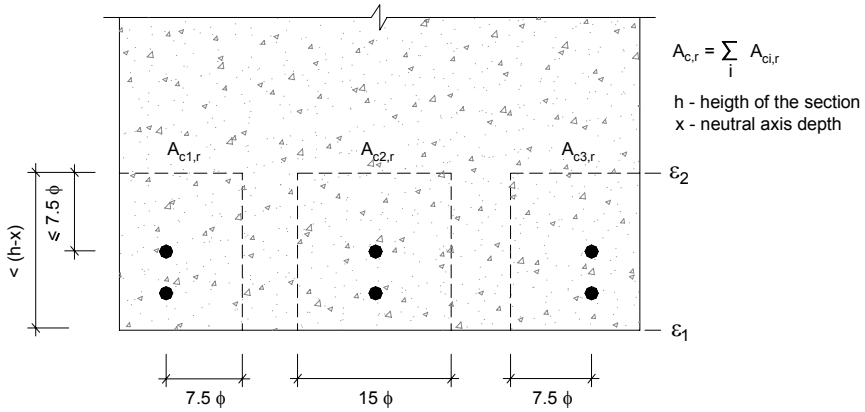

Figure 7.13 *- Effective concrete surrounding the tension reinforcement, according to REBAP (1983).*

CEB Model Code (1993)

Following the CEB Model Code (1993) suggestion, the average crack spacing, at stabilized cracking phase, may be estimated using the length over which slip between steel and concrete occurs according to Eq. (7.12).

$$s_{rm} \approx \frac{2}{3} \cdot \ell_{s,max} \tag{7.12}$$

where

$\ell_{s,max} = \dfrac{\phi_s}{3.6 \cdot \rho_{s,ef}}$ for stabilized cracking

$\ell_{s,max}$ is the length of slipping between steel and concrete

ϕ_s is the steel bar diameter

$\rho_{s,ef}$ is the effective reinforcement ratio ($= A_s / A_{c,ef}$)

$A_{c,ef}$ is the effective area of concrete in tension, the area of concrete surrounding the tension reinforcement (see ***Figure 7.14***, for slabs).

For the slabs strengthened with CFRP material, each laminate was converted in a equivalent steel bar (of area A_s^{eq} and diameter ϕ_s^{eq}) as described in previous sections.

The parameters, therefore, can be adjusted for strengthened members:

$$\ell_{s,max} = \frac{\phi_m}{3.6 \cdot \rho_{s,ef}} \tag{7.13}$$

where

ϕ_m is the mean bar diameter (average of steel and equivalent steel bars, $= \dfrac{\phi_s \cdot A_s + \phi_s^{eq} \cdot A_s^{eq}}{A_s + A_s^{eq}}$)

$\rho_{s,ef}$ is the effective reinforcement ratio ($= \dfrac{A_s + A_s^{eq}}{A_{c,r}}$)

$A_{c,r}$ is the area of concrete surrounding the tension reinforcement, steel and equivalent steel bars (see ***Figure 7.14***), and was computed using the mean concrete cover and mean bar diameter.

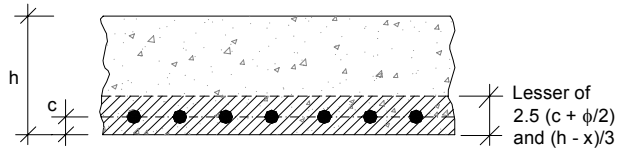

Figure 7.14 *- Effective concrete tension area in slabs, according to the CEB Model Code (1993).*

EUROCODE 2 (2000)

EUROCODE 2 (2000) provides Eq. (7.14) for RC members subjected mainly to flexure and direct tension. The final average crack spacing can be given by

$$s_{rm} = 50 + 0.25 \cdot k_1 \cdot k_2 \cdot \frac{\phi_s}{\rho_r} \quad (7.14)$$

where

k_1 accounts for the bond properties of the bar and, for flexural cracking, k_1 = 0.8 for high bond bars and k_1 = 1.6 for plain bars;

k_2 depends on the strain distribution and k_2 = 0.5 for bending and k_2 = 1.0 for pure tension;

ϕ_s is the steel bar diameter;

ρ_r is the effective reinforcement ratio ($= A_s / A_{c,ef}$), where A_s is the area of reinforcement contained within the effective tension area, $A_{c.ef}$;

$A_{c,ef}$ is the effective area of concrete in tension, the area of concrete surrounding the tension reinforcement (see ***Figure 7.14***, for slabs).

For the slabs including CFRP laminates, the cross-section area of each CFRP laminate (A_{CFRP}) is transformed in an equivalent steel area (A_s^{eq}) as given in Eqs. (7.9) and (7.10). The parameters in Eq. (7.14) can, therefore, be adjusted for strengthened members:

c is the mean concrete cover, cf. ***Figure 7.14***, (average of steel and equivalent steel bars, $= \frac{c_s + c_s^{eq}}{2}$);

ϕ_s is the mean bar diameter (average of steel and equivalent steel bars, $= \frac{\phi_s \cdot A_s + \phi_s^{eq} \cdot A_s^{eq}}{A_s + A_s^{eq}}$);

ρ_r is the effective reinforcement ratio ($= \frac{A_s + A_s^{eq}}{A_{c,r}}$);

$A_{c,r}$ is the effective area of concrete in tension, surrounding the tension reinforcement, steel and equivalent steel bars (see ***Figure 7.14***), and was computed using the mean concrete cover and mean bar diameter.

EUROCODE 2 (2004)

EUROCODE 2 (2004) provides Eq. (7.15) for RC members subjected mainly, to flexure and direct tension. The final average crack spacing can be evaluated from:

$$s_{rm} = k_3 \cdot c + k_1 \cdot k_2 \cdot k_4 \cdot \frac{\phi}{\rho_{p,eff}} \quad (7.15)$$

where

ϕ is the bar diameter;

c is the cover to the longitudinal reinforcement;

k_1 accounts for the bond properties of the bar and, for flexural cracking, k_1 = 0.8 for high bond bars and k_1 = 1.6 for plain bars;

k_2 is a coefficient which takes into account of the distribution of strain and k_2 = 0.5 for bending and k_2 = 1.0 for pure tension;

The recommended values of k_3 and k_4 are 3.4 and 0.425, respectively;

$\rho_{p,eff}$ is the effective reinforcement ratio ($= A_s / A_{c,ef}$), where A_s is the cross-section area of the reinforcement contained within the effective tension area, $A_{c.ef}$;

$A_{c,ef}$ is the effective area of concrete in tension, the area of concrete surrounding the tension reinforcement (see ***Figure 7.14***, for slabs).

For slabs having CFRP laminates, the cross-section area of each CFRP laminate area (A_{CFRP}) is transformed in an equivalent steel area (A_s^{eq}) as given in Eqs. (7.9) and (7.10). The parameters in Eq. (7.15) can, therefore, be adjusted for strengthened members.

c is the mean concrete cover, cf. ***Figure 7.14***, (average of steel and equivalent steel bars, $= \frac{c_s + c_s^{eq}}{2}$);

ϕ is the mean bar diameter (average of steel and equivalent steel bars, $= \frac{\phi_s \cdot A_s + \phi_s^{eq} \cdot A_s^{eq}}{A_s + A_s^{eq}}$);

$\rho_{p,eff}$ is the effective reinforcement ratio ($= \frac{A_s + A_s^{eq}}{A_{c,r}}$);

$A_{c,ef}$ is the effective tension area of concrete, surrounding the tension reinforcement, steel and steel equivalent bars (see ***Figure 7.14***), and was computed using the mean concrete cover and mean bar diameter.

FIB (2001)

For FIB bulletin, assuming stabilized cracking, the meam crack spacing, s_{rm}, taking into account the effect of both the internal reinforcement and external strengthening (EBR), can be calculated as:

$$s_{rm} = \frac{2 \cdot f_{ctm} \cdot A_{ct,eff}}{\tau_{sm} \cdot u_s} \cdot \frac{E_s \cdot A_s}{E_s \cdot A_s + \xi_b \cdot E_s \cdot A_s} \tag{7.16}$$

where

$\xi_b = \dfrac{\tau_{CFRPm} \cdot E_s \cdot \phi_s}{\tau_{sm} \cdot E_{CFRP} \cdot u_{CFRP}}$;

$A_{ct,eff}$ is the effective area of concrete in tension, the area of concrete surrounding the tension reinforcement (see ***Figure 7.14***, for slabs);

$\tau_{sm} = 1.8 \cdot f_{ctm}$, is the average bond stress of the steel (CEB Model Code, 1993);

τ_{CFRPm}, is the average bond stress of the CFRP strengthening: $\tau_{CFRPm} = 1.25 \cdot f_{ctm}$ for EBR (FIB bulletin) and $\tau_{CFRPm} \approx \tau_{bm}$ for NSM, with $\tau_{bm} \geq 12\,N/mm^2$ and $f_{cm} \geq 35\,N/mm^2$ (SENA-CRUZ, 2004). In the present work τ_{bm} was considered equal to 16.1 N/mm^2;

$u_{CFRP} = t_{CFRP} + 2 \cdot w_{CFRP}$, is the bond perimeter of the CFRP laminate;

ϕ_s is the bar diameter of the internal steel reinforcement;

E_S is the modulus of elasticity the steel reinforcement;

w_{CFRP} is the width of the CFRP laminate;

t_{CFRP} is the thickness of the CFRP laminate, and

E_{CFRP} is the modulus of elasticity of the CFRP laminate.

CERONI & PECCE (2005)

Based on a parametric study and validated against their experimental data obtained from 32 beams and 12 ties tests, CERONI & PECCE (2004 and 2005) proposed a new formulation to compute the crack widths in EBR strengthened members, as follows:

$$w_m = k \cdot \frac{A_{ct,eff}{}^a}{\phi^b} \cdot \frac{\sigma_s}{E_s} \cdot \beta \cdot \left(1 - \left(\frac{A_{CFRP}}{A_{ct,eff}}\right)^c \cdot \left(\frac{E_{CFRP}}{E_s}\right)^d \cdot \left(\frac{B_{CFRP}}{B}\right)^e\right) \qquad (7.17)$$

where

$\beta = \dfrac{H - x_c}{h - x_c}$ and $h = (H - c)$;

H is the total height of the section;

c is the concrete cover in tension;

x_c is the depth of the neutral axis;

B is the width of the section;

$A_{ct,eff}$ is the effective area of concrete in tension, the area of concrete surrounding the tension reinforcement (see ***Figure 7.14***, for slabs);

ϕ is the diameter of steel bar;

A_{CFRP}, B_{CFRP} and E_{CFRP} are the area, the width and the elastic modulus of external composite, respectively;

σ_s and E_s are the stress at service crack limit state and the elastic modulus of the steel bar;

$k = 5.4$, $a = 0.4$, $b = 0.70$, $c = 0.30$, $d = 0.50$ and $e = 1$, are coefficients calibrated from the data obtained in the experimental program, presented in CERONI & PECCE (2005).

For RC elements the average crack width (w_m) is usually evaluated by multiplying the average final crack spacing (s_{rm}) by the mean strain in the reinforcement (ε_{sm}), as follows,

$$w_m = s_{rm} \cdot \varepsilon_{sm} \tag{7.18}$$

The average final crack spacing (s_{rm}) can be computed using Eqs (7.17) and (7.18). However, concerning NSM strengthened members it is suggested that the last term relating to EBR in Eq. (7.17) should rather be taken as:

$$\left(\frac{B_{CFRP}}{B}\right)^{e} = \left(n_{CFRP} \cdot L_{per}\right)^{\frac{\beta - 1.35}{3}} \tag{7.19}$$

where

n_{CFRP} is the number of NSM CFRP strips;

L_{per} is the perimeter length of the cross-section of the failure plane, defined in ***Figure 7.15***, where the failure plane of length L_{per} should be assumed to be 1 mm from the plate as shown.

Crack development in RC elements strengthened with composite materials is a complex process, and there is no universally accepted model for estimating crack width and crack spacing. Compared to the expressions of REBAP and EUROCODE 2, the expressions of CEB, FIB and CERONI & PECCE lead to better results of predicted crack spacing for the unstrengthened and NSM strengthened slabs. However, it is shown that the use of various code equations to estimate crack spacing in the same member can result in significantly different values (c.f. ***Table 7.5***). Therefore, there is no agreement on the most appropriate model to predict width and spacing of flexural cracks in both EBR and NSM strengthened RC elements. More experimental and analytical related investigations are needed to validate a feasible model for predicting crack phenomena in RC members strengthened with composites.

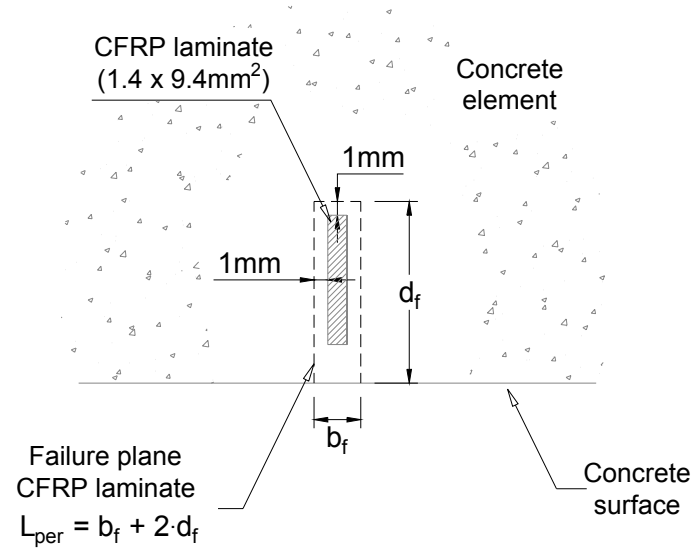

Figure 7.15 *- Perimeter length of idealised failure plane for NSM CFRP strip (cross section), reproduced from CIDAR Guideline (2006).*

Table 7.5 *- Experimental and analytical crack spacing.*

Strengthening	Slab	Average crack spacing (mm)						
		Experimental[a]	REBAP[b] (1983)	CEB[c] (1990)	EUROCODE 2 (2000)	EUROCODE 2 (2004)	FIB (2001)	CERONI & PECCE (2005)
Reference	SL1	80	166	67	86	117	-	67
		(81)	*(164)*					
	SL2	82	162					
CFRP laminate strengthening	SL3S	45	75	42	73	77	48	44
		(45)	*(75)*					
	SL4S	45	75					
CFRP + SFRC overlay strengthening	SL5SO	53	89	59	82	91	68	52
	SL6SO	51	89					
		(52)	*(89)*					
	SL7SO	53	89					
	SL8SO	50	87					

a Measures taken in the side close to the bottom surface of the slab strip (see *Figure 7.12*)
b The cross section strain distribution was derived from the strain gauges data, for an elongation close to the first yield of the conventional reinforcement
c The neutral axis depth, c, was derived from the strain gauges data, for an elongation close to the first yield of the conventional reinforcement
Where the strain gauge data was not recorded, a cross section analysis was carried out
(value) average value, when is the case

Ductility Analysis

Safety is the most important consideration for the design of new and strengthened structures. When minimum requirements of ductility and energy dissipation capacity are guaranteed, the structure, if overload, will exhibit stress redistribution and notable

deformation, providing a set of visible warning prior to collapse, i.e. an unexpected sudden failure of the structure is prevented (DUTHINH & STARNES, 2001; KELLEY, BRAINERD & VATOVEC, 2000).

On the contrary, strengthening of RC structures with EBR often leads to an increase in strength and stiffness, which is attained at the expense of a loss in ductility, or capacity of the structures to deflect inelastically while sustaining load at the ultimate state (DUTHINH & STARNES, 2001). Since ductility is an important property for safe design of strengthening of any structural element and moreover, NSM strengthening with CFRP is a fairly new innovation, understanding the effect of this strengthening technique on the ductility of a RC member is critical. A method, based on the ductility index commonly used, is considered in this section to analyse the ductility of the composite slab specimens.

Ductility of RC members has generally been measured by a ratio called bending ductility index or factor (μ). The ductility index is usually expressed as a ratio of the rotation (θ), curvature (χ), or deflection (Δ) at the ultimate load[§] (subscript U) to the corresponding property at the yield load (subscript Y), as follows:

$$\mu_\theta = \frac{\theta_U}{\theta_Y} \qquad \mu_\chi = \frac{\chi_U}{\chi_Y} \qquad \mu_\Delta = \frac{\Delta_U}{\Delta_Y} \tag{7.21}$$

Another common way of measuring ductility consists in computing the ratio of reinforcing steel strain at failure of the element to the yield strain of the steel (KELLEY, BRAINERD & VATOVEC, 2000).

For this study, deflection was used to measure the ductility of the slab specimens tested. ***Table 7.6*** lists the ductility ratio for each of the specimens and the average ductility ratio for the unstrengthened and strengthened situations. Values for the NSM strengthened slabs were in the range from 1.98 to 3.90, to be compared with 3.38 and 4.13 for the companion control slabs.

By examining the ***Table 7.6***, a decrease of about 42% in the averaged ductile ratio of the NSM strengthened slabs comparatively to the reference slabs can be noticed. As aforementioned, the deformational behavior of the slabs strengthened using NSM was limited by crushing of concrete in extreme compressive fibre. Furthermore, no significant changing in the ductility index of the slabs strengthened using NSM and SFRC overlay with respect to the unstrengthened control slabs was observed. In the slabs strengthened with the hybrid system, the tough SFRC overlay prevent any compression crushing of concrete and also the ductility level of bare slabs was re-

[§] The ultimate load is considered here as the load corresponding to a concrete strain of 3‰ in the strain gauges on top of slab

established. However, the deformability of these slabs was directly limited by the shear failure.

Table 7.6 *- Ductility ratios of the slab specimens tested.*

Strengthening	Slab	Δ_Y (mm)	Δ_U (mm)	Ductile ratio, μ_Δ (mm/mm)	Average μ_Δ (mm/mm)
Reference	SL1	16.76	56.59	3.38	3.75 (*14.22%*)
	SL2	17.29	71.41	4.13	
CFRP laminate strengthening	SL3S	18.00	41.96	2.33	2.16 (*11.49%*)
	SL4S	17.99	35.64	1.98	
CFRP + SFRC overlay strengthening	SL5SO	12.20	46.93	3.85	3.84 (*1.34%*)
	SL6SO	11.65	43.95	3.77	
	SL7SO	12.12	47.23	3.90	
	SL8SO	11.84	45.52	3.84	

(*value*) Coefficient of Variation (COV) = (Standard deviation/Average) x 100

According to recommendations of the FIB (2001), the ductility index should exceed a certain value to prevent from sudden failure with no or very little warnings in strengthened flexural members. The minimum acceptable ductility index ensures that the internal reinforcement experiences sufficient yield securing additional warnings prior to failure of the member. For the slabs tested herein, according to the FIB (2001), the curvature ductility index should exceed the value of 1.70 suggested for steel S500 and concrete types C35/45 or lower. The values included in ***Table 7.6*** are reasonable larger compared with the minimum FIB requirement.

To understand in depth the ductility behaviour of RC flexural members strengthened with composite materials, it is important to examine and perceive the behaviour at failure prior and after strengthening. This requires other than traditional evaluation of the limits associated with the rupture of the steel or composite, or the crushing of the concrete. In other words, issues as failure mechanism of the composite-concrete substrate bond system and the ratio of strengthening area to the existing steel reinforcement area are crucial (KELLEY, BRAINERD & VATOVEC, 2000).

Accordingly, the bond mechanism of the composite reinforcement for high strengthening ratios, in flexural strengthening of RC members, not only limits the load carrying capacity, but can also result in non-safe strengthened members when EBR systems are used. Therefore, the enhanced bond condition provides a much more ductile behaviour for the NSM strengthening technique comparatively to the EBR strengthening technique and, as illustrated before in ***Figure 1.4*** (Section “Brief Background”), the bond ductility when the composite material is applied into silts is comparable to the bond ductility of embedded steel rebars.

8 Summary and Conclusions

An experimental program was conducted in order to: (a) investigate the NSM strengthening technique for reinforced concrete slabs, and (b) evaluate structural performance of a hybrid strengthening technique for existing concrete slabs, comprised by CFRP laminates and SFRC overlay. For this purpose a total of eight slabs were tested.

The following conclusions can be drawn from this experimental study:

- The experimental program carried out demonstrated that the hybrid strengthening technique has great potential application towards flexural strengthening of RC slabs, not only in terms of increasing the slab ultimate load capacity, but also its stiffness up to concrete crack initiation;

- A CFRP strengthening ratio of 0.25% (CFRP reinforcement to the conventional steel reinforcement ratio close to 40%) increased about 55% the service load of the 1.8 m RC slabs with a steel reinforcement ratio of 0.63%. However, the slabs strengthened by NSM technique and SFRC showed an increase of approximately 244% in the service load with respect to the reference slabs. Comparatively to the NSM technique, the hybrid strengthening strategy lead to an increase of about 122% in load at the service load level;

- The hybrid strengthening system also lead to an increase of about 350% in the RC slab maximum load carrying capacity with respect to the reference slabs and an increase of about 80% in comparison to the slabs strengthened only with NSM technique. When compared to the reference slabs, close to 150% of increase in the load carrying capacity was attained when applying the NSM strengthening technique;

- The concrete cracking spacing measured at the bottom of the slabs, indicates that NSM technique provides a significant improvement in the crack behavior of RC slabs. In the results obtained, the average crack spacing of the lightly RC slabs strengthened with measured after failure were about 45% lower than that measured in reference slabs. Almost the same reduction (about 36%) in the average crack spacing was observed in the hybrid strengthened slabs;

- For the stabilized cracking phase and taking into account appropriate considerations for the NSM strengthening system, the average crack spacing of the strengthened slabs may be achieved with acceptable accuracy using the

analytical expressions suggested by the CEB (1990), FIB (2001) and CERONI & PECCE (2005);

- When compared to the bond strength, which was recorded in pull out-bending tests, a very low bond stress profile was observed through the interfaces CFRP laminate-epoxy adhesive-concrete along the laminate strips in slabs where NSM strengthening was applied;

- In general, for all slabs strengthened with NSM system and SFRC overlay, the ductility indexes, based on deflections measurements, were the same to those of the reference slabs. The slabs strengthened only with NSM laminates had ductility indexes 42% lower when compared to the reference slabs. This reduction in ductility was mainly conditioned by the low resistance of the concrete, as compression failure was observed at the top surface of the slabs;

- The NSM strengthening system has also provided a significant increase in the stiffness and deformability, consistent with the high stress redistribution (closely spaced crack pattern) owing to the prominent composite action between the CFRP reinforcement and concrete. Since the hybrid strengthening system lead to substantial increase in flexural resistance, the shear capacity of the composite slabs limited their deformability; however, the stiffness of the slabs has increased significantly and the ductility level maintained; and

- The SFRC overlay bonding procedures can be considered adequate, because no slip was observed, the connection between SFRC overlay and the RC slab was able to transfer horizontal shear stress, forming consequently a monolithic flexural cross-section.

Acknowledgements

The authors acknowledge the financial support of the Portuguese Science and Technology Foundation (FCT), PhD grant number *SFRH / BD / 11232 / 2002*.

Thanks also for the companies “Companhia Geral de Cal e Cimento S.A. (SECIL)”, Sika S.A., “Central do Pego”, “Pedreiras Bezerras”, Bekaert NV, “Degussa Construction Chemicals Portugal S.A.”, S&P® Reinforcement, which generously have supplied cement; overlay bond product; fly ash; aggregates; steel fibres; superplasticizer and CFRP adhesive; and CFRP laminate, respectively.

References

ACI Committee 318. Building code requirements for structural concrete and Commentary (ACI 318-04), Reported by committee 318, American Concrete Institute, Detroit, 351 pp., 2004.

ACI 503R. Use of epoxy compounds with concrete, ACI Manual of Concrete Practice, Part 5, Reported by Committee 503, American Concrete Institute, 28 pp., 1993 (Reapproved 1998).

ACI 503.2. Standard specification for bonding plastic concrete to hardened concrete with a multi-component epoxy adhesive, ACI Manual of Concrete Practice, Part 5, Reported by Committee 503, American Concrete Institute, 5 pp., 1992 (Reapproved 1997).

ACI 503.5R. Guide for the selection of polymer adhesives with concrete, ACI Manual of Concrete Practice, Part 5, Reported by Committee 503, American Concrete Institute, 4 pp., 1997.

ACI 503.6R. Guide for the application of epoxy and latex adhesives for bonding freshly mixed and hardened concretes, ACI Manual of Concrete Practice, Part 5, Reported by Committee 503, American Concrete Institute, 16 pp., 1992 (Reapproved 1997).

AHMED, O., GEMERT, D. V., and VANDEWALLE, L. Improved model for plate-end shear of CFRP strengthened RC beams, Cement and Concrete Composites, Vol. 23, N°. 01 , pp. 3-19, February 2001.

AL-CHAAR, G. K., and LAMB, G. E. Design of fiber-reinforced polymer materials for seismic rehabilitation of infilled concrete structures, US Army Corps of Engineers, Engineer Research and Development Center, Construction Engineering Research Laboratory, Report N°. A810114, pp. 83, December 2002.

ALKHRDAJI, T., NANNI, A. Surface bonded FRP reinforcement for strengthening/repair of structural reinforced concrete. In ICRI-NR Workshop. Baltimore, MD, October 30, 1999.

ALKHRDAJI, T., NANNI., A., CHEN, G., BARKER, M. Upgrading the transportation infrastructure: solid RC decks strengthened with FRP, Concrete International: Design and Construction, Vol. 21, No.10, pp. 37-41, October 1999.

ASTM C 143. Standard test method for slump of hydraulic cement concrete, American Society for Testing and Materials, Annual Book of ASTM Standards, Vol. 4.02, West Conshohocken, PA 1998.

ASTM D 3039/D 3039 M. Standard test method for tensile properties of polymer matrix composite materials, American Society for Testing and Materials, Annual Book of ASTM Standards, Vol. 15.03, pp. 118-127, West Conshohocken, PA 1993.

ASTM A370. Standard test methods and definitions for mechanical testing of steel products. American Society for Testing and Materials, 2002.

BALAGURU, P. N., SHAH, S. P. Fiber reinforced cement composites. McGraw-Hill International Editions, Civil Engineering Series, 530 pp., 1992.

BARROS, J. A. O. Comportamento do betão reforçado com fibras - análise experimental e simulação numérica (Behavior of fiber reinforced concrete - experimental analysis and numerical simulation). PhD Thesis, Civil Eng. Dept., Faculty of Engineering, University of Porto, Portugal, 1995. (in Portuguese)

BARROS, J. A. O., FIGUEIRAS, J. A. Experimental behaviour of fibre concrete slabs on soil. Mechanics of Cohesive-frictional Materials, Vol. 3, No. 03, pp. 277-290, July 1998.

BARROS, J. A. O., SENA-CRUZ, J. M. Strengthening a prestressed concrete slab by epoxy - bonded FRP composites and SFRC overlayer, 7th Internacional Conference on Inspection Appraisal Repairs & Maintenance of Buildings & Structures, Nottingham Trent University, UK, 11-13 September, 2001.

BARROS, J. A. O., DIAS, S. J. E. Shear strengthening of reinforced concrete beams with laminate strips of CFRP, International Conference Composites in Constructions - CCC2003, Cosenza, Italy, pp. 289-294, 16-19 September, 2003.

BARROS, J. A. O., CUNHA, V. M. C. F., RIBEIRO, A. F., ANTUNES, J. A. B. Post-cracking behaviour of steel fibre reinforced Concrete, Materials and Structures, Vol. 38, No. 275, pp. 47-56, January 2004.

BARROS, J. A. O., FORTES, A. S. Flexural strengthening of concrete beams with CFRP laminates bonded into slits, Cement and Concrete Composites, Vol. 27, No. 4, pp. 471-480, April 2005.

BONALDO, E., BARROS, J. O., LOURENÇO, P. B. Bond characterization between concrete base and repairing SFRC by pull-off tests, Report 04-DEC/E-13, May 2004.

BETTOR MBT. MBrace Laminate, Technical sheet, Rio de Mouro, Portugal, 2 pp. 2003.

BETTOR MBT - Degussa Construction Chemical Portugal, S.A., http://www.bettormbt.pt/MBTPortugal/Home/default.htm, Portugal, 2004. (available on September 24, 2004)

BETTOR MBT. MBrace Resin 220, Technical sheet, http://www.degussa-cc.es, Spain, 3 pp., 2005. (available on January 25, 2005)

BLASCHKO, M., ZILCH, K. Rehabilitation of concrete structures with CFRP strips glued into slits, In Proceeding of the 12th International Conference on Composites Materials. Paris, 5-9 July, 1999.

BUYUKOZTURK, O., GUNES, O., KARACA, E. Characterization and modelling of debonding in RC beams strengthened with FRP composites, 15th ASCE Engineering Mechanics Conference, Columbia University, New York, NY, pp. 8, June 2-5, 2002.

CEB-FIP Model Code. Design code. Comité Euro-International du Béton, Bulletin d'Information No. 213/214, Lausanne, Switzerland, 1993.

CAROLIN, A. Strengthening of concrete structures with CFRP - Shear strengthening and full-scale applications. Licentiate Thesis, Division of Structural Engineering, Luleå University of Technology, Luleå, Sweden, pp. 120, June 2001. ISBN: 91-89580-01-X, ISSN: 1402-1757.

CAROLIN, A. Carbon fibre reinforced polymers for strengthening of structural elements. Doctoral Thesis, Division of Structural Engineering, Luleå University of Technology, Luleå, Sweden, pp. 190, June 2003. ISBN: 91-89580-04-4, ISSN: 1402-1544.

CERONI, F., PECCE, M. Modelling of tension stiffening behaviour of RC ties strengthened with FRP sheets, Journal of Composites for Constructions, Vol. 8, No. 6, pp. 510-518, November-December 2004.

CERONI, F., PECCE, M. Modelling of cracking in RC elements strengthened with FRP sheets, In Proceeding of the 3rd International Conference on Composites in Construction CCC2005. Lyon, France, pp. 115-121, 21-23 July, 2005.

CHRISTOPHER, L., YANG, Y. A fracture-based model for debonding of FRP plate from concrete substrate, 15th ASCE Engineering Mechanics Conference, Columbia University, New York, NY, pp. 7, June 2-5, 2002.

CIDAR. Design Guideline for RC structures retrofitted with FRP and metal plates: beams and slabs, DRAFT 3, Submitted to Standards Australia 02/02/06, Centre for Infrastructure Diagnosis, Assessment and Rehabilitation (CIDAR), The University of Adelaide (http://www.civeng.adelaide.edu.au/index.html), pp. 109, February 2006. (available on March 8, 2006)

COMYN, J. Adhesion Science, The Royal Society of Chemistry, Cambridge, UK, 149 pp., 1997.

COUTINHO, A. S. Manufacturing and properties of concrete, National Civil Engineering Laboratory, 3 volumes, Lisbon, Portugal, 1988. (in Portuguese)

CSA Standard. Design of concrete structures for buildings - CAN3-A23.3-M84, Canadian Standards Association, Rexdale, Ontario, pp. 281, 1984.

DE LORENZIS, L., NANNI, A. Shear strengthening of reinforced concrete beams with near-surface mounted reinforced polymer rods. ACI Structural Journal, Vol. 98, No. 01, January-February 2001a.

DE LORENZIS, L., NANNI, A. Characterization of FRP rods as near-surface mounted reinforcement. Journal of Composites for Construction, Vol. 05, No. 02, May 2001b.

DORELL, J., NORDBERG, E. Begränsning av krypsprickor vid pågjutningar med fiberbetong. Master of Science Thesis, Division of Structural Engineering, Luleå University of Technology, Luleå, Sweden, December 1993.

DRAMIX: product data sheet, N. V. Bekaert S.A., 1998.

DUTHINH, D., STARNES, M. Strength and ductility of concrete beams reinforced with carbon FRP and steel, National Institute of Standards and Technology Technology Administration (NIST), U.S. Department of Commerce, NISTIR 6830, 33 pp., November 2001.

EN 10 002-1. Metallic materials - Tensile testing. Part 1: Method of test (at ambient temperature). European Standard, CEN, Bruxelas, 35 pp., November 1990.

EN 12 390-3 Testing hardened concrete - Part 3: Compressive strength of test specimens. European Standard, CEN, Bruxelas, 18 pp., 2001.

ENV 1992-1-1, Eurocode 2: Design of concrete structures - Part 1-1: General rules and rules for buildings, CEN, Bruxelas, 2000.

EN 1992-1-1, Eurocode 2: Design of concrete structures - Part 1-1: General rules and rules for buildings, CEN, Bruxelas, 225 pp., 2004.

FIB. Externally bonded FRP reinforcement for RC structures - Technical report on the "Design and use of externally bonded fibre reinforced polymer reinforcement (FRP EBR) for reinforced concrete structures", by 'EBR' working party of fib TG 9.3, 138 pp., July 2001, ISBN 2-88394-054-1.

FISCHER, G., LI, V. C. Deformation behavior of fiber-reinforced polymer reinforced engineered cementitious composite (ECC) flexural members under reversed cyclic loading conditions. ACI Structural Journal, Vol. 100, No. 01, pp. 25-35, January-February 2003.

GRZYBOWSKI, M. Determination of crack arresting properties of fiber reinforced cementitious composites, Publication TRITA-BRO-8908, ISSN 1100-648X, Royal Institute of Technology, Stockholm, Sweden, 190 pp., June 1989.

GRZYBOWSKI, M., and SHAH, S. P. Shrinkage cracking of fiber reinforced concrete, ACI Material Journal, Vol. 87, No. 02, pp. 138-148, March-April 1990.

HILTI - Hilti Corporation, www.hilti.com, 2004. (available on December 28, 2004)

HOLLAWAY, L. C., LEEMING, M. B. Strengthening of reinforced concrete structures: using externally-bonded FRP composites in structural and civil engineering, Published by Boca Raton, Fla.: CRC Press and Cambridge, England: Woodhead Pub., pp. 327, 1999. (ISBN 1-5912-4605-9, electronic book - online version available at: http://www.knovel.com/knovel2/Toc.jsp?BookID=828&VerticalID=0)

ISO 527-1. Plastics - Determination of tensile properties - Part 1: General principles, International Organization for Standardization, Genèva, Switzerland, 9 pp., 1993.

ISO 527-2. Plastics - Determination of tensile properties - Part 2: Test conditions for moulding and extrusion plastics, International Organization for Standardization, Genèva, Switzerland 5 pp., 1993.

ISO 527-5. Plastics - Determination of tensile properties - Part 1: Test conditions for unidirectional fibre-reinforced plastic composites, International Organization for Standardization, Genèva, Switzerland, 9 pp., 1993.

JSCE Committee. Standard specification for design and construction of concrete structure, Part 1 (Design), Japan Society of Civil Engineers, Tokyo, 1996.

KELLEY, P. L., BRAINERD, M. L., VATOVEC, M. Design philosophy for structural strengthening with FRP, Concrete International, Vol. 22, No. 2, pp. 77-82, February 2000.

KOTYNIA, R. Strengthening of reinforced concrete structures with near surface mounted FRP reinforcement, 5th International Conference - Analytical models and new concepts in concrete and masonry structures AMCM 2005, 8 pp., Gliwice - Ustroń, 12-14 June, 2005a.

KOTYNIA, R. Plate end de-bonding mitigated by side plates, FRP Photo Competition '05, International Institute for FRP in Construction, Ref. No. PC05-085, November 2005b.

KOTYNIA, R. Midspan cover delamination of NSM CFRP strips, FRP Photo Competition '05, International Institute for FRP in Construction, Ref. No. PC05-140, November 2005c.

MAYS, G. C., HUTCHINSON, A. R. Adhesives in Civil Engineering, Cambridge University Press, New York, USA, 333 pp., 1992.

MOSALLAM, A. S., MOSALLAM, K. M. Strengthening of two-way concrete slabs with FRP composite laminates, Construction and Building Materials, Vol. 17, No. 1, pp. 43-54, February 2003.

NANNI, A. FRP Reinforcement for bridge structures. Proceedings, Structural Engineering Conference, The University of Kansas, Lawrence, KS, 5 pp., 16 March, 2000.

NIWA, J., YAMADA, K., YOKOZAWA, K., OKAMURA, H. Reevaluation of the equation for shear strength of reinforced concrete beams without web reinforcement, JSCE Concrete Library International, No. 9, pp. 65-84, June 1987.

OKAMURA, H., HIGAI, T. Proposed design equation for shear strength of reinforced concrete beams without web reinforcement, Proceedings of Japanese Society of Civil Engineers, Vol. 300, pp. 131-141, 1980.

REBAP. Regulamento de estruturas de betão armado e pré-esforçado (Portuguese design code for reinforced and prestressing concrete structures), 191 pp., Porto Press, 1983. (in Portuguese)

RILEM. FMC1 - Determination of the fracture energy of mortar and concrete by means of three-point bend tests on notched beams, Materials and Structures, Vol. 18, No. 106, pp. 285-290, July-August 1985.

RILEM. Technical Committee 162-TDF - Test and design methods for steel fibre reinforced concrete. Recommendation for bending test (Chairlady L.

Vandewalle), Materials and Structures, Vol. 33, No. 225, pp. 3-5, January-February 2000.

RILEM. Technical Committee 162-TDF - Test and design methods for steel fibre reinforced concrete. Final Recommendation, Materials and Structures, Vol. 35, pp. 579-582, November 2002.

RILEM. Technical Committee CPC8 - Modulus of elasticity of concrete in compression, Technical recommendations for the testing and use of construction materials, pp. 25-27, 1994.

RDP. LVDTs calibration certificates, RDP Group, October1995.

SAYED, W. E. E., EBEAD, U. A., NEALE, K. W. Modeling of debonding failures in FRP-strengthened two-way slabs, 7th International Symposium on Fiber-Reinforced (FRP) Polymer Reinforcement for Concrete Structures (FRPRCS-7), ACI, SP 230-27, Kansas City, Missouri, 7-10 November, 2005.

SENA-CRUZ, J. M., BARROS, J. A. O., Modeling of bond between near-surface mounted CFRP laminate strips and concrete, Computers and Structures, Vol. 82, No. 17-19, pp. 1513-1521, July 2004a.

SENA-CRUZ, J. M., BARROS, J. A. O., Bond between near-surface mounted CFRP laminate strips and concrete in structural strengthening, Journal of Composites for Construction, Vol. 8, No. 6, pp. 519-527, November-December 2004b.

SENA-CRUZ, J. M., Strengthening of concrete structures with near-surface mounted CFRP laminate strips. PhD Thesis, Department of Civil Engineering, University of Minho, 198 pp., December 2004.

SIKA, Technical data sheet - construction, Sika - Chemical Industry, S.A., Edition No. 5, 434 pp., 2002. (in Portuguese)

S&P - Clever Reinforcement Company, http://www.sp-reinforcement.ch, Switzerland, 2004. (available on September 24, 2004)

SOROUSHIAN, P., and LEE, C. D. Constitutive modelling of steel fiber reinforced concrete under direct tension and compression, Proceeding: Fiber reinforced cement and concrete recent developments, Edited by: R. N. Swamy and B. Barr, University of Wales College of Cardiff, UK, pp. 363-377, NY, September 1989.

TAERWE, L. R. Influence of steel fibers on strain-softening on high-strength concrete, ACI Materials Journal, Vol. 88, No. 6, pp. 54-60, January-February 1992.

TÄLJSTEN, B., CAROLIN, A. Concrete Beams strengthened with near surface mounted CFRP laminates. 5th International Conference on Fibre Reinforced Plastics for Reinforced Concrete Structures - FRPRCS-5 (Edited by Chris Burgoyne), Cambridge, UK, Vol. 01, pp. 107-116, 16-18 July, 2001.

TANN, D. B. Determination of ductility and deformability indices for FRP strengthened RC slabs, Repair and renovation of concrete structures. Proceedings of 6th International Conference: Global Construction: Ultimate Concrete Opportunities, Edited by, Ravindra K. Dhir, M. Roderick Jones and Li Zheng, University of Dundee, Scotland, UK, pp. 311-320, 5-7 July 2005 (ISBN 0-7277-3405-9).

TENG, J. G., SMITH, S. T., YAO, J., CHEN, J. F. Intermediate crack-induced debonding in RC beams and slabs, Construction and Building Materials, Vol. 17, No. 6-7, pp. 447-462, September-October 2003.

TML - Tokyo Sokki Kenkyujo Co., Ltd., http://www.tokyosokki.co.jp/e/index.html, Japan, 2004. (available on September 24, 2004)

WAFA, F. F., and ASHOUR, S. A. Mechanical properties of high-Strength fiber reinforced concrete, ACI Materials Journal, Vol. 89, No. 05, pp. 449-455, September-October 1992.

WU, Z., HEMDAN, S. Debonding in FRP-strengthened flexural members with different shear-span ratios, 7th International Symposium on Fiber-Reinforced (FRP) Polymer Reinforcement for Concrete Structures (FRPRCS-7), ACI, SP 230-24, Kansas City, Missouri, November 7-10, 2005.

ZHANG, A. H., JIN, W. L., LI G. B. Behavior of preloaded RC beams strengthened with CFRP laminates, Journal of Zhejiang University SCIENCE A, Vol. 7, No. 3, pp. 436-444, 2006. ISSN 1009-3095

ANNEXES

Annex A - Physical properties of the aggregates

Annex B - Particle sizing of the aggregates

Annex C - Data of the compressive strength of the substrate concrete and of the SFRC overlay

Annex D - Flexural tensile behavior of the plain concrete and SFRC overlay

Annex E - Epoxy adhesive dosages adopted and respective proportions

Annex F - Load-deflection curves of the lateral LVDTs

Annex G - Side view of the slabs after test

Annex H - Side view of the slabs after test

Annex I - Measurements of the NSM slit geometry

Annex A - Physical properties of the aggregates

Table A1 *- Specific gravity and water absorption of fine aggregate 4/11.*

P_1	WEIGHT OF THE SAMPLE DRIED IN AIR	4795.2 g
P_2	WEIGHT OF THE SATURATED SAMPLE IN THE AIR WITH DRY SURFACE	4857.6 g
P_3	WEIGHT OF THE SATURATED SAMPLE IN WATER	3023.0 g
G_a	SPECIFIC GRAVITY OF THE WATER AT TEST TEMPERATURE	1000.0 kg/m^3
$\frac{P_1}{P_2 - P_3} \times G_a$	SPECIFIC GRAVITY OF THE DRY PARTICLES	2613.8 kg/m^3
$\frac{P_1}{P_1 - P_3} \times G_a$	SPECIFIC GRAVITY OF THE IMPERMEABLE MATERIAL OF PARTICLES	2705.8 kg/m^3
$\frac{P_2}{P_2 - P_3} \times G_a$	SPECIFIC GRAVITY OF SATURATED PARTICLES WITH DRY SURFACE	2647.8 kg/m^3
$\frac{P_2 - P_1}{P_1} \times 100$	ABSORPTION	1,3 %

Table A2 *- Specific gravity and water absorption of coarse aggregate 11/16.*

P_1	WEIGHT OF THE SAMPLE DRIED IN AIR	5324,0 g
P_2	WEIGHT OF THE SATURATED SAMPLE IN THE AIR WITH THE DRY SURFACE	5378,0 g
P_3	WEIGHT, IN WATER, OF THE SATURATED SAMPLE	3359,2 g
G_a	SPECIFIC GRAVITY OF THE WATER AT TEST TEMPERATURE	1000,0 kg/m^3
$\frac{P_1}{P_2 - P_3} \times G_a$	SPECIFIC GRAVITY OF THE DRY PARTICLES	2637.2 kg/m^3
$\frac{P_1}{P_1 - P_3} \times G_a$	SPECIFIC GRAVITY OF THE IMPERMEABLE MATERIAL OF PARTICLES	2709.7 kg/m^3
$\frac{P_2}{P_2 - P_3} \times G_a$	SPECIFIC GRAVITY OF SATURATED PARTICLES WITH DRY SURFACE	2664.0 kg/m^3
$\frac{P_2 - P_1}{P_1} \times 100$	ABSORPTION	1,0 %

***Table A3** - Specific gravity and water absorption of fine river sand.*

P_1	WEIGHT OF THE SATURATED SAMPLE WITH DRY SURFACE	500.1 g
P_2	WEIGHT OF THE FULL WATER BOTTLE	709.6 g
P_3	WEIGHT OF THE FULL BOTTLE WITH SATURATED SAMPLE AND WATER	1014.33 g
P_4	WEIGHT OF THE DRY SAMPLE	494.7 g
G_a	SPECIFIC GRAVITY OF THE WATER AT TEST TEMPERATURE	1000.0 kg/m^3
$\frac{P_4}{P_1+P_2-P_3}\times G_a$	SPECIFIC GRAVITY OF THE DRY PARTICLES	2532.6 kg/m^3
$\frac{P_4}{P_4+P_2-P_3}\times G_a$	SPECIFIC GRAVITY OF THE IMPERMEABLE MATERIAL OF PARTICLES	2604.3 kg/m^3
$\frac{P_1}{P_1+P_2-P_3}\times G_a$	SPECIFIC GRAVITY OF SATURATED PARTICLES WITH DRY SURFACE	2560.1 kg/m^3
$\frac{P_1-P_4}{P_4}\times 100$	ABSORPTION	1,1 %

***Table A4** - Specific gravity and water absorption of coarse river sand.*

P_1	WEIGHT OF THE SATURATED SAMPLE WITH DRY SURFACE	500.0g
P_2	WEIGHT OF THE FULL WATER BOTTLE	709.6 g
P_3	WEIGHT OF THE FULL BOTTLE WITH THE SATURATED SAMPLE AND WATER	1006.6 g
P_4	WEIGHT OF THE DRY SAMPLE	491.3 g
G_a	SPECIFIC GRAVITY OF THE WATER AT TEST TEMPERATURE	1000.0 kg/m^3
$\frac{P_4}{P_1+P_2-P_3}\times G_a$	SPECIFIC GRAVITY OF DRY PARTICLES	2420.3 kg/m^3
$\frac{P_4}{P_4+P_2-P_3}\times G_a$	SPECIFIC GRAVITY OF THE IMPERMEABLE MATERIAL OF PARTICLES	2528.3 kg/m^3
$\frac{P_1}{P_1+P_2-P_3}\times G_a$	SPECIFIC GRAVITY OF SATURATED PARTICLES WITH DRY SURFACE	2463.1 kg/m^3
$\frac{P_1-P_4}{P_4}\times 100$	ABSORPTION	1,8 %

Annex B - Particle sizing of the aggregates

Table B1 *- Sieve analysis of the fine river sand.*

Sieve		Weight retained	% Retained	% Accumulated retained	% Pass
nº	(mm)				
1″	25.400				
¾″	19.100				
½″	12.700				
⅜″	9.520				
4″	4.760				
8″	2.380				100
16″	1.190	16.46	1.55	1.55	98.45
30″	0.595	81.47	7.66	9.21	90.79
50″	0.297	516.96	48.60	57.80	42.20
100″	0.149	283.82	26.68	84.48	15.52
200″	0.074	109.50	10.29	94.77	5.23
RESIDUE		55.61	5.23	100	0
TOTAL		1063.81	100		

D_{max} = 1.31 mm, according to COUTINHO (1988)

Table B2 *- Sieve analysis of the coarse river sand.*

Sieve		Weight retained	% Retained	% Accumulated retained	% Pass
nº	(mm)				
1″	25.400				
¾″	19.100				
½″	12.700				
⅜″	9.520				100
4″	4.760	18.80	1.88	1.88	98.12
8″	2.380	130.70	13.06	14.94	85.06
16″	1.190	259.50	25.94	40.88	59.12
30″	0.595	279.70	27.96	68.84	31.16
50″	0.297	205.90	20.58	89.42	10.58
100″	0.149	100.20	10.01	99.43	0.57
200″	0.074	5.30	0.53	99.96	0.04
RESIDUE		0.40	0.04	100	0
TOTAL		1000.50	100		

D_{max} = 5.10 mm, according to COUTINHO (1988)

Table B3 *- Sieve analysis of the fine aggregate 4/11.*

Sieve		Weight retained	% Retained	% Accumulated retained	% Pass
nº	(mm)				
1″	25.400				
¾″	19.100				
½″	12.700				100
⅜″	9.520	64.30	2.14	2.14	97.86
4″	4.760	1977.00	65.92	68.07	31.93
8″	2.380	802.80	26.77	94.83	5.17
16″	1.190	61.40	2.05	96.88	3.12
30″	0.595	22.10	0.74	97.62	2.38
50″	0.297	15.50	0.52	98.14	1.86
100″	0.149	17.20	0.57	98.71	1.29
200″	0.074	30.40	1.01	99.72	0.28
RESIDUE		8.30	0.28	100	0
TOTAL		2999.00		100	

D_{max} = 9.60 mm, according to COUTINHO (1988)

Table B4 *- Sieve analysis of the coarse aggregate 11/16.*

Sieve		Weight retained	% Retained	% Accumulated retained	% Pass
nº	(mm)				
1″	25.400				
¾″	19.100				100
½″	12.700	495.16	14.16	14.16	85.84
⅜″	9.520	1855.12	53.05	67.21	32.79
4″	4.760	1080.73	30.91	98.12	1.88
8″	2.380	21.20	0.61	98.72	1.28
16″	1.190	3.60	0.10	98.83	1.17
30″	0.595	2.63	0.08	98.90	1.10
50″	0.297	4.11	0.12	99.02	0.98
100″	0.149	7.95	0.23	99.25	0.75
200″	0.074	11.18	0.32	99.57	0.43
RESIDUE		15.19	0.43	100	0
TOTAL		3496.87		100	

D_{max} = 14.35 mm, according to COUTINHO (1988)

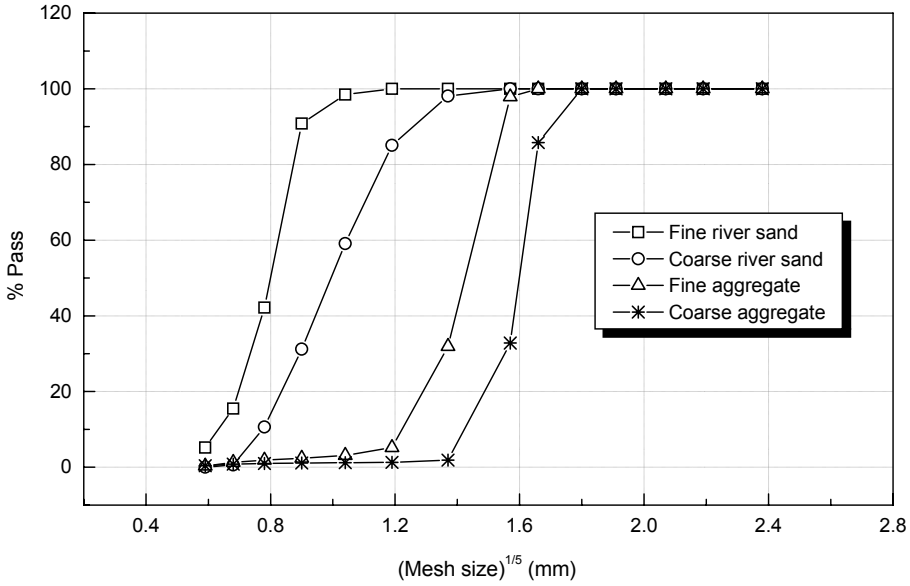

Figure B1 *- Sieve analysis of the aggregates.*

Annex C - Data of the compressive strength of the substrate concrete and of the SFRC overlay

Table C1 *- Compressive strength of concrete substrate and SFRC overlay at the age of 28 days.*

Designation	Cylinder test	Apparent density (kg/m^3)	f_c (N/mm^2)	f_{cm} (N/mm^2)	Std. dev. (N/mm^2)	COV (%)
B1	1	2274	23.65	24.16	0.44	1.83
	2	2284	24.39			
	3	2274	24.45			
B2	1	2235	22.59	23.39	0.71	3.05
	2	2241	24.29			
	3	2228	23.16			
	4	2377	23.54			
O[a]	1	2348	40.69	40.66	0.04	0.09
	2	2359	40.62			
	3	2377	40.66			

Note: Coefficient of Variation (COV) = (Standard deviation/Average) x 100
[a] SFRC

Table C2 *- Compressive strength of concrete substrate and SFRC overlay at slab testing age.*

Designation	Age at testing (days)	Cylinder test	Apparent density (kg/m^3)	f_c (N/mm^2)	f_{cm} (N/mm^2)	Std. dev. (N/mm^2)	COV (%)
B1	95	1	2277	25.58	26.35	0.89	3.36
		2	2263	26.30			
		3	2266	27.60			
		4	2294	25.91			
B2	89	1	2220	25.71	25.97	0.56	2.16
		2	2232	25.61			
		3	2257	25.76			
		4	2260	26.81			
O[a]	64	1	2304	43.06	43.23	2.27	5.24
		2	2353	42.17			
		3	2348	41.53			
		4	2361	47.17			
		5	2359	42.24			

Note: Coefficient of Variation (COV) = (Standard deviation/Average) x 100
[a] SFRC

Annex D - Flexural tensile behavior of the plain concrete and SFRC overlay

Plain Concrete Slab

The recommendation FMC1, from RILEM (1985), specifies a three-point bending test to characterize mortar and concrete post-cracking behaviour (see ***Figure D1***). From FMC1 method, the flexural tensile strength and the fracture energy (G_F) can be derived.

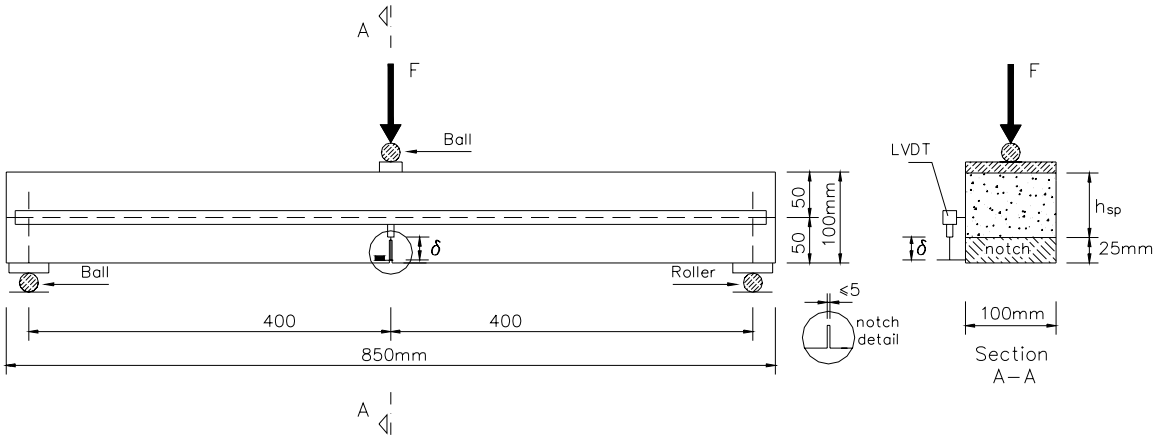

Figure D1 *- Specimen dimensions, loading and support conditions, and arrangement of the displacement transducer, according to RILEM FMC1 recommendation.*

The fracture energy is calculated from the equation:

$$G_F = \frac{(W_o + m \cdot g \cdot \delta_o)}{A_{lig}} \qquad [N/m\ (J/m^2)] \qquad (D1)$$

where

W_o = area under the load - displacement curve, ***Figure D2***, F-δ (N/mm);

m = $m_1 + 2 \cdot m_2$ (kg);

m_1 = weight of the beam between the supports, calculated as the beam weight multiplied by ℓ/L ratio (ℓ is the span and L is length of the beam, 800 mm and 850 mm, respectively, in the present case);

m_2 = weight of the part of the loading arrangement which is not attached to the machine, but follows the beam until failure;

g = gravity acceleration, 9.81 m/s^2;

δ_o = deformation at the final failure of the beam (m); and

A_{lig} = area of the ligament, $h_{sp} \cdot b$ (m^2), where b is width of the beam.

To characterize the post-cracking behaviour of the plain concrete of each mix, three bending tests were carried out, in notched 100 mm x 100 mm x 850 mm beams, according to the RILEM recommendations. The experimental set up is illustrated in ***Figure D3***. The imposed mid-span deflection, in the 3-point bending test, was measured from a LVDT yoke fixed at mid-height of the tested specimen itself (sometimes referred to as the "Japanese yoke" or "suspension yoke").

The flexural tensile strength ($f_{ct,fl}$), axial tensile strength ($f_{ct,ax}$), fracture energy (G_F) and the load-displacement responses obtained are reported in ***Table D1*** and ***Figure D4***, respectively. The value of axial tensile strength ($f_{ct,ax}$) is estimated from the flexural tensile strength, $f_{ct,fl}$, according to (D2) from CEB.

$$f_{ct,ax} = f_{ct,fl} \cdot \frac{1.5 \cdot (h_{sp} / h_o)^{0.7}}{1 + 1.5 \cdot (h_{sp} / h_o)^{0.7}} \qquad [N/mm^2] \qquad (D2)$$

where

$$f_{ct,fl} = \frac{3}{2} \cdot \frac{F_{max} \cdot \ell}{b \cdot (h_{sp})^2} \qquad [N/mm^2] \qquad (D3)$$

and

$f_{ct,fl}$ is the value of the flexural tensile strength;
h_{sp} is the depth of beam (mm), h_{sp} = 75 mm in the present case;
h_o = 100 mm;
F_{max} maximum applied load (refer to ***Figure D2***);
b is width of the beam; and
ℓ is the beam span length.

The residual flexural tensile strength ($f_{ctres,fl}$), at the final failure of the beam was determinated as follows:

$$f_{ctres,fl} = \frac{3}{2} \cdot \frac{F_{res} \cdot \ell}{b \cdot (h_{sp})^2} \qquad [N/mm^2] \qquad (D4)$$

where

F_{res} is the residual applied load at the final failure of the beam (refer to ***Figure D2***).

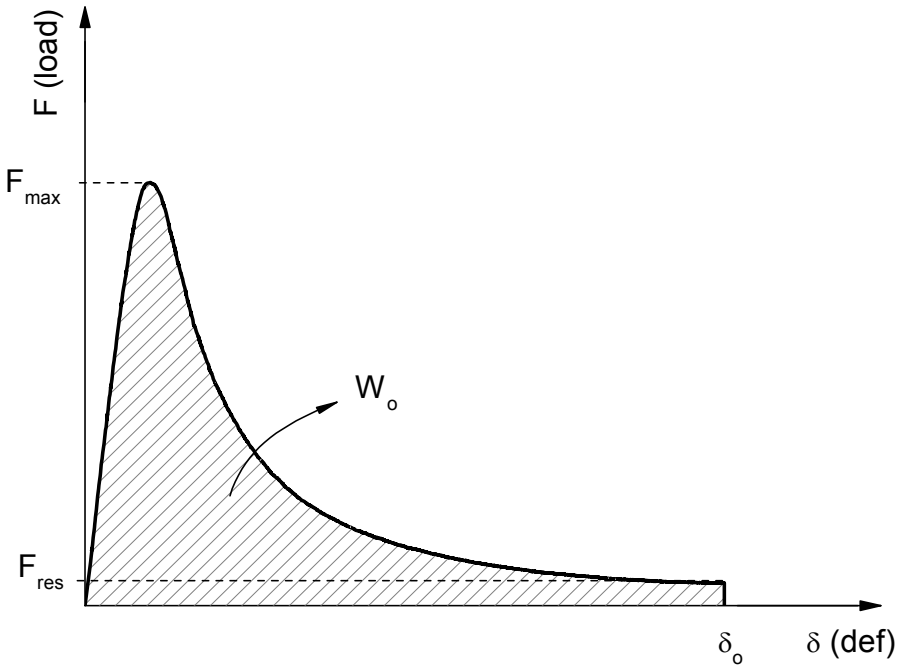

Figure D2 *- Typical load-mid span displacement curve.*

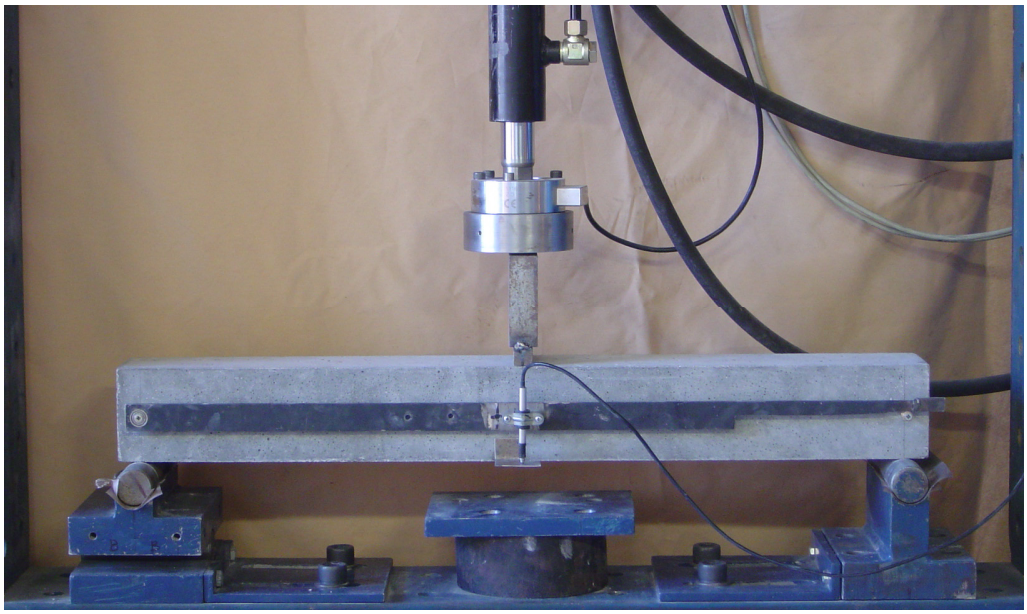

Figure D3 *- Illustration of the flexural tensile test setup for a plain concrete specimen.*

Table D1 *- Flexural tensile strength parameters of the plain concrete.*

Mix designation	Age at testing (days)	Beam	Weight (kg)	$f_{ct,fl}$ (N/mm^2)	$\delta_{fct,fl}$ (mm)	$f_{ctres,fl}$ (N/mm^2)	$f_{ct,ax}$ (N/mm^2)	G_F (N/m)
B1	43	1	19.84	3.08	0.12	0.04	1.48	145
		2	19.60	4.19	0.14	0.04	1.99	163
		3	19.90	2.51	0.11	0.02	1.20	186
B2	36	1	19.54	3.03	0.11	0.03	1.45	156
		2	19.68	2.14	0.09	0.03	1.03	105
		3	19.38	2.84	0.09	0.03	1.37	121
		4	19.72	3.62	0.16	0.02	1.73	160

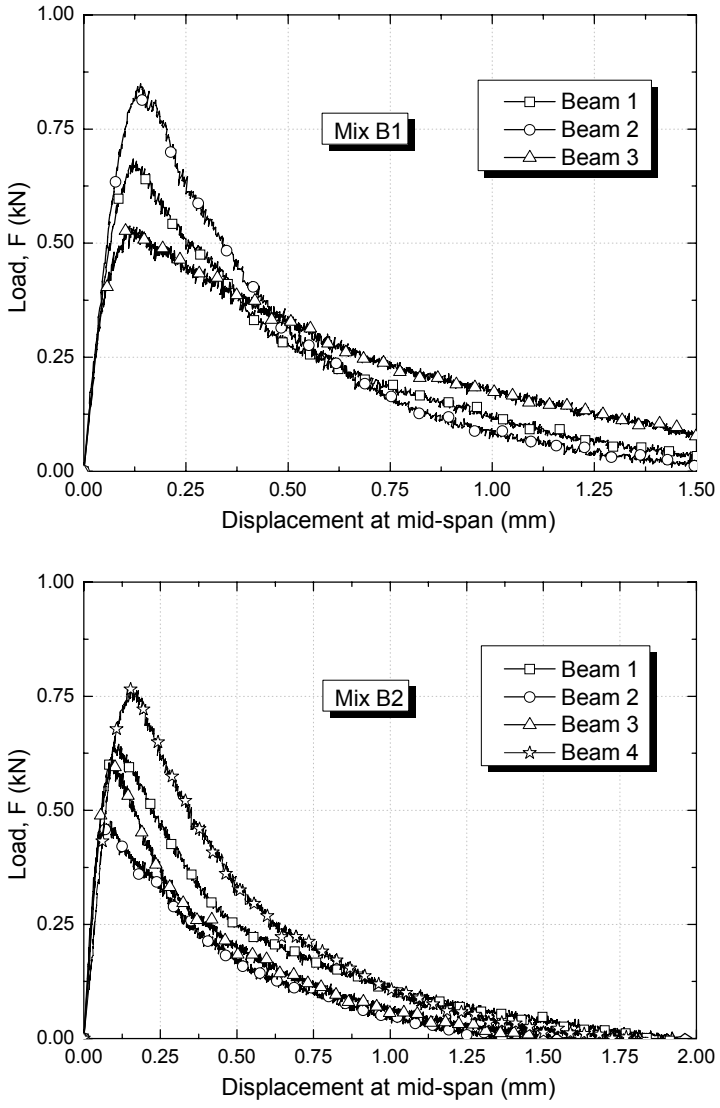

Figure D4 *- Load-deformation at mid span for all plain concrete mix.*

Concrete Overlay

RILEM TC 162-TDF Committee (RILEM, 2000 and 2002) has proposed a specimen configuration, test procedures and flexural tensile strength parameters to characterize the flexural tensile post-cracking behaviour of the SFRC.

The standard test specimen recommended by RILEM TC 162-TDF is represented ***Figure D5***. The production method for casting the specimen, the curing procedures, the position on the notch sawn into the test beam, the load and specimen support conditions, the characteristics for both the equipment and measuring devices, and the test procedures are given elsewhere RILEM (2000, 2002) documents.

From the bending test, a force-deflection relationship is obtained. From this relationship it can be evaluated the load at the limit of proportionality (F_L), the equivalent flexural tensile strength parameters ($f_{eq,2}$ and $f_{eq,3}$) and the residual flexural tensile strength parameters ($f_{R,1}$ and $f_{R,4}$). F_L is equal to the highest value of the load registered up to a deflection of 0.05 mm. The parameters $f_{eq,2}$ and $f_{eq,3}$ are related to the energy absorption capacity up to a deflection of δ_2 and δ_3 ($\delta_2 = \delta_L + 0.65$ mm, $\delta_3 = \delta_L + 2.65$ mm where δ_L is the deflection correspondent to F_L) provided by fibre reinforcement mechanisms, ($D^f_{BZ,2}$ and $D^f_{BZ,3}$), see ***Figure D6*** and ***Figure D7***. The parameters $f_{R,1}$ and $f_{R,4}$ are the stresses due to forces $F_{R,1}$ and $F_{R,4}$, respectively, corresponding to a deflection of $\delta_{R,1} = 0.46$ mm and $\delta_{R,4} = 3.0$ mm (see ***Figure D6*** and ***Figure D7***). The expressions for evaluating f_{eq} and f_R are inset on ***Figure D6*** and ***Figure D7***, where b (= 150mm), h_{sp} (~125mm) and L (= 500 mm) are the width of the specimen, the distance between the tip of the notch and the top of the cross section, and the span of the specimen, respectively. All these expressions were defined assuming a linear stress distribution on the cross section of the beam.

The experimental set up is illustrated in ***Figure D8***. For sake of test stability and measurement accuracy, the imposed mid-span deflection, in the 3-point flexural test, was measured from a reference bar leaning on the tested specimen itself (sometimes referred as “Japanese yoke” or “suspension yoke”).

The load-deflection relationships obtained on the specimens reinforced with 30 kg/m³ hooked ends DRAMIX® RC-80/60-BN steel fibres are reported in ***Figure D9***. The values of the load at the limit of proportionality (F_L), equivalent flexural tensile strength ($f_{eq,2}$ and $f_{eq,3}$), residual flexural tensile strength ($f_{R,1}$ and $f_{R,4}$), and flexural modulus of elasticity (E_{cf}) are included in ***Table D2***. Three and four bending tests were carried out for the SFRC mix O1 and O2, respectively.

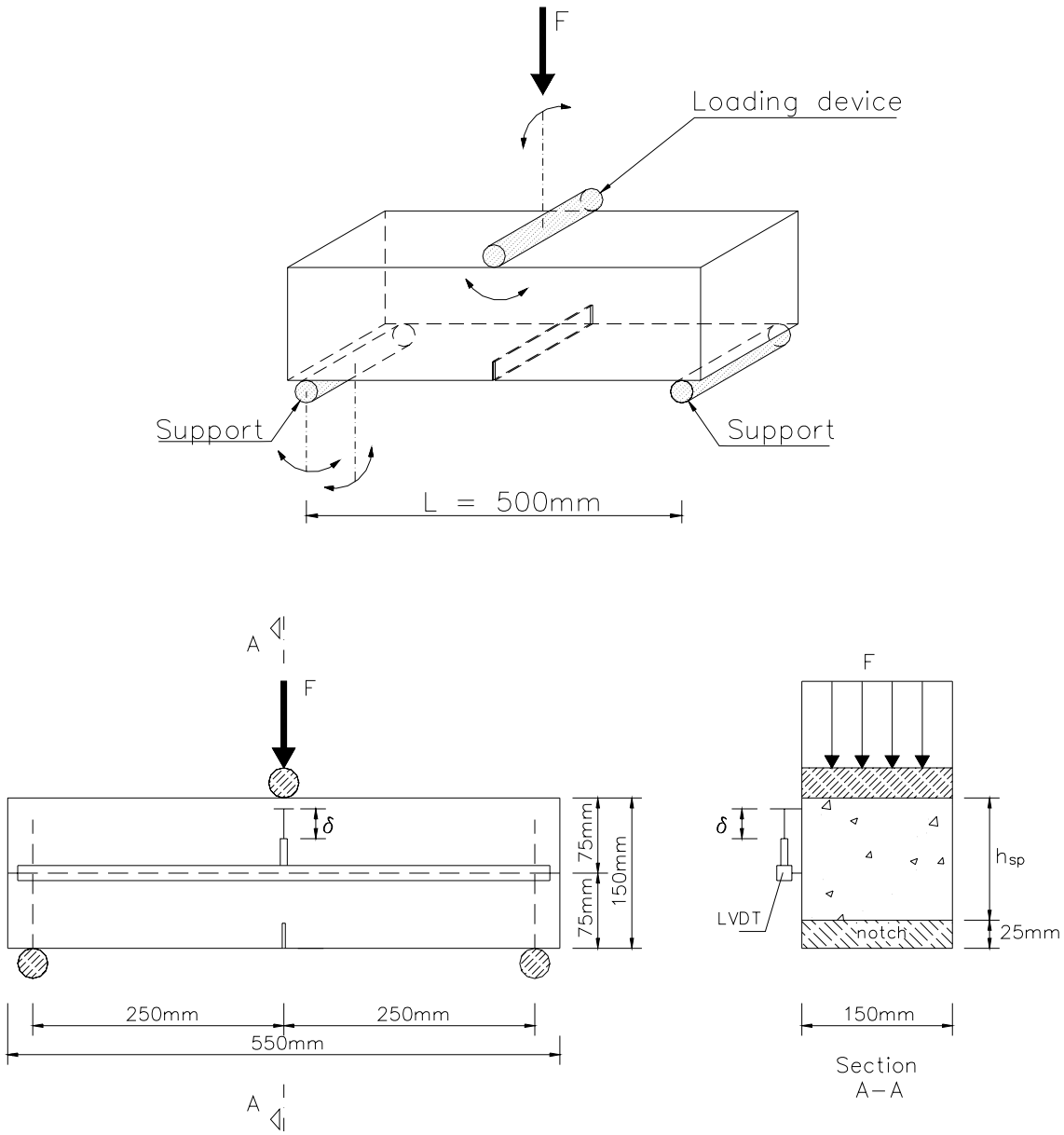

Figure D5 *- Specimen dimensions, loading and support conditions, and arrangement of the displacement transducers of the RILEM flexural tensile test.*

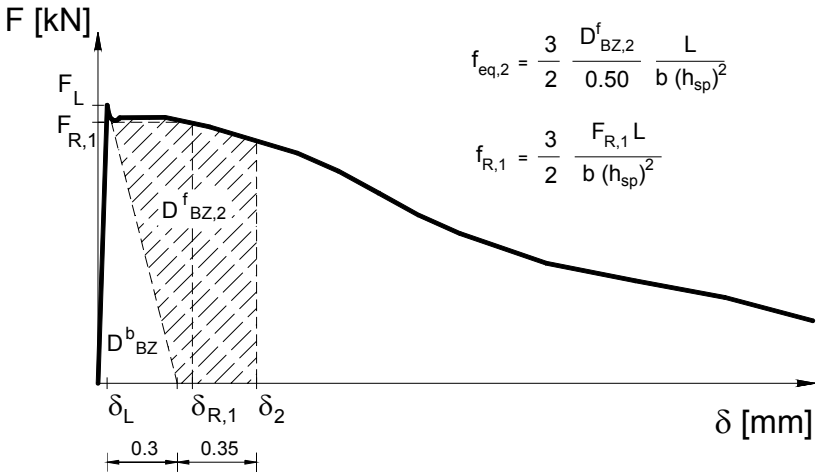

Figure D6 *- Evaluation of the equivalent two ($f_{eq,2}$) and residual one ($f_{R,1}$) flexural tensile strength parameters.*

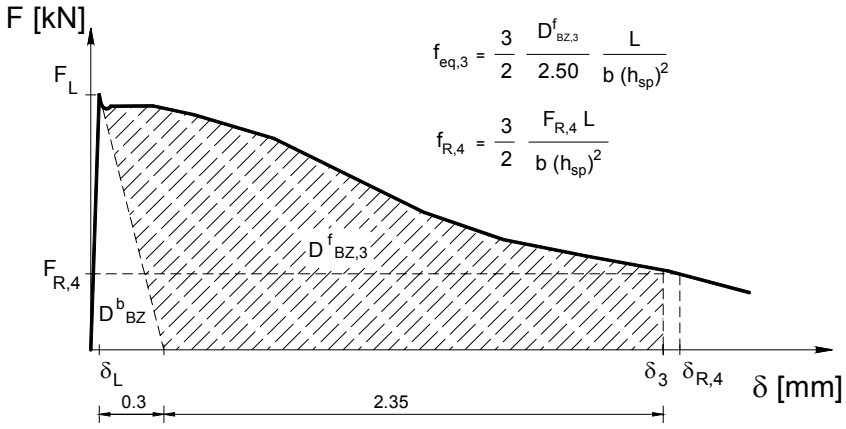

Figure D7 *- Evaluation of the equivalent three ($f_{eq,3}$) and residual four ($f_{R,4}$) flexural tensile strength parameters.*

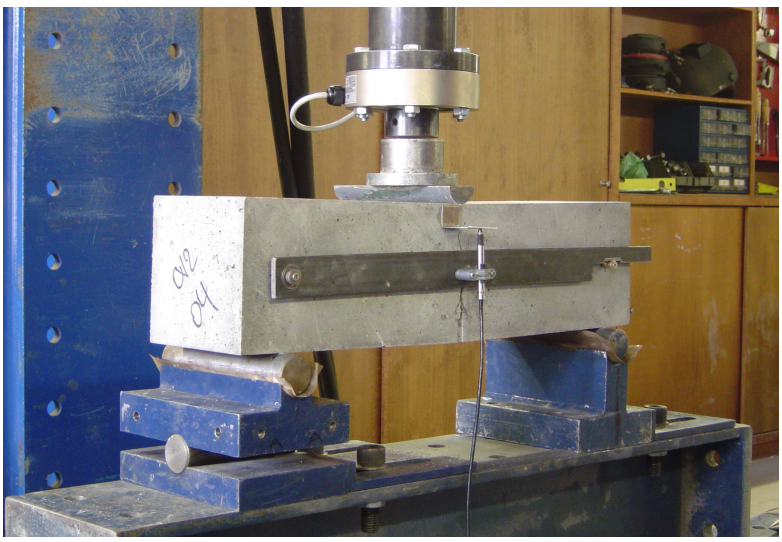

Figure D8 *- Illustration of the flexural tensile test setup for a SFRC specimen.*

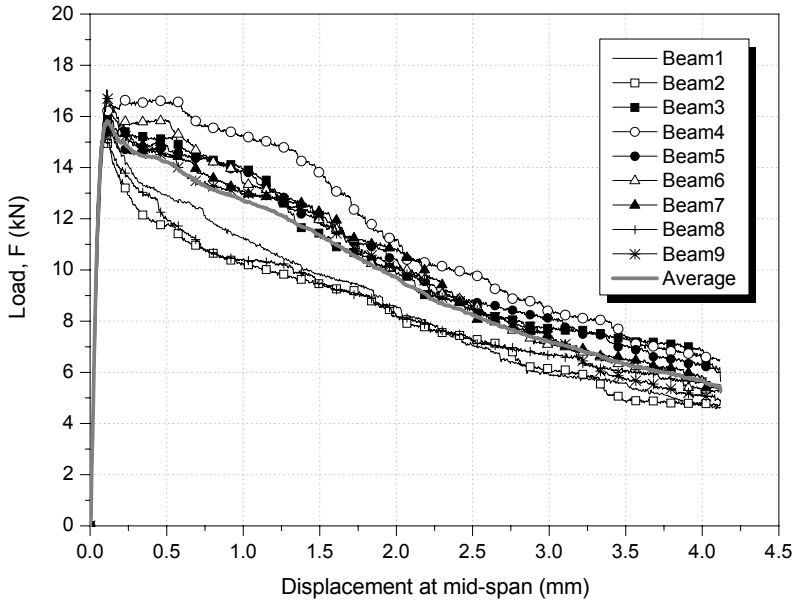

Figure D9 *- Load-deflection relationships of notched beams specimens under 3-point loading for the SFRC mix.*

Table D2 *- Flexural tensile strength parameters of the SFRC mix.*

Beam[a]	F_L (kN)	$f_{eq,2}$ (N/mm^2)	$f_{eq,3}$ (N/mm^2)	$f_{R,1}$ (N/mm^2)	$f_{R,4}$ (N/mm^2)	E_{cf}[b] (kN/mm^2)
1	17.04	3.83	3.04	4.04	1.83	24.60
2	15.75	3.48	2.89	3.66	1.90	29.03
3	16.70	4.33	3.56	4.51	2.27	21.60
4	15.98	5.07	4.11	5.15	2.61	21.97
5	15.44	4.49	3.68	4.58	2.53	28.45
6	15.65	4.79	3.71	4.93	2.20	24.63
7	15.25	4.52	3.66	4.64	2.32	26.24
8	15.16	3.73	2.98	3.83	2.08	26.40
9	16.70	4.31	3.54	4.48	2.26	21.49

[a] The age at testing of the specimens was 37 days
[b] Calculated according the equation included in the reference BARROS (1995)

Annex E - Epoxy adhesive dosages adopted and respective proportions

SFRC overlay bond product **SIKADUR® 32 N**

Dosage = 0.90 kg/m^2

For each slab:

Weigth of component A = 360 g

Weight of component B = 180 g

CFRP-concrete bond product **Mbrace® RESIN 220**

Dosage = 0.13 kg per meter of slit

For each slit:

Weigth of component I = 194.06 g

Weigth of component II = 60.94 g

Annex F - Load-deflection curves of the lateral LVDTs

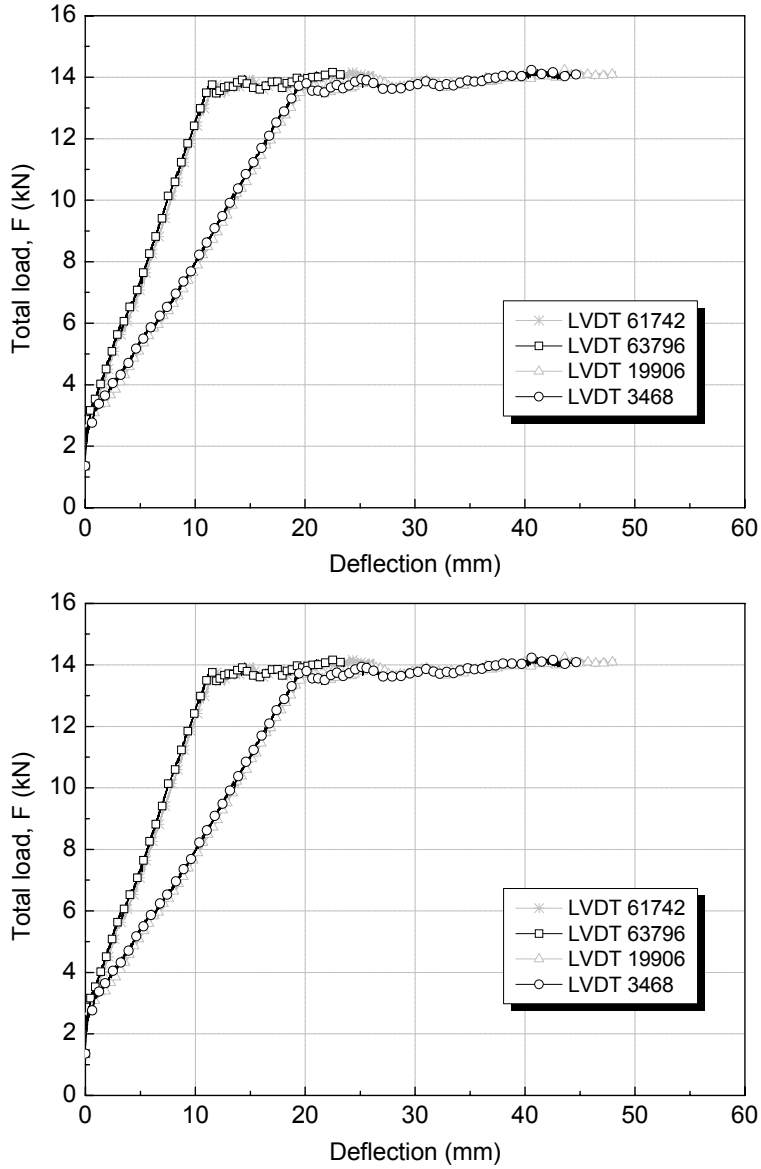

Figure F1 *- Relationship between applied load and deflection at the lateral LVDTs for the reference slabs: (a) SL1 and (b) SL2.*

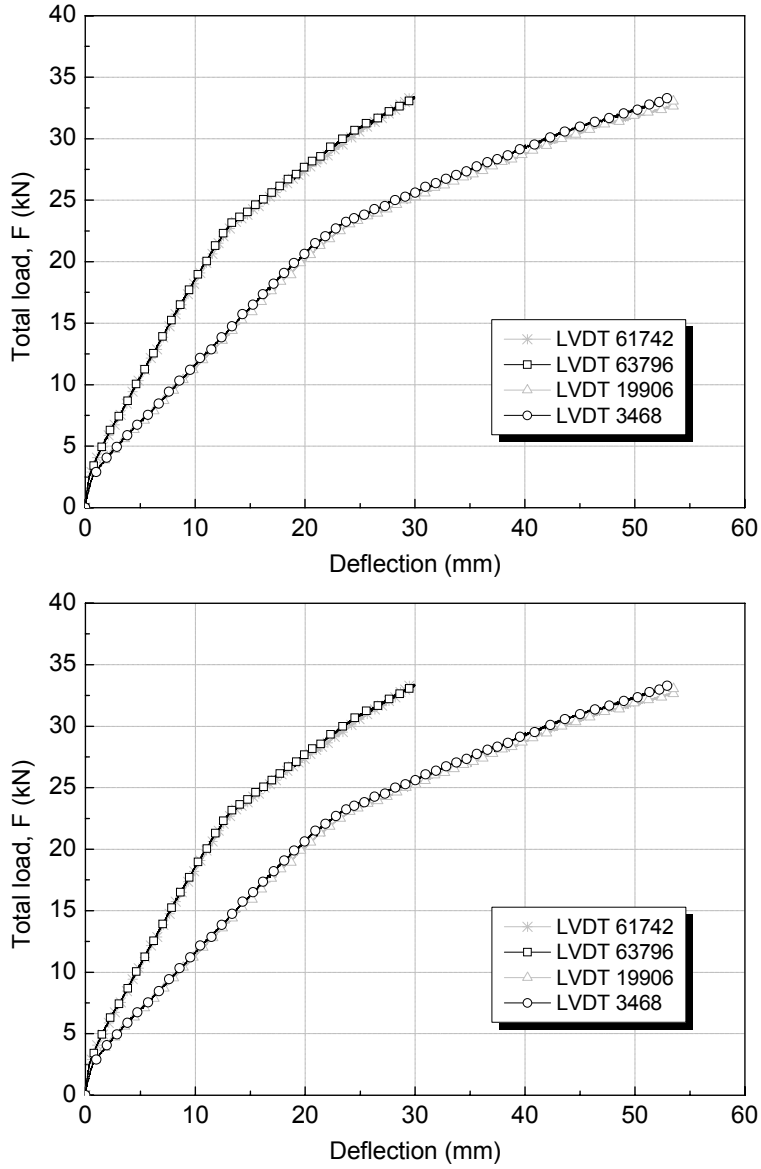

Figure F2 *- Relationship between applied load and deflection at the lateral LVDTs for the NSM CFRP strengthened: (a) SL3S and (b) SL4S.*

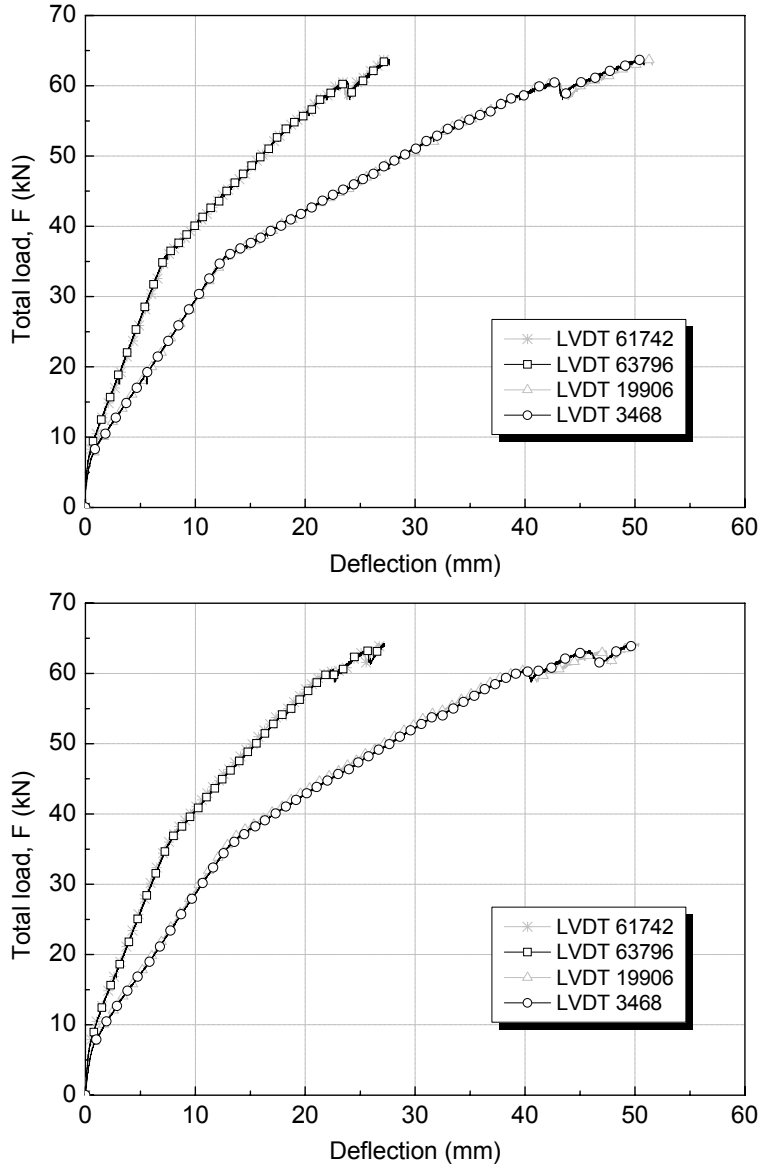

Figure F3 *- Relationship between applied load and deflection at the lateral LVDTs for the NSM CFRP strengthened: (a) SL5SO, and (c) SL6SO.*

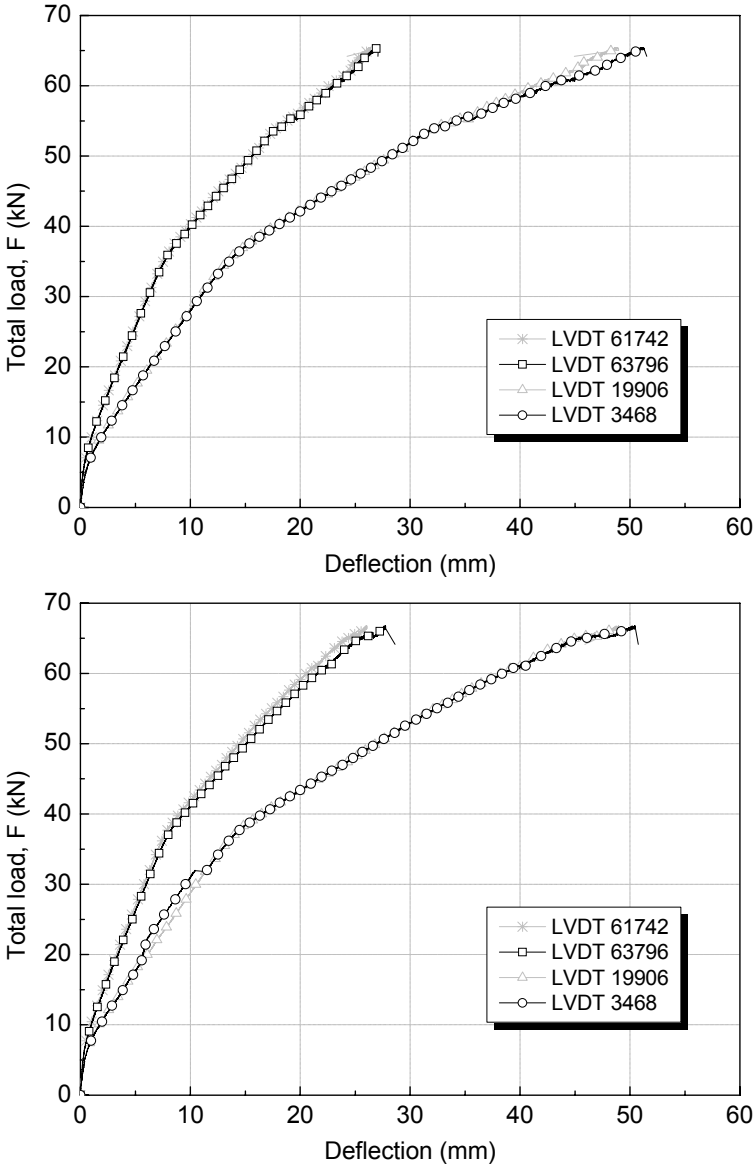

Figure F4 *- Relationship between applied load and deflection at the lateral LVDTs for the NSM CFRP strengthened: (a) SL7SO, and (c) SL8SO.*

Annex G - Theoretical predictions of ultimate diagonal shear crack load

ACI 318 (2004)

$$V_c = \left(0.14 \cdot \sqrt{f_c'} + 17.2 \cdot \rho_w \cdot \frac{V_u \cdot d}{M_u} \right) \cdot b_w \cdot d \qquad \text{(G.1)}$$

where

- $f_c' =$ cylinder concrete compressive strength (N/mm^2)
- the quantity $\frac{V_u \cdot d}{M_u}$ was taken equal to 1.0
- $\rho_w =$ longitudinal tensile steel ratio, taken as $\rho_w = \rho_{\ell,ef}$
- $\rho_{\ell,ef} = \frac{A_s}{b \cdot d_s} + n \cdot \frac{A_{CFRP}}{b \cdot d_{CFRP}}$; $n = \frac{E_{CFRP}}{E_s}$
- $b_w =$ cross-section width
- $d =$ effective depth of the cross-section, taken as $d = d_{ef}$
- $d_{ef} = \frac{A_s \cdot d_s + n \cdot A_{CFRP} \cdot d_{CFRP}}{A_s + n \cdot A_{CFRP}}$

REBAP (1983)

$$V_{cd} = \tau_1 \cdot b_w \cdot d \qquad \text{(G.2)}$$

where

- $\tau_1 =$ shear strength, value taken from ***Table G.1***
- $b_w =$ cross-section width
- $d =$ effective depth of the cross-section, taken as $d = d_{ef}$
- $d_{ef} = \frac{A_s \cdot d_s + n \cdot A_{CFRP} \cdot d_{CFRP}}{A_s + n \cdot A_{CFRP}}$

Table G.1 *- Values of the stress* τ_1 *(in N/mm^2)*

Concrete strength class	C12/15	C16/20	C20/25	C25/30	C30/37	C35/45	C40/50	C45/55	C50/60
τ_1	0.50	0.60	0.65	0.75	0.85	0.90	1.00	1.10	1.15

For slabs:

$$V_{cd\_Slab} = \alpha \cdot V_{cd} \qquad \text{(G.3)}$$

where

- $\alpha = 0.6 \cdot (1.6 - d)$, and $\alpha \geq 0.6$

For mean values:

$$V_c = \gamma_c \cdot V_{cd} \tag{G.4}$$

where

- $\gamma_c = 1.50$

CEB (1993)

$$V_{Rd1} = 0.12 \cdot \xi \cdot (100 \cdot \rho \cdot f_{ck})^{1/3} \cdot b_{red} \cdot d \tag{G.5}$$

where

- $\xi = 1 + \sqrt{\left(\frac{200}{d}\right)}$ (with d in mm)
- $\rho =$ longitudinal tensile steel ratio, taken as $\rho = \rho_{\ell,ef}$
- $\rho_{\ell,ef} = \frac{A_s}{b \cdot d_s} + n \cdot \frac{A_{CFRP}}{b \cdot d_{CFRP}}$; $n = \frac{E_{CFRP}}{E_s}$
- $b_{red} =$ cross-section width
- $d =$ effective depth of the cross-section, taken as $d = d_{ef}$
- $d_{ef} = \frac{A_s \cdot d_s + n \cdot A_{CFRP} \cdot d_{CFRP}}{A_s + n \cdot A_{CFRP}}$
- $f_{ck} =$ characteristic value of the cylinder concrete compressive strength

OKAMURA & HIGAI (1980)

$$V_v = 0.20 \cdot f_c'^{1/3} \cdot (1 + \beta_p + \beta_d) \cdot \left[0.75 + \frac{1.4}{\left(\frac{a}{d}\right)}\right] \cdot b_w \cdot d \tag{G.6}$$

where

- $f_c' =$ concrete compressive strength (N/mm^2)
- a = shear span

- $d =$ effective depth of the cross-section (≤ 1.1m), taken as $d = d_{ef}$
- $d_{ef} = \dfrac{A_s \cdot d_s + n \cdot A_{CFRP} \cdot d_{CFRP}}{A_s + n \cdot A_{CFRP}}$
- $b_w =$ breadth of the web
- $\beta_p = \sqrt{p_w} - 1 \leq 0.732$ (with d in mm)
- $\beta_d = d^{-1/4} - 1$ (with d in m)
- $p_w =$ longitudinal tensile steel ratio ($\leq 3\%$), taken as $p_w = 100 \cdot \rho_{\ell,ef}$
- $\rho_{\ell,ef} = \dfrac{A_s}{b \cdot d_s} + n \cdot \dfrac{A_{CFRP}}{b \cdot d_{CFRP}}$; $n = \dfrac{E_{CFRP}}{E_s}$

NIWA et al (1987)

$$V_v = 0.20 \cdot \left(p_w \cdot f_c'\right)^{1/3} \cdot d^{-1/4} \cdot \left[0.75 + \frac{1.4}{\left(\frac{a}{d}\right)}\right] \cdot b_w \cdot d \qquad \text{(G.7)}$$

where

- $f_c' =$ concrete compressive strength (N/mm^2)
- a = shear span length
- $d =$ effective depth of the cross-section, taken as $d = d_{ef}$
- $d_{ef} = \dfrac{A_s \cdot d_s + n \cdot A_{CFRP} \cdot d_{CFRP}}{A_s + n \cdot A_{CFRP}}$
- $b_w =$ breadth of the web
- $p_w =$ longitudinal tensile steel ratio, taken as $p_w = 100 \cdot \rho_{\ell,ef}$
- $\rho_{\ell,ef} = \dfrac{A_s}{b \cdot d_s} + n \cdot \dfrac{A_{CFRP}}{b \cdot d_{CFRP}}$; $n = \dfrac{E_{CFRP}}{E_s}$

CSA (1984)

$$V_{cr} = \left(\frac{220}{1000 + d}\right) \cdot \sqrt{f_c'} \cdot b_w \cdot d \qquad \text{(G.8)}$$

where

- $f_c' =$ compressive strength of concrete (N/mm^2)
- $b_w =$ effective cross-section width
- $d =$ effective depth of the cross-section, taken as $d = d_{ef}$
- $d_{ef} = \dfrac{A_s \cdot d_s + n \cdot A_{CFRP} \cdot d_{CFRP}}{A_s + n \cdot A_{CFRP}}$

JSCE (1996)

$$V_{cd} = 0.2 \cdot \beta_d \cdot \beta_p \left(f_c'\right)^{1/3} \cdot b_w \cdot d \qquad \text{(G.9)}$$

where

- $f_c' =$ compressive strength of concrete (N/mm^2)
- $b_w =$ effective cross-section width
- $\beta_d = \left(\frac{1}{d}\right)^{1/4} \leq 1.5$ (with d in m)
- $d =$ effective depth of the cross-section, taken as $d = d_{ef}$
- $d_{ef} = \frac{A_s \cdot d_s + n \cdot A_{CFRP} \cdot d_{CFRP}}{A_s + n \cdot A_{CFRP}}$
- $\beta_p = (p_w)^{1/3} \leq 1.5$
- $p_w =$ longitudinal tensile steel ratio, taken as $p_w = 100 \cdot \rho_{\ell,ef}$
- $\rho_{\ell,ef} = \frac{A_s}{b \cdot d_s} + n \cdot \frac{A_{CFRP}}{b \cdot d_{CFRP}}$; $n = \frac{E_{CFRP}}{E_s}$

Annex H - Side view of the slabs after test

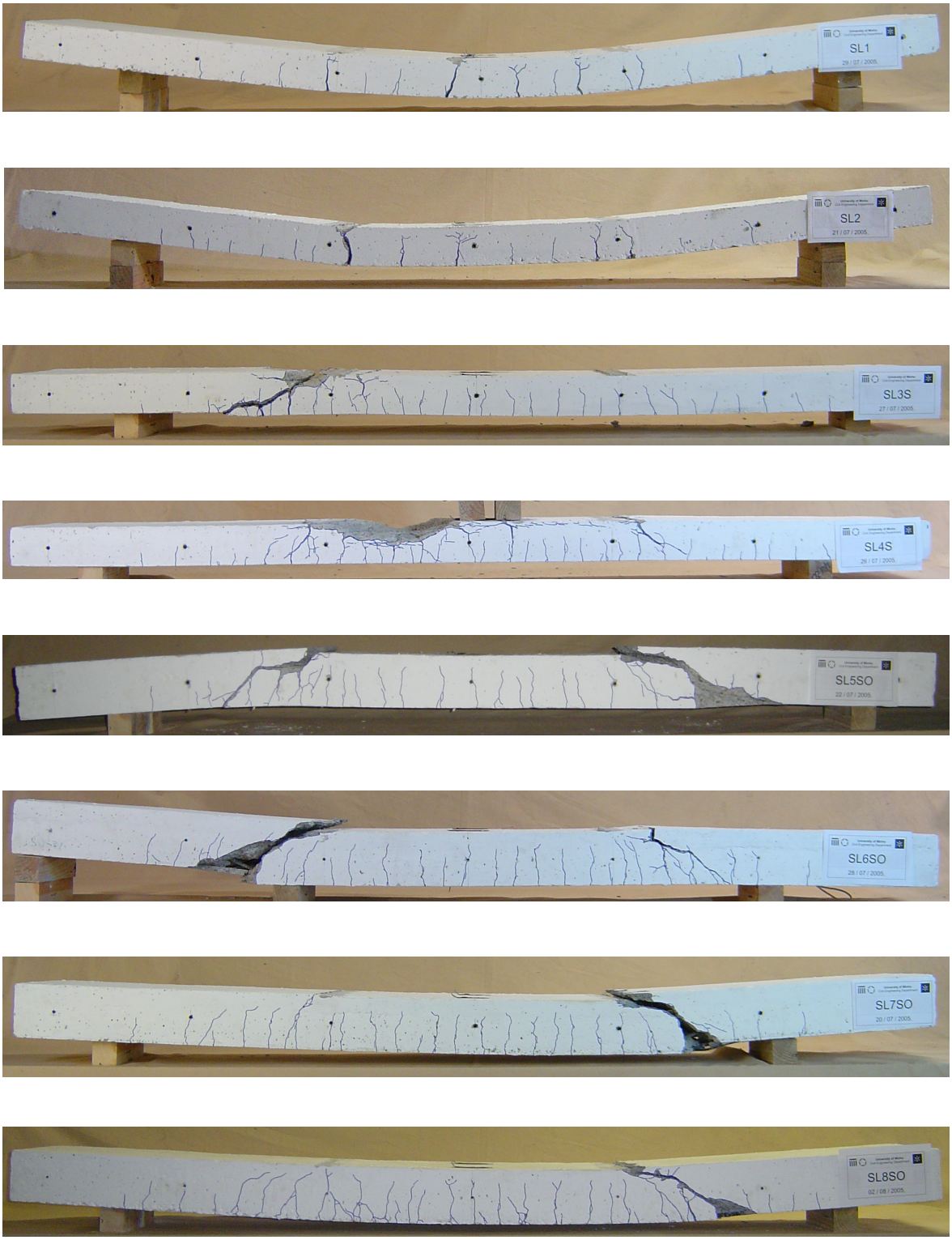

Figure H1 *- Side view of the slabs after having been tested.*

Annex I - Measurements of the NSM slit geometry

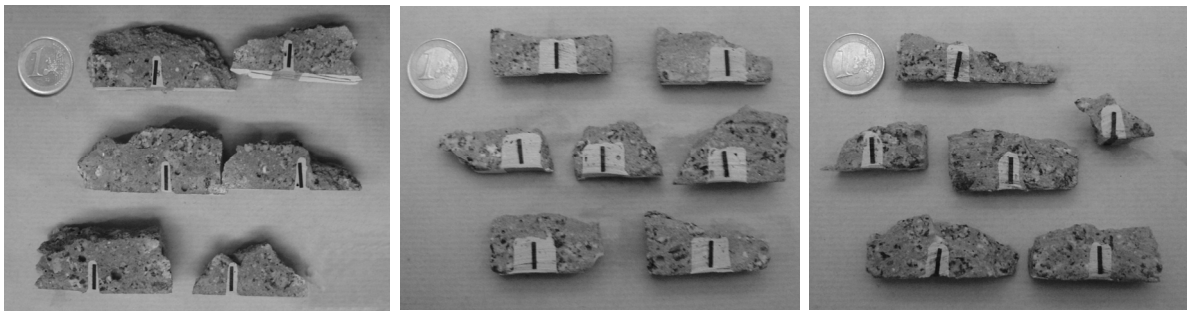

(a) *(b)* *(c)*

***Figure I1** - Pieces of NSM strengthening extracted[§] from the slabs after demotion: (a) SL6SO, (b) SL7SO and (c) SL8SO.*

***Table I1** - Measurements of width and depth of the NSM slit after demolition.*

Reading	SL6SO		SL7SO		SL8SO	
	Width (mm)	Depth (mm)	Width (mm)	Depth (mm)	Width (mm)	Depth (mm)
1	3.73 4.18	11.53	14.34 14.49	12.82	7.43 7.57	12.59
2	4.02 4.04	12.50	15.19 14.96	12.28	8.03 8.00	13.25
3	3.93 3.85	17.57	13.93 13.43	12.45	7.68 7.53	12.44
4	4.07 3.96	12.22	13.89 13.59	12.55	7.25 7.17	13.25
5	4.00 4.04	15.53	13.39 13.60	12.37	7.00 6.83	12.05
6	3.93 3.80	12.04	12.97 12.79	12.29	6.74 6.74	12.60
7	3.78 3.51	12.27	12.34 13.43	12.18	7.82 7.42	12.92
8	3.85 4.03	12.12	13.35 13.44	12.28	7.41 7.62	12.10
9	3.97 3.73	12.46	14.83 14.91	12.18	7.36 7.76	11.54
10	3.72 3.59	12.12	14.30 14.39	12.56	6.45 6.45	13.25
11	3.66 3.92	12.24	13.74 13.60	12.51	7.55 8.23	12.23
Average	*3.88*	*12.96*	*13.86*	*12.41*	*7.36*	*12.57*
Std. dev.	*0.17*	*1.85*	*0.74*	*0.19*	*0.51*	*0.57*
COV	*4.41%*	*14.27%*	*5.37%*	*1.57%*	*6.88%*	*4.50%*

Note: Coefficient of Variation (COV) = (Standard deviation/Average) x 100

[§] **The pieces were extracted from the region between the load points**